Incorporating contact area in soft finger grasp models

A thesis submitted in fulfilment
of the requirements for the degree

of Masters of Engineering

in Mechanical Engineering

The University of Waikato

By

Tara Fernandez-Ritchie

2021

Abstract

The ability to grasp is a significant function of many robotic hands, whether it be for fruit-picking or manufacturing tasks. Two major theories often used in conjunction to model grasping are Nguyen's theorem and Coulomb's friction law. Both theories model the contact between the fingers and the object in grasp as at a point. This runs true when the fingers and the object in grasp are made of hard materials. However, when the fingers or the object are soft, they deform around each other and result in a contact area between the objects rather than a contact point. This contact area means that soft-fingered grasps can apply an additional moment to balance any external moments, of which hard fingers cannot. To account for this, the soft-fingered grasp is often modelled as a point contact with a moment about the normal direction. However, in scenarios where there is no external moment both soft and hard fingers would exert a moment of 0 Nm and their grasps are modelled identically using Nguyen's theorem and Coulomb's law. Since soft-fingered grasping has been used extensively due to its superiority to hard-fingered grasping it does give rise to the question of whether the soft fingered grasp should be modelled identically to the hard fingered grasp in this case.

This research expands the current grasp models to better showcase the differences between soft and hard finger grasps. The approach taken to achieve this was to incorporate the contact area of soft fingered grasping into the contact model so as to highlight the differences between soft and hard fingers when grasping an object. The research utilised this expansion in the contact model employing Nguyen's theorem and Coulomb's friction law. Nguyen's theorem is a condition that must be met for a grasp to be in force closure, while Coulomb's friction model limits the forces that can be applied by a finger onto an object to being within a friction cone at a point for no slipping to occur. Both Nguyen's and Coulomb's theories model the friction cone of the soft finger at the centre-point of the area of contact. A set-of-cones theory was proposed, where the area of contact is comprised of many friction cones corresponding to the points that make up the contact area instead of a single friction cone.

An experiment was devised for a two-fingered symmetrical grasp of a cylinder, where the maximum angle of contact above the horizontal before slipping was investigated. The set-of-cones approach was made into a resultant friction cone model. The resultant cone model and the original centre-point cone model were used to predict the forces due to Coulomb's theory at the maximum angle of contact. The predictions were compared to the data obtained from the experiment. It was found that the resultant cone contact model predicted the normal force applied at the maximum angle before slipping more accurately than the centre-point contact model for both soft finger materials being investigated in this research.

When the resultant cone model was translated for use in the prediction of a force closure grasp by using Nguyen's theorem, the range of positions where the object was grasped in force closure increased as compared to when using the centre-point contact model. If further verified, the resultant cone model would be used for soft fingers while the centre-point model would be used for hard fingers. This extends of the modelling of soft finger contact so as to illustrate the differences in the stability of a grasp between hard and soft finger contact.

Acknowledgements

I would like to thank my supervisor, Dr Chi Kit Au. Throughout both my undergraduate and postgraduate studies, he has been a great support and somehow always has the time to help. I would like to thank him for his patience with all my questions, no matter how basic they were.

I would also like to thank the technicians at the Large Scale Laboratories at the University of Waikato, Jack Hies and Jonathan van Harselaar. To Jack, for his quick and efficient 3D printings of my endless design iterations and for showing me where to find all the necessary equipment. To Jonathan for showing me how to use the Mold star to make the molds for my silicone rubber fingertips.

To my parents for their bountiful advice given their own experiences in academic research.

To all my friends and my lovely volleyball/netball team, having nice breaks from all the stresses of the research managed to keep me sane and life happy.

Table of Contents

List of Figures

List of Tables

1 Introduction

1.1 Background

The human hand is a masterpiece in its own right. From manipulating a pen, turning a doorknob, or typing out a text message, human hands have proven to be a vital part of our daily life. Their complex structure is considered to be an outstanding example of natural engineering. Made up of 27 bones, it is a fragile skeleton. The primary functions of the hand include gripping, grasping, and forming precise movements. These functions have helped in the development of many major industries.

The usefulness of the human hand has been noted in the robotics and prosthetics industries, with many attempts to recreate it. The first ever replication of a human hand was recorded in 77AD by Pliny the Elder, a Roman scholar (Zuo & Olson, 2014). It was made for a soldier who had lost his hand during a war so that he could return for another battle. When electronics came into play, the artificial hand industry also expanded. The first industrial robotic arm can be seen in Figure 1 and was the Unimate arm, invented by George Devol (Moran, 2007). Devol designed it to be programmed to grasp and lift objects repeatedly. The first Unimate arm marketed could grasp hot die cast metal parts and stack them accordingly. This arm served as the prototype for the expansion of the robotic arm and automated grasping industries that continue to grow today. Robotic hands are now being used in harvesting, weeding, mining, surgery, manufacturing, warehousing and more.

Figure 1: First Unimate robotic arm (Kucher, 2020)

1.2 Modelling importance in robotic grasping industries

As with any engineering design, modelling is an important part of the robotic grasping industry's design process. It is a vital tool for planning and problem-solving in engineering design. Modelling can be done physically or theoretically. Before the official product or design is made, it must be prototyped and tested to ensure that the features work as desired. For robotic grasping, modelling is required to ensure that the hand or fingers are restraining the object in a force closure grasp without slipping (L. E. Zhang, Ciocarlie, & Hsiao, 2011). Force closure is a condition where the fingers are positioned such that they can oppose any external forces or moments on the object in grasp. As well as physical prototypes, it is essential to have a good mathematical model. In engineering design, mathematical equations are used to ensure that the design will do the task or have its features working as anticipated. When the initial design is validated through mathematical modelling, it can then be prototyped and eventually transformed into the final design.

In terms of robotic grasping, it is necessary to have accurate grasp models. There are a few widely used grasp models that ensure an object is restrained well in a grasp; from Coulomb's friction law, Hertzian contact stresses to Nguyen's theorem. Many variables can affect how effective a grasp is. Models attempt to incorporate all these different grasp variables and find ways to accurately portray whether the grasp is enough to keep the object held in place. Some of these variables include the placement of the robotic fingers on the object, whether the grasp is a precision or power grasp, the shape, material and weight of the objects and fingers in contact, and the force that is applied to the object. In particular, determining the range of positions where the grasp is force closure is an important aspect of grasping to model. This is because the more positions for grasping where the object is held in force closure, the less positional accuracy needed from the robot (Nguyen, 1987). Another important aspect of consideration for robotic hand modelling is the actual purpose of the hands. Whether it be to simply grasp and lift an object or for dextrous manipulation. Models that check whether the grasp of an object will be successful differ from models looking at how the fingers can manipulate an object to orientate it however desired.

As well as considering the many variables that make up a robotic grasp, the application of the grasp should be considered. The field of application for robotic grasping is becoming wider every day. Originally, robotic arms and hands were used to replace human limbs and almost exclusively focused on grasping (Khurshid, Ghafoor, & Malik, 2011). Grasping is easier to model than dextrous manipulation. Nowadays, the sectors that robotic hands are used for are more extensive. One such area is manufacturing works that include arc welding, painting, drilling, picking, packing, gluing and other industrial works (Shake, 2020). Other major industries employing robotic arms include food preparation, military, and agriculture.

In particular, the agriculture industry has overseen the growth of robotic arms and hands, with its primary function being picking and harvesting. Mimicking the human hand, a robotic end-effector attached to the robot arm works to minimise the need for humans to do repetitive tasks and save plenty of time and money in the harvesting industry (Team, 2017). The ability of a robot to grasp ripe produce in a stable grasp and place them where necessary is the backbone of the robot industry in agriculture. Sometimes this need not be done with a hand-like end-effector but for the more delicate operations, it is necessary. The challenge is that the robot gripper needs to replicate or even improve the performance of a human hand in such operations. While it is simple for a human hand to pick, grasp, lift, and place various objects of various sizes, weights, surface characteristics and shapes, a robotic hand requires a lot more thoughtful engineering(B. Zhang et al., 2020). The robotic hands are the grippers or end-effectors on the end of the arm of the robot. The opening-and-closing grasp action is achieved through the use of power, whether that be pneumatic or electrical. As well as grasping the object, robotic graspers have the task of locating the objects to be picked. This takes the use of a variety of sensors and visual aids. The combination of these sensors with control programming makes the robotic grasp capable of these tasks (B. Zhang et al., 2020).

Figure 2: Robot grippers grasping a tomato (Slater, 2020)

As can be seen from Figure 2, robot grippers have changed significantly since the first days of its use. When automated processes were first used for harvesting, it was done in a completely mechanical way, where produce was physically shaken until they dropped or other forceful methods were used (Slater, 2020). However, these methods can bruise or damage the harvested produce and thus, other methods were explored. Nowadays, harvesting robots are much more sophisticated. The robot holding the tomato in Figure 2 is doing this through the aid of machine vision that can be seen as the part above the gripper. Machine vision helps the gripper establish the location and even the colour of the produce by using a camera to mimic human vision (Sonka, Hlavac, & Boyle, 2014). Using wave interpreters, harvesting robots can even measure the thermal radiation coming off an object.

Every type of produce needs to be approached differently when modelling and designing robot grippers. This is mainly due to their different shapes, ways of attachment to their holder plant and how much force they can take without damage. Therefore, robot grippers are typically designed for a specific product rather than being able to adapt to many different types of objects. This is similar for any object and task that robotic grippers have to grasp in any industry. That is where the typical robot hand still has not quite replicated the adaptive abilities of a human hand.

1.3 Research Objective

The main theories other than the classic law of equilibrium used for predicting whether a grasp is stably restraining an object are Nguyen's theorem and Coulomb's friction law. Nguyen's theorem states a condition for a force closure grasp, while Coulomb's friction law is used to predict whether the contact between the robot fingers and the object in grasp will result in slipping. These two theories work together as conditions in keeping the object restrained.

Robotic fingers used for grasping can be made of a variety of materials, ranging from very hard to soft and deformable. Soft fingers deform against the object in contact. The contact area means that the soft finger can apply a moment about the applied normal force's direction to offset any external moments acting on the object. Hard fingers only have a point contact so they cannot apply any additional moment to the grasped object. Thus, soft finger grasps are generally seen as superior to hard finger grasps. Both soft and hard finger grasps are modelled as point contacts but with soft finger models incorporating the extra moment component.

Interestingly, there are grasping scenarios where no external moments are acting on the object in grasp, and the soft fingers do not have to apply any moment for equilibrium. In these cases, both soft and hard finger grasps are modelled identically. Assuming the coefficient of static friction is a constant for both the hard and soft finger, the positions for effective placement of the fingers on the object, found by using Nguyen's and Coulomb's theorems, are the same in such a scenario. Since soft fingers are thought of as superior to hard fingers in grasping, it is questionable that the soft fingers would not be able to grasp the object more stably in a wider range of positions that the equivalent hard finger in such a scenario.

The objective of this research is to propose and investigate a grasping model that can better showcase the difference between a soft and hard finger grasp than the current models do. The thesis begins with a review of current grasping and contact models (Chapter 2). It will lead to the research approach to answer some of the questions formed by the literature review (Chapter 3), and then an alternative model will be proposed (Chapter 4). The experiment's methodology will be outlined (Chapter 5), with the experimental results then covered (Chapter

6). Verification of the alternative model will follow (Chapter 7), and a final chapter will explore further insight into Nguyen's theorem (Chapter 8).

2 Literature Review

2.1 Introduction to Grasping

The human hand acts in a wide range of ways to complete an assortment of complex tasks, but one of the most important uses of the hand is grasping. Grasping is the ability to restrain an object. There are many ways we use our hands to grasp in everyday life, from holding a mug to picking up a ball. This facility is what the robotics and prosthetics industries continuously attempt to recreate and potentially improve.

The desirable properties of a grasp can be simplified into two properties. Firstly, the capability to combat external forces such as the force due to gravity. The grasping fingers need to be able to apply an opposing set of forces to balance out the external forces. Secondly, the capability to manipulate objects dextrously. This can be referred to as a manipulatable grasp. A task may require a grasp to move the object being restrained around the fingers, which will require the grasping fingers to have some level of independent motion (Murray, Li, Sastry, & Sastry, 1994). These properties are dependent on the materials in contact and the finger positioning on the object.

Of course, the human hand is not a simple phenomenon, with its five digits, nine tendons and a palm. All these elements work together to allow the hand to restrain a wide range of objects. This means that there is not just one type of grasp position used to restrain objects. In a 1956 study by J.R. Napier, he observed that there initially appeared to be an unlimited number of positions that the hand can choose to be in when grasping. But upon further examination, he noticed a pattern where the typical grasp types can be limited to two categories: Power grasping and precision grasping. The factors that influence the posture of the hand during grasping are the shape of the object, size, weight, texture, temperature, other miscellaneous reasons and the purpose of the grasp (Napier, 1956).

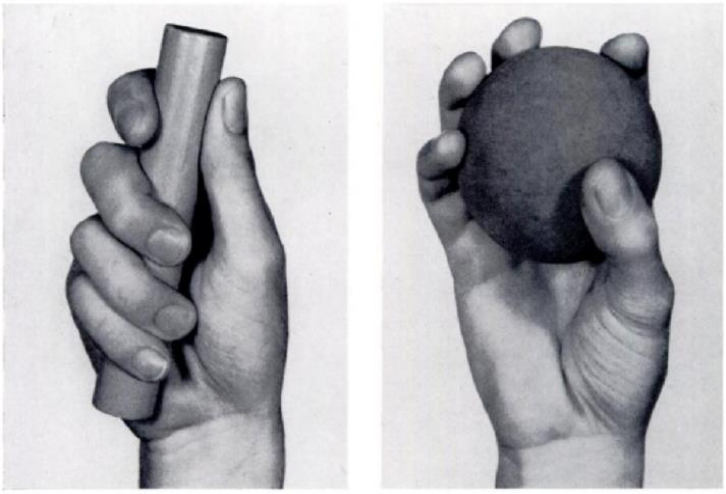

Figure 3: Power grasp (left) and Precision grasp (right) (Napier, 1956)

The two grasp types proposed by Napier can be seen in Figure 3. The power grasp is characterised by sizeable contact areas between the fingers, palm, and the object in question. There is little room for the motion of the individual fingers in the power grasp. On the other hand, the precision grasp is characterised by the object being held by the fingertips and the thumb with hardly any contact with the palm. Both power and precision grasps are useful for different reasons. Power grasps are generally used to ensure that the object is stable and secure, whereas precision grasps are used for dextrous manipulation and sensitivity (Cutkosky, 1989). This was demonstrated in Napier's research, where the hand positions were analysed in the act of opening a large jar. In the start of the jar-opening, the hand was stretched out in a power grasp, with the palm placed firmly against the lid. This was done until the jar was loosened and then the hand changed to a precision grasp position, with the fingertips in contact with the lid until it was completely unscrewed and lifted off the jar (Napier, 1956).

Both power and precision grasps are undoubtedly useful in different applications, but they can also be used together to complete a task, as seen in the jar-opening example. This illustrates the importance of the positioning of the grasping fingers and that it should be considered in the design of a grasping hand. In actuality, robotic graspers may not need to exactly replicate the human hand at all. An extensive range of grippers and fixtures in industry are solely used for

restraining an object (Bicchi & Kumar, 2000). End-grippers are commonly placed on the end of a robotic arm and have a minimum of two fingers. A common two-fingered gripper consists of two-parallel grippers, like the one in Figure 4. This type of gripper is best for cylinders or symmetric objects with parallel faces. Out of the two grasp types proposed by Napier, this would be closer to the power grasp because of the large area of the grippers on the object being grasped.

Figure 4: Parallel grippers grasping a can (Harada et al., 2014)

Traditionally, robotic graspers have consisted of an arm with various detachable end-effectors, such as the parallel gripper previously mentioned. This is to encompass a range of shapes and sizes of the object being picked up and ensures that there is an appropriate gripper to restrain the variety of objects that the machine may need to grasp. The potential drawback to the detachable end-effectors is that any movement or manipulation of an object would have to be achieved through the movement of the entire arm. This would be fine for power grasping and lifting since the set of tasks to complete would be relatively simple and linear. For precision grasping and manipulation, it would be more difficult. For example, it would be similar to writing with a pencil by moving one's whole arm instead of manipulating the angle of the pencil with one's fingers (Murray et al., 1994). Hence, controlling multiple independent fingers is necessary for precision grasping in many dexterous operations and this has been further developed in modern robotic graspers.

2.2 Stability

For the popular task of picking up and holding an object, robotic hands or end-effectors are designed to provide stability to the object in grasp. The subject of stability is often mentioned in the world of robotic grasping, with an optimal grasp being one that is classified as stable. A stable grasp can be defined as a grasp that fully restrains an object so that it can resist external forces and disturbances and return to an equilibrium state if removed from such a state (Montana, 1992). Stability can be defined as either contact grasp stability or spatial grasp stability. Contact grasp stability refers to the contact points between the fingers and the object. The inclination of the points of contact to return to their original position after a disturbance is the contact grasp stability. Spatial grasp stability is the tendency of the object to return to its original position when displaced because of an external force (Montana, 1991). Both contact and spatial grasp stability are effective ways to analyse the stability of a grasp and ideally could be used in conjunction with each other. Spatial grasp stability has a long history of use and is arguably more widely used than contact grasp stability since it has been used to quantify the stability of grasps. It does this through the analysis of the forces and torques applied on the object.

One way of describing the spatial grasp analysis is through a balanced force system (Li, Li, Yang, & Wang, 2013). As is the topic of Newton's first law of motion, an object is in equilibrium if the sum of the forces and torques applied on the object is equal to zero.

$$\sum F = 0 \tag{1}$$

$$\sum \tau = 0 \tag{2}$$

For example, an object being held by two fingers has an external force acting on the object that is the force of gravity on the object. The forces exerted by the two fingers have to balance the downward gravitational force on the object for the object to be in equilibrium. This is required for spatial grasp stability.

Another way to describe spatial grasp stability is through the concepts of form closure and force closure (Reuleaux, 2013). These concepts date back to 1876 but have been further defined in

research leading up to the present day. A grasp is form closure if there exists a set of contact points that are geometrically positioned such that the object is completely constrained regardless of the magnitude of the contact forces applied. A grasp is force closure if the grasping contacts on the object are positioned such that they can apply forces and moments to oppose any arbitrary external disturbance (Nguyen, 1987). Of the two spatial grasp stability concepts, force closure is used more widely. This is because force closure grasping has had plenty of research to support the theory and suitable mathematical descriptions have been developed to describe it. Form closure has had less research and a divergence in the concepts describing it exists (Rimon & Burdick, 1996).

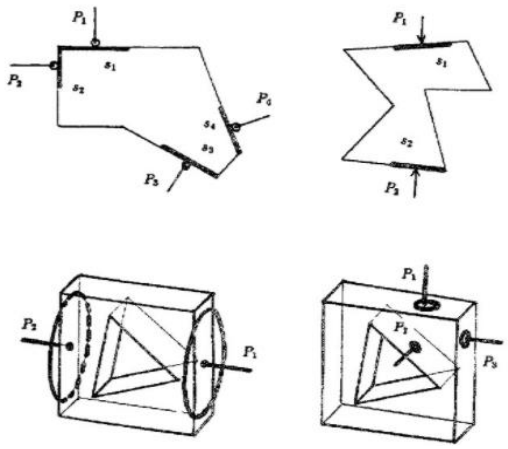

Figure 5: Force closure examples in 2D and 3D (Nguyen, 1987)

Figure 5 shows a few examples of force closure grasps. These contact forces are positioned so that the grasp would be able to resist any external disturbances for these specific shapes. The shape and size of the object are significant factors in determining the positions of contact of the fingers that will result in the object being in a force closure grasp. This is because the moments acting on the object due to the positioning of the forces have to balance to a net moment of zero and are dependent on the shape and size of the object. The distribution of the weight also influences the moments due to the object's shape and size, and this is why the positioning of th contact forces that will result in the object being in force closure will vary for the shapes such as those seen in Figure 5.

The most basic definition for a force-closure grasp is that for any external force/moment wrench, F_e, applied to the object, there are forces that can applied from the fingers in contact, f_c (Murray et al., 1994). They exist such that:

$$Gf_c = -F_e \tag{3}$$

Other theories have been proposed from this basic definition that can help determine the magnitude of the contact forces and positions for a force-closure grasp for different objects in greater detail. This is particularly useful because of the possibility of more complicated object shapes, such as the ones seen in Figure 5. It should be noted that a force-closure grasp does not imply equilibrium but rather that there is the potential for the fingers to keep the object in equilibrium at a particular positioning. Equilibrium analysis of the object in grasp should also be done when modelling a grasp.

Another aspect influencing the stability of a grasp is due to the object slipping. Slipping is self-explanatory from the name and is a concept commonly used in daily conversation. In terms of grasping, slipping is when the object or the fingers in contact with the object do not stay in their original position but are completely displaced from their original position due to an external disturbance. This can result in the object moving entirely out of the fingers' grasp.

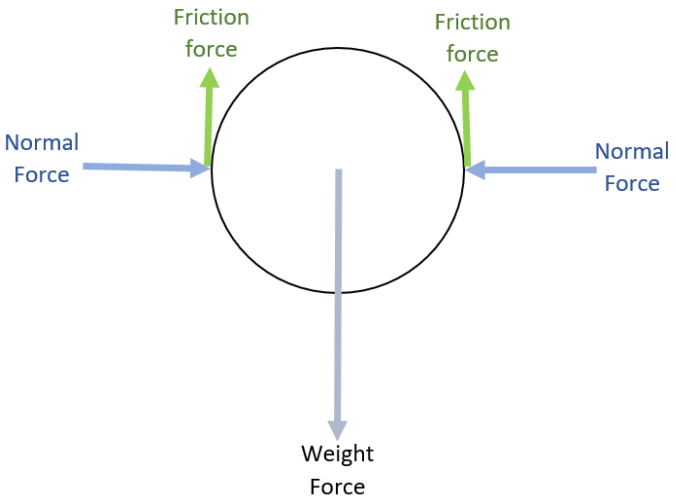

Figure 6: Contact forces on a disk in 2D

Slipping is linked to the frictional forces in play when fingers are grasping an object. When fingers are grasping an object, there is a normal force applied as well as friction forces that are perpendicular to the normal force. As in the typical two-dimensional (2D) grasp shown in Figure 6, friction forces are responsible for keeping the object grasped and in equilibrium. In other scenarios, the normal force applied may be the main force keeping the object in equilibrium rather than just the friction force.

Coulomb's friction law is the main way slipping is modelled in grasping. The famous law provides a relationship between the normal force and the frictional forces between the fingers and the object in grasp. Coulomb's equation follows where F_t is the tangential friction force, F_n is the normal force and μ is the coefficient of static friction.

$$F_t \leq \mu F_n \tag{4}$$

As long as F_t is less than μF_n then no slipping will occur. This can be visualized geometrically with a friction cone. The forces must keep within the boundaries of the friction cone for no slipping of the object in grasp to occur.

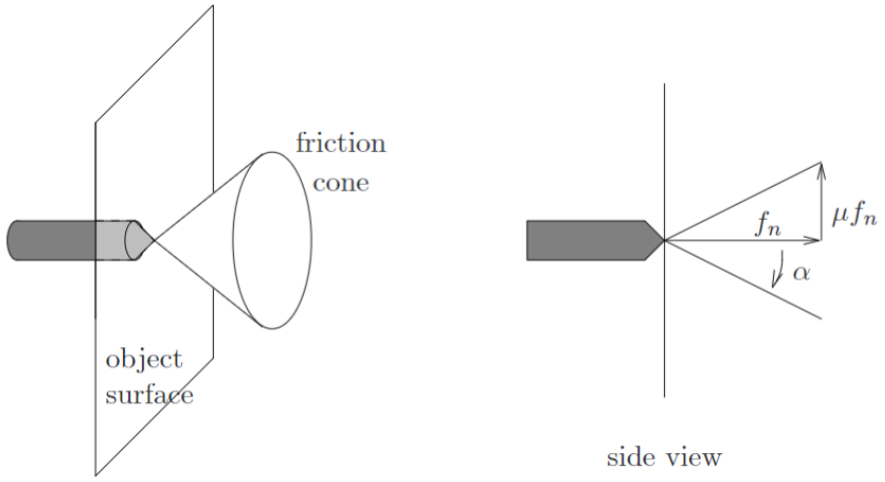

Figure 7: The friction cone represented geometrically (Murray, et al., 1994)

When considering the forces in 3-dimensions, visually represented with the friction cone on the left in Figure 7, the criteria for no slipping becomes:

$$\sqrt{{f_1}^2 + {f_2}^2} \leq f_3 , \qquad f_3 \geq 0 \tag{5}$$

where f_1 and f_2 are the frictional forces, tangential to f_3, the normal force. Note that f_3 has to be greater than or equal to zero. This is because in grasping, the normal force applied to an object can only be a "push" force, not a "pull" force, as a negatively signed force would imply. The friction cone model seen in Figure 7 applies to point contacts with friction, otherwise known as hard contacts. For the case where the finger in contact with the object is soft, an additional moment can be applied due to the contact being an area rather than a point. The contact area means that the forces applied from the finger are distributed around the area as opposed to a single point force. The distribution of forces about a larger space is useful in grasping because the distance of the outer forces from the centre point of the application can generate a moment when needed to balance external disturbances. The friction cone model and equations still apply, but the additional moment must be accounted for. A torsional frictional coefficient, γ, can be used for simplicity to demonstrate that there is a limit to the moment that can be applied, $|f_4|$, in a cone about the normal force before slipping (Murray et al., 1994).

$$|f_4| \leq \gamma f_3 \tag{6}$$

To summarise, frictional forces that can be applied for a specific normal force without slippage occurring can be modelled as being within a cone around the normal force. This is similar for the torques applied in soft-finger contact. When the frictional forces or frictional torques are larger than the limits of the frictional cones, slipping will occur. This is compromising the stability of the object being grasped. When modelling the design of a robotic hand grasping an object, Coulomb's law can be used to estimate whether the object would slip. If this proves to be the case, there will need to be iterations to the applied force, material, finger shape, finger size and positioning until Coulomb's law shows that no slipping would occur.

While Coulomb's law is effective for individually analysing whether slipping would occur between an individual finger of a robotic hand and an object, grasping is never just done with a single finger contact that can be analysed completely independent of the other fingers that may be in contact with the object. Such is the complexity of the human hand; it has five fingers to work

with. Coulomb's friction cone must be used for both fingers. In a typical grasp, there must be at least two contacts that are restraining an object. Therefore, Coulomb's friction cone theory has to incorporate all the fingers being used in the grasp, with the idea that if even one of the fingers does not meet Coulomb's friction law, then the object will begin to slip.

This is where Nguyen's theorem comes into play. Nguyen proposed a condition for a stable two-fingered grasp with no slipping. Nguyen still proposed the use of Coulomb's friction cone theory to model slipping, but he also suggested that for an object to be held without slipping, there needs to be a line segment that points exactly into the centre of the friction cone for each point contact (Nguyen, 1986). This can be seen in Figure 8 (i), where there is a line connecting the contact points within their friction cones so that no slipping occurs. This was modelled simply for point contacts by Nguyen and thus, this theory has widely been used for hard finger contacts with minimal area contact.

Nguyen's theorem of the line connecting the two contact points is derived from the direction of the resultant of the frictional and normal forces from each contact point. This method is a simple way of analysing whether an object is held in a force closure grasp. Every object being grasped has a range of possible positions for the fingers to contact the object in a force closure grasp. A way to prove that a grasp is force closure is through the convex hull test. Nguyen used the convex hull test to establish that it was always a force closure grasp when the line connecting the two contact points lay within their friction cones. He also used the convex hull test to establish that the grasp was not in force closure when the line connecting the two contact points lay outside their friction cones.

The definition of a convex hull for a set of vectors S = {v_1, … , v_k) is (Murray et al., 1994):

$$co(S) = \left\{ v = \sum \alpha_i v_i : \sum \alpha_i = 1, \alpha_i \geq 0 \right\} \quad (7)$$

Where α_i is a set of arbitrary constants that must be greater or equal to zero.

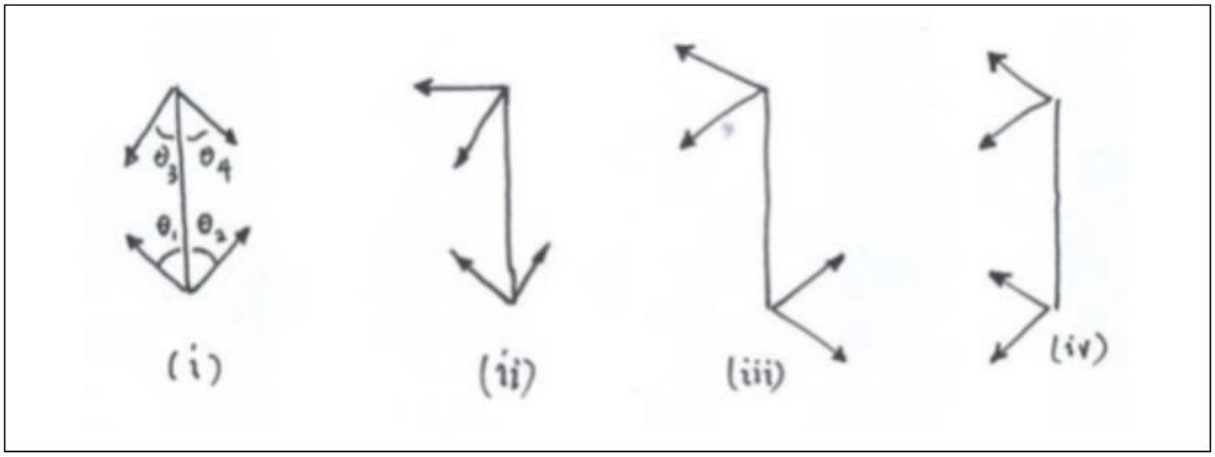

Figure 8: Possible contact situations (SeoulNationalUniversity, n.d.)

In Figure 8 the reference frame for each of these contact scenarios is the origin at the midpoint of the connecting line, with the y-axis following this line's direction. Scenario (i) has the connecting line lying inside both friction cones. Scenario (ii) has the connecting line lying inside only one friction cone. Scenario (iii) has the connecting line outside both friction cones and the friction cones are pointing towards opposite sides from the line of contact. Scenario (iv) has the connecting line outside both friction cones but with the cone pointing towards the same side from the line of contact.

Planar convex hull tests of each scenario show that only situation (i) is in force closure (SeoulNationalUniversity, n.d.). Θ is the angle that the connecting line makes with the outer edge of the friction cone and can be seen labelled in Scenario (i) of Figure 8.

$$\begin{bmatrix} -sin\theta_1 & sin\theta_2 & -sin\theta_3 & sin\theta_4 \\ cos\theta_1 & cos\theta_2 & -cos\theta_3 & -cos\theta_1 \\ -sin\theta_1 & sin\theta_2 & sin\theta_3 & -sin\theta_4 \end{bmatrix} \begin{bmatrix} x_1 \\ x_2 \\ x_3 \\ x_4 \end{bmatrix} = \begin{bmatrix} b_1 \\ b_2 \\ b_3 \end{bmatrix} \quad (8)$$

If for every $b_i \in R^3$, there exists $x_i \geq 0$ that satisfies the equation above, then the grasp is in force closure. The use of the convex hull test on the remaining scenarios shows that they are not force closure since the equation cannot be satisfied. Nguyen's theorem hence proves to be an important aspect to be considered when modelling robotic grasps and it greatly simplifies the task of evaluating whether a grasp will be in force closure. Nguyen's theorem does incorporate

Coulomb's friction cones because the line connecting the contact points must be within the friction cones at those points. However, it must be noted that Nguyen's theorem is generally still used in conjunction with Coulomb's friction law, i.e. a grasp must be in force closure and have frictional forces within friction cones for the object to be stably restrained without slipping.

There have been attempts to expand Nguyen's theorem for use in modelling force-closure grasps for a soft contact grasp of a planar object instead of just for hard point contact grasps. One study stated that for a polyhedral object with planar area contact of a two-fingered grasp, no slipping would occur if the line of force from each point in the area goes directly into the friction cone of the corresponding point of the other contact area (Caraza & Yun, 1991). This can be thought of as a set of contact points that form a set of friction cones. This theory has been used primarily for planar face contact grasping, such as palms grasping a polyhedral object which is why the angle of the friction cone with respect to the horizontal is the same for each point along the flat segment. Nguyen's theory has been modelled for point or planar contact grasps (Fakhari, Kao, & Keshmiri, 2019). When an object is instead curved, as it is for a sphere or cylinder or other non-polyhedral objects, the angle of the friction cone with respect to the horizontal will change depending on the position of the contact point. Ponce et al. (1993) expanded Nguyen's theorem to address the change in orientation of the cone for contacts on piecewise-smooth, curved objects. Their research also assumed that the contacts were hard point contacts with friction and this assumption was used to create an algorithm to compute force closure grasps for curved 2D objects. If the grasp were done by soft fingers with an area contact instead, the orientation of the set of friction cones would change within the contact area. There has been no specific research on how to compute whether a soft finger grasp is in force closure, as all previous research on it has assumed a point contact grasp.

Overall, an object being grasped by two or more fingers will be restrained successfully and without slip as long as Coulomb's and Nguyen's laws are met. In other words, an object will be grasped effectively if the frictional forces produced are within Coulomb's friction cone and there is a line connecting the points of each finger contact position that lies within the corresponding friction cones.

2.3 Extensions of stability theories

While the friction cone theory is used extensively in hard contact grasps, there have been a few iterations made of it that are used for soft grasp contact. Extending from the friction cone theorem used at a point contact, there has been a development of a friction limit surface for planar contact. A publication by A. Fakhari et al. in 2019 suggested that Coulomb's friction law for finger-contact was best used for point contacts since it dealt with the net forces involved in the grasp (Fakhari et al., 2019). The friction limit surface is a proposed way to extend the friction cone to a planar area contact since it incorporates the additional torque due to the contact area. It was originally used as a way to model the slipping between a planar surface and a rigid body. The limit surface is usually modelled with a set of ellipsoids but has also been modelled as polyhedral cones. The limit surface model depends on the shape of the contact area in question and thus, the pressure distribution within the contact area. This can be determined using contact models such as Hertzian's contact model.

As can be seen from the ellipsoid in Figure 9, it is merely an approximation of the friction cone that incorporates the additional torque that the soft finger can apply into it.

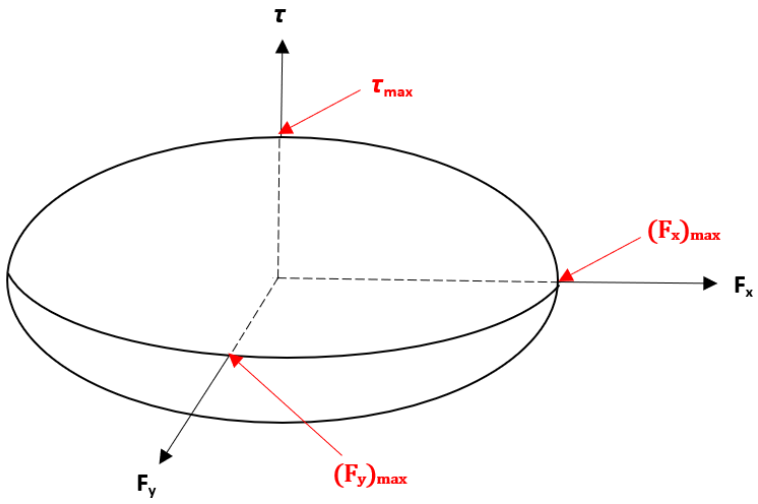

Figure 9: Friction limit surface

$$\frac{{F_x}^2}{{(F_t)_{max}}^2} + \frac{{F_y}^2}{{(F_t)_{max}}^2} + \frac{\tau^2}{{\tau_{max}}^2} = 1, \quad F_t = \sqrt{{F_x}^2 + {F_y}^2} \tag{9}$$

The friction limit surface can be defined as the set of all allowable frictional forces and torques before slipping may occur. The F_x and F_y forces are the frictional forces while the torque, $\boldsymbol{\tau}$, represents the torque produced about the direction of the applied normal force. The limit surface is computed by integrating the elliptic integrals using the pressure distribution for the materials in contact (Xydas & Kao, 1999). The friction limit surface is particularly useful for soft finger contact grasps since it contains the limitations of the applied torque in its surface while the friction cone does not.

It can be noted than when $\boldsymbol{\tau}$ is equal to zero, such as in the case of the hard finger grasp, both sides of the equation become identical and cancel each other. It is Coulomb's law that applies in this scenario with $\sqrt{{F_x}^2 + {F_y}^2} = \mu N$. This makes the shape a circle when $\boldsymbol{\tau}$ is equal to zero, hence the ellipsoid is just an approximation of the friction cone that is extended to include the torque. The friction limit surface is a simplified process of modelling Coulomb's friction laws. The major difference is that the friction limit surface does not visually include the effect of the normal force on the frictional forces and the moment. Instead, it is simply modelling the relationship between the frictional forces and the frictional moment for a given frictional interface. While this is certainly a useful relationship to have, it cannot be used as a visual representation of force closure like the friction cone can. Nguyen's theorem proves that a grasp is force closure if there is a line within the contact points' friction cones. This is because the cone is a direct visual representation of the relationship between the normal force applied and the maximum frictional forces allowed.

2.4 Types of contact models

While grasp models are used to assess an object's stability in a grasp, how the actual contact between the object and the fingers has been decided to be modelled greatly influences the grasp models. Finger contacts on an object are modelled three different ways, both in 2D and 3D. The first is a frictionless point contact, which is the simplest model that rarely occurs in practical scenarios. The frictionless contact consists of a single point contact in the direction normal to point on the surface as can be seen in the schematic in Figure 10. There is no frictional force acting between the object and the finger. This contact model is best used for situations with minimal friction forces or when there is an unknown friction force. It can be used to assure that the grasp is not dependent on the frictional forces when manipulating or restraining the object (Murray et al., 1994).

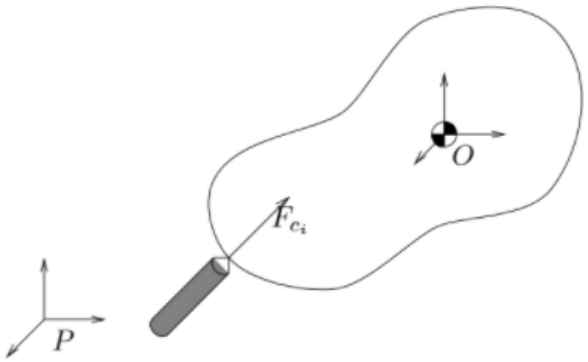

Figure 10: Frictionless point contact diagram (Murray et al., 1994)

The next type of contact model is the point contact with friction model, which can be seen on the left in Figure 11. This is also a point contact like in the frictionless contact model except it also encompasses the frictional forces. This is also known as a hard finger contact since hard fingers grasping a hard object contact each other at a point with friction. Lastly, there is the soft finger contact model. Soft finger contacts can deform around an object, therefore making the contact an area surface rather than a point. Like the previous contact model, this contact is still modelled as a point contact with applied normal force and frictional forces. To account for the fact that the contact would actually be an area contact instead of a point, it includes a torque that can be applied about the applied normal force (Murray et al., 1994). This model can be seen on the right

in Figure 11. The soft fingers ability to apply torque arises for the contact being an area rather than a point.

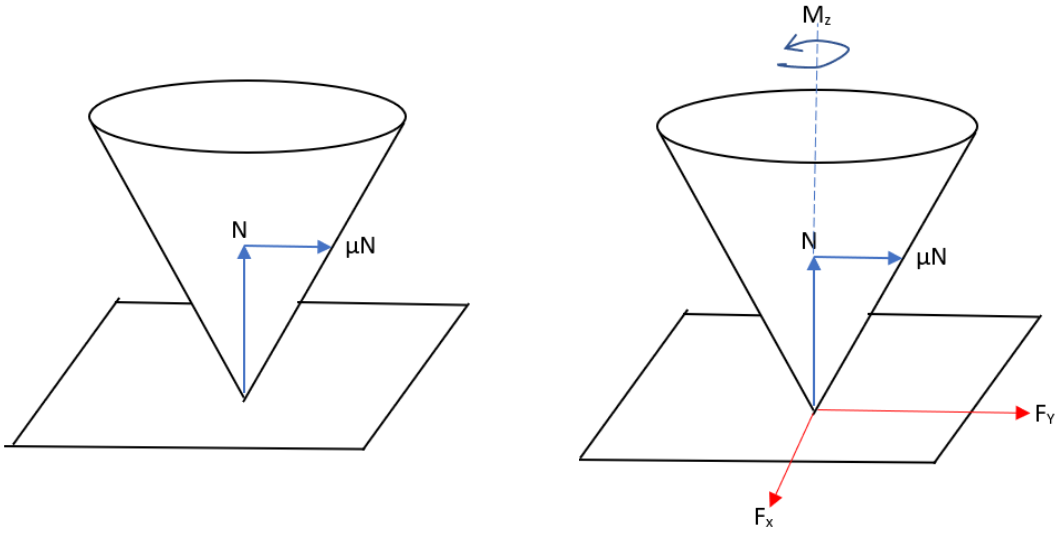

Figure 11: Schematics of the friction cone for hard contact with friction (left) and soft contact (right)

The most appropriate contact model to use when modelling a grasp ultimately depends on the material properties of the object and fingers in the grasping situation and how they interact with each other.

2.5 Contact model matrix operations

The different contact models are often represented with mathematical matrices. Since the main types of contact realistically used in robot grasping are hard frictional contact and soft contact, these two contact models will be explored in this section.

The set of contact forces that are allowable by an applied contact is modelled by:

$$F_{c_i} = B_i f_{c_i}, \quad f_{c_i} \epsilon FC_{c_i} \tag{10}$$

where B_i is the force/torque basis, f_{ci} is the matrix of applied forces at the contact point that must be an element of the friction cone. The basis for the force and torques, otherwise known as the wrench basis, differs depending on the type of contact model in use.

The matrix of the applied forces, f_{c_i}, is displayed as a single column matrix with the first three rows representing the forces in each direction and the last three rows representing the torque about each direction. This can be seen in equation 11. The direction of the x, y and z axes is determined as the coordinate axis at the contact point.

$$f_{c_i} = \begin{bmatrix} f_x \\ f_y \\ f_z \\ \tau_x \\ \tau_y \\ \tau_z \end{bmatrix} \tag{11}$$

Using the wrench basis for point contact with friction in equation 12 is as follows (Murray et al., 1994):

$$F_{c_i} = \begin{bmatrix} 1 & 0 & 0 \\ 0 & 1 & 0 \\ 0 & 0 & 1 \\ 0 & 0 & 0 \\ 0 & 0 & 0 \\ 0 & 0 & 0 \end{bmatrix} f_{c_i}, \qquad f_{c_i} \in FC_{c_i} \tag{12}$$

Each column indicates the number of forces or torques being applied. There are only three columns because a point contact with friction does not apply any torque. Hence the last three rows of the f_{c_i} contain zeroes. The unit digits in the wrench basis represent a potential force in each direction of the coordinate axis. There is no column to indicate that any torque is produced.

$$F_{c_i} = \begin{bmatrix} 1 & 0 & 0 & 0 \\ 0 & 1 & 0 & 0 \\ 0 & 0 & 1 & 0 \\ 0 & 0 & 0 & 0 \\ 0 & 0 & 0 & 0 \\ 0 & 0 & 0 & 1 \end{bmatrix} f_{c_i}, \qquad f_{c_i} \in FC_{c_i} \tag{13}$$

Equation 13 contains the wrench basis for soft finger contact wrenches. There is an extra column to represent the torque that is produced about the normal force. The direction normal to the

surface is usually denoted as the z-axis and this is why the additional column shows the applied torque being about the z-axis, which is shown by the last row in the wrench basis. A summary of the wrench bases can be seen in Table 1.

Table 1: Wrench basis and slipping rules for different contact types (Murray et al., 1994)

Contact type	Picture	Wrench basis	FC
Frictionless point contact		$\begin{bmatrix}0\\0\\1\\0\\0\\0\end{bmatrix}$	$f_1 \geq 0$
Point contact with friction		$\begin{bmatrix}1&0&0\\0&1&0\\0&0&1\\0&0&0\\0&0&0\\0&0&0\end{bmatrix}$	$\sqrt{f_1^2+f_2^2} \leq \mu f_3$ $f_3 \geq 0$
Soft-finger		$\begin{bmatrix}1&0&0&0\\0&1&0&0\\0&0&1&0\\0&0&0&0\\0&0&0&0\\0&0&0&1\end{bmatrix}$	$\sqrt{f_1^2+f_2^2} \leq \mu f_3$ $f_3 \geq 0$ $\lvert f_4 \rvert \leq \gamma f_3$

The wrench basis and the subsequent matrices operations simplify the use of the contact models and ensure a grasp is in force closure and not slipping. Confirming whether a grasp is force-closure or not can be done using matrix operations for point contacts due to their simplicity. For a point contact without friction, there are numerous ways to tell if the grasp is force closure. Let $G \in R^{p \times m}$ be the grasp matrix of this particular grasp and $\{G_i\}$ be the columns of the grasp matrix (Murray et al., 1994). Then, the grasp is considered force closure if:

- The columns of G positively span R^p
- The convex hull of $\{G_i\}$ contains a neighbourhood of the origin
- There is no vector $v \in R^p$ that is unequal to 0 that for i = 1,…..,k, $v.G_i \geq 0$

The previous statements are equivalent and can be checked using various matrices operations. These methods of determining force closure can be extended for point contact grasps with friction and soft finger spatial contact, although the calculations can become more complicated.

Nguyen's theorem is a simpler way to confirm that a grasp is force closure and is based on the convex hull test.

The wrench basis simplification of the contact models is an effective way of determining whether a grasp is force closure, but it is also widely used to calculate the unknown forces or torques required for equilibrium. This is done using a grasp map, which essentially maps the contact forces exerted on the object to the object wrench through the centre of mass. Refer to Appendix 1 and Appendix 2 to see the matrix operations for the equilibrium analysis of a point contact with friction grasp and a soft finger grasp of a cylinder in various positions.

2.6 Contact deformation models

Even though the three contact models are modelled at points, the soft contact grasp would actually have a contact area rather than a point due to the deformation of the soft finger around the object. This interaction of the grasping fingers with the object in grasp is significant in grasp modelling. Different materials and loading scenarios can influence the contact area, applied torques and forces, and pressure distribution. These factors ultimately affect the effectiveness of a grasp. There is a range of contact deformation models that are used when there is deformation of the fingertip in the grasp. One of the earliest and most widely used is the Hertzian contact theory.

Hertzian's theory assumes that the deformed material has linear elastic behaviour and that the contact is frictionless. Hertzian completed his initial research by examining the effects of the contact of a soft linear-elastic hemisphere with a hard material. The theory links the normal force between the objects, N, and the radius of the contact area, a, as outlined in the equation below.

$$a \propto N^{\frac{1}{3}} \tag{14}$$

From this basic theory, a set of equations for the contact between various shapes has been developed and can predict the pressure distribution throughout the contact. An example is two spheres in contact. They will have a circular area of contact and the maximum pressure will be

occurring at the centre of this area. The maximum pressure can be calculated using the applied force, F, and the radius of the contact area, a:

$$P_{max} = \frac{3F}{2\pi a^2} \tag{15}$$

The pressure distribution away from this maximum pressure centre follows a semi-elliptic pattern (Zhu, 2012). Knowing the contact area of a grasp is very useful because once it is known, it can be used to predict other important factors such as applied forces, pressure distribution and torque capabilities. This may need to be utilised instead of direct measurement devices such as force sensors for when theoretically modelling a design before physical prototyping. The ability to predict the torque that can be applied in a grasp is necessary for modelling whether slipping will occur in a grasp as there is a maximum value of torque that can be applied for a given applied normal force.

The main limitation of Hertzian's theory is that it is not as accurate for large inelastic deformations (Fakhari, Keshmiri, Kao, & Hadian Jazi, 2016). Other limiting factors of Hertzian's theory are that the bodies in contact must be elastic, there must be no rigid body movement, and the area of contact between the two bodies must be significantly smaller than the dimensions of the bodies themselves (Hongyan, Ran, & Ligang, 2016). There has been further research done that focuses on expanding Hertzian's theory for a greater range of contact scenarios.

In their research in 1999, Xydas and Kao investigated how the Hertzian contact deformation model could be extended for use for non-linear elastic materials (Xydas & Kao, 1999). Since materials for robotic fingers are often non-linear elastic materials such as silicon rubber, research such as this is useful for the grasping industry. However, expansions of the original Hertzian theory mean that more work and experimentation needs to be done to verify the new constants that would need to be in use. For smaller amounts of deformation, the original Hertzian theory is often still used as a predictor of the contact characteristics.

Another major contact deformation theory is the Winkler foundation theory. This theory is used extensively in civil engineering. The basis of the theory is that the restoring force, q, of an elastic beam is directly proportional to its deflection, w (Dillard, 2018)

$$q = kw \tag{16}$$

The Winkler theory essentially likens the elastic foundation of the robotic fingers to a group of springs of spring constant, k, (Naeini, Ziaie moayed, & Allahyari, 2014) and this is shown in Figure 12. This theory has been applied to a wide range of scenarios to estimate the applied force or the deformation of the grasping fingers, including the use of nonlinear elastic objects that Hertzian theory cannot always apply to.

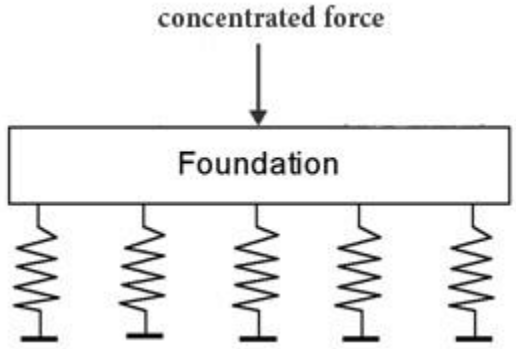

Figure 12: Winkler foundation theory (Naeini, Ziaie moayed & Allahyari, 2014)

Although the Winkler foundation model can be used for a wider range of materials than the Hertzian model, there are some limitations to the model. A limitation of the Winkler theory is that it suggests the deformation of the body is limited to the areas where the load is applied. In actual fact, this is not the case due to the foundation being a continuous object. Another limitation is that the k constant equivalent of the spring model of the elastic foundation being used can be quite difficult to represent accurately. This makes an otherwise simple model complicated to use (Chandra, 2014). In the case of representing the contact deformations and forces in the robotic hand grasp, the Hertzian theory provides an easier-to-use model than Winkler, although the range of materials it can be applied to is more limited.

2.7 Measuring frictional forces and coefficients

For robotic grasping, a reason slipping occurs is because the frictional forces in the grasp exceed the limits of the friction cone. This is why it is necessary to estimate the frictional forces in a grasp accurately. Friction is a complex topic that is still being researched today. Currently, the two main reasons for friction can be summarised as either mechanical or chemical. Mechanically, it is the collision of the two surfaces on a molecular level that causes the energy dissipation that results in frictional forces. Chemically, it is the adhesion between the two surfaces that causes the frictional forces (Kim & Kim, 2009).

Applied forces can be directly measured using devices such as a spring force meter or an electronic force sensor. Frictional forces on an object in a grasp arise due to unbalanced forces that would result in the object not being in equilibrium. Static friction forces can be found by using a free-body-force-diagram and making the friction forces equal and opposite to the forces causing the potential motion.

While having a proven friction law such as Coulomb's is a milestone in friction theory, it needs to be implemented in practical applications for it to be useful. To reiterate, Coulomb's law shows that if the frictional forces in a grasp exceed the limits of the friction cone then slipping will occur. To use this theory to determine if an object will slip, one must first identify the coefficient of friction that defines the friction cone. The coefficient of static friction is the ratio of the normal force applied on the object to the frictional force that opposes any accelerating motion (i.e. slipping) between the objects (Younis, 2010). If slipping were to begin, then there would be a new frictional coefficient to be used, known as the coefficient of kinetic friction.

The coefficient of static friction between two objects is entirely dependent on the materials in contact and their interaction. It does not depend on weight, contact area, forces, or any other variable. This is why measuring the coefficient of static friction can be done quite simply. The coefficient values for many common materials can be found in tables such as Table 2.

Table 2: Example table of frictional coefficients with differing surface conditions (EngineeringToolBox, 2004)

Materials and Material Combinations		Surface Conditions	Frictional Coefficient	
			Static - μ_{static} -	Kinetic (sliding) - $\mu_{sliding}$ -
Aluminum	Aluminum	Clean and Dry	1.05 - 1.35	1.4
Aluminum	Aluminum	Lubricated and Greasy	0.3	
Aluminum-bronze	Steel	Clean and Dry	0.45	
Aluminum	Mild Steel	Clean and Dry	0.61	0.47
Aluminum	Snow	Wet 0°C	0.4	
Aluminum	Snow	Dry 0°C	0.35	
Brake material[2)]	Cast iron	Clean and Dry	0.4	
Brake material[2)]	Cast iron (wet)	Clean and Dry	0.2	
Brass	Steel	Clean and Dry	0.51	0.44
Brass	Steel	Lubricated and Greasy	0.19	
Brass	Steel	Castor oil	0.11	
Brass	Cast Iron	Clean and Dry		0.3
Brass	Ice	Clean 0°C		0.02
Brass	Ice	Clean -80°C		0.15
Brick	Wood	Clean and Dry	0.6	

It is important to note that there are a few conditions other than the material itself than can impact the coefficient of static friction. As seen in the third column of Table 2, the conditions of the material's surface can greatly impact the coefficient of frictions, both static and kinetic. These conditions include any irregularities in its surface like bumps that could lead to an increase in friction produced and the lubrication of the surface since lubrication acts like another medium between the materials and needs to be accounted for.

The coefficient of static friction does not depend on the weight or contact area, as shown by Coulomb (Popov, 2010). Taking a rectangular prism with a square cross-section like the one in Figure 13, for example, when the largest side, A, is placed on another material, the prism's weight acts as the normal force acting over this area. When the smaller cross-section, B, is placed on the same material instead, the force per unit area would be greater, but the total net force downward would be the same as in the first scenario. Thus, the net friction force that is allowable would be the same for both scenarios. This shows how the contact area between materials does not influence the coefficient of static friction, instead the overall net force does.

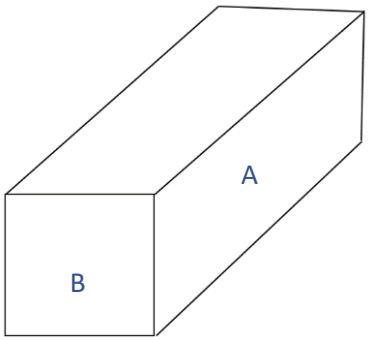

Figure 13: A rectangular prism for reference

The coefficient of static friction is used to describe the Coulomb friction cone, and this can be used to model when slipping occurs in a grasp. If the friction force for a specific applied normal force lies outside the friction cone, slipping will occur. This means that, for an object in grasp, the normal force applied must be measured to determine if the friction force that will keep the object in equilibrium is within the friction cone. Friction is a complicated subject and, while it is known that the allowable frictional forces are proportional to the applied normal force, the actual relationship varies depending on the materials in contact. The idea that friction force is equal to μN is a common over-simplification used in the discussion of friction. In reality, it is only when an object is about to slip that the friction force is equal to μN. After the object slips, the static friction force becomes kinetic friction.

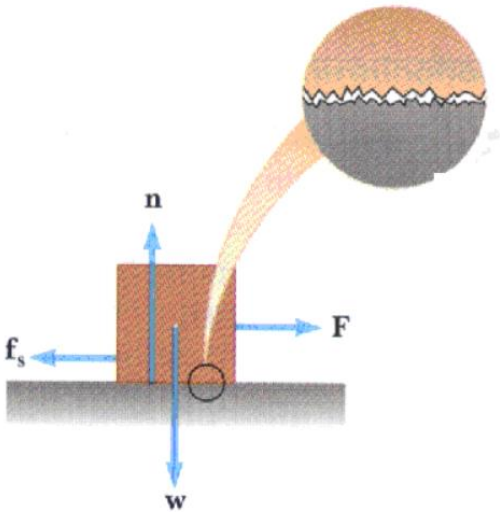

Figure 14: Schematic of block being pushed by force, F (Davis, 2002)

As can be seen from Figure 14, a block of weight, w, has a normal force, n. When F force is applied to attempt to initiate the block moving, the friction force f_s tries to oppose this. As F increases, it will eventually overcome the allowable friction force, fs, and then slipping will occur as the block slides over the surface (Davis, 2002). Since static friction is a force that is meant to respond to and oppose any motion, it also increases as F increases in an equal and opposite manner. This would continue until the frictional force reaches its maximum value of μN and then slipping would occur.

If one were to use the Coulomb friction model to predict at what force, F, slipping were to occur for an object of a given weight, w, one would have to consider the normal force due to the weight and calculate μN. This would be equal to the maximum friction force between the block and the surface that could be applied for the given normal force before sliding would start. It is important to note that the Coulomb model shows that objects with a higher normal force can exert higher frictional forces until sliding due to the maximum frictional force being proportional to the normal force.

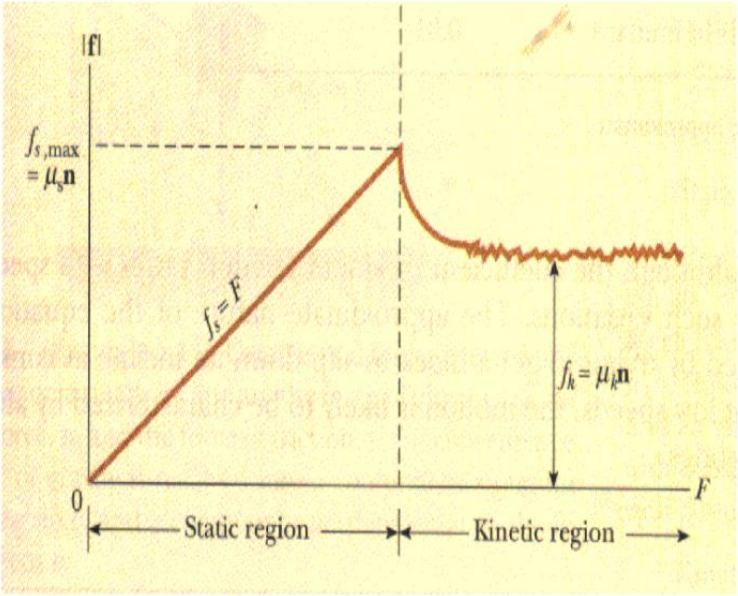

Figure 15: Graph of relationship between push force and friction force (Davis, 2002)

Figure 15 is a visual representation of the relationship between friction, f_s, and the push force on the block, F, and how f_s increases as F increases until it reaches μN and slips. Once slipping begins in the kinetic region, the friction decreases. The larger the normal force acting on the block is, the larger the maximum allowable frictional force would be, and thus, it would take more force to overcome this friction force to cause the block to move.

The modelling of the situation shown in Figure 14 is very simple using the Coulomb friction law, assuming Nguyen's theorem is met. If one recalls, slipping occurs if either Coulomb friction law or Nguyen's theorem are not met. Since the weight force is in the same but opposite direction to

the normal force, it makes the frictional force perpendicular to the weight force. Thus, it is straightforward to calculate the maximum force the object can take before slipping since there are no complicated angles involved.

Grasping is one situation where frictional forces are used to restrain an object and keep it from slipping out. There are more complicated grasping scenarios, such as the one in Figure 16 where two fingers are used to keep the object in equilibrium. The normal force applied has a component that adds to the downward weight force of the object. This means that the vertical component of the frictional force is the only force keeping the object in equilibrium.

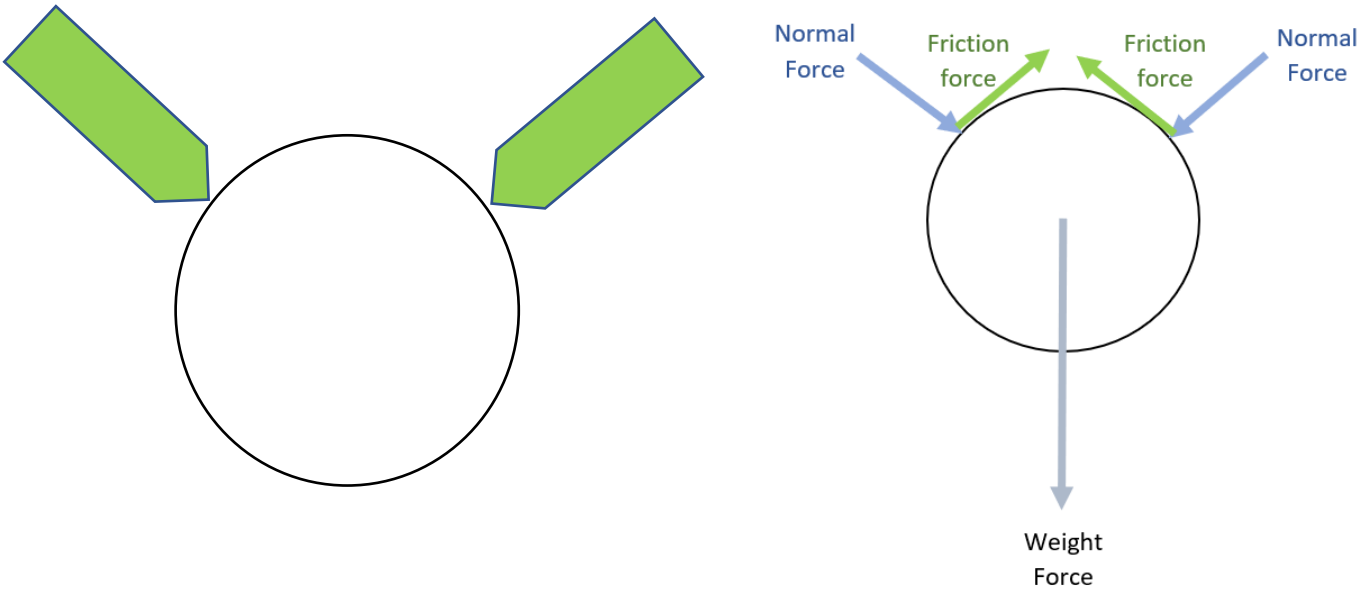

Figure 16: (Left) A two-finger grasping scenario (Right) The force diagram of the scenario

This is an interesting scenario because, since the normal force contributes to the weight force, more friction is required to offset both the weight force and the downward component of the normal force. The higher the point of contact of the fingers along the object's circumference, the smaller the component of the friction force is that offsets the weight force is and hence, the friction force will need to increase accordingly. This may require the normal force to increase to avoid slipping.

2.8 Hard vs Soft Finger

There is plenty of research that is being done to improve and eventually perfect the grasping of a variety of objects in the robotic grasping industry. As mentioned previously, an ideal grasp is one that is stable in equilibrium and force-closure.

The hardness of a finger that is being used to grasp an object contributes to the effectiveness of a grasp. A material's hardness can be defined as the ability of a material to resist deformation (Chen, Niu, Li, & Li, 2011). Softer and more compliant materials have been used mainly for robotic grasping and manipulation. This is because softer fingers result in deformation around an object and can apply a larger amount of allowable frictional forces and moments to withstand any external disturbances before slipping occurs (Khurshid et al., 2011). In particular, the moment that the soft finger can apply is what makes the soft finger grasp preferable over the hard finger grasp. If there are any external moments on the object in grasp, the soft finger may be able to balance this by applying a moment while the hard finger cannot since it is simply a point contact. The human finger is a testimony to this, with its soft material around the bone.

Although it is widely known that soft fingers provide better grasping and manipulation capabilities than hard fingers, their grasps are modelled quite similarly. In the most commonly used models, hard finger and soft finger contacts are modelled as a point contact with forces in two or three dimensions. The only difference in the models is that the soft finger has the additional torque applied about the applied normal force. The point models make modelling the contacts very simple and it is easy to work with in research. However, it does beg the question of whether it portrays the soft finger contact accurately enough to show that it is superior in most grasping situations to the hard finger.

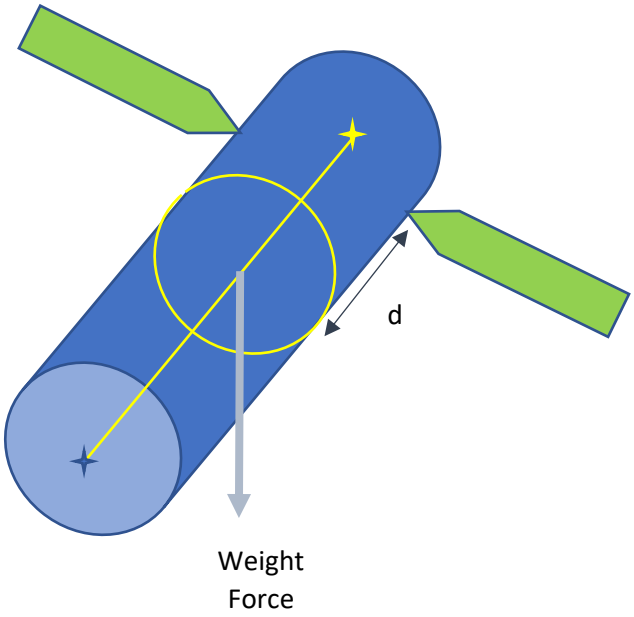

Figure 17: Two-fingered grasp away from the centre of mass

An example of such a scenario would be of two soft fingers holding a cylinder. The setup shown in Figure 17 has the two soft fingers grasping the cylinder at a distance away from the centre of mass. The grasp here can only be force closure with no slipping if the fingers are soft. The hard fingers will not be able to hold it because they cannot provide a moment to counteract the moment produced from the cylinder's weight being the distance, d, from the finger placement. Matrix operations demonstrating this can be found in Appendix 1. In the setup shown in Figure 18, both hard and soft fingers would be able to grasp the object stably since no external moments are acting on the object, as the fingers are placed precisely in the line of the centre of mass of the cylinder. Matrix operations demonstrating this can be found in Appendix 2. The moment applied from the soft fingers is zero since the positioning at the centre of mass means that there are no external moments to oppose. Since the classic point models are used, and both the hard and soft fingers are not applying any moment, the grasps are modelled as identical. However, the soft fingers would still be a better choice for grasping than the hard fingers since it would have an area contact rather than a point contact. This introduces a limitation of the point-contact model in modelling soft fingers since it asks the question of how accurate the point-contact

model is for area contact model since one cannot distinguish between the effectiveness of the two in certain situations.

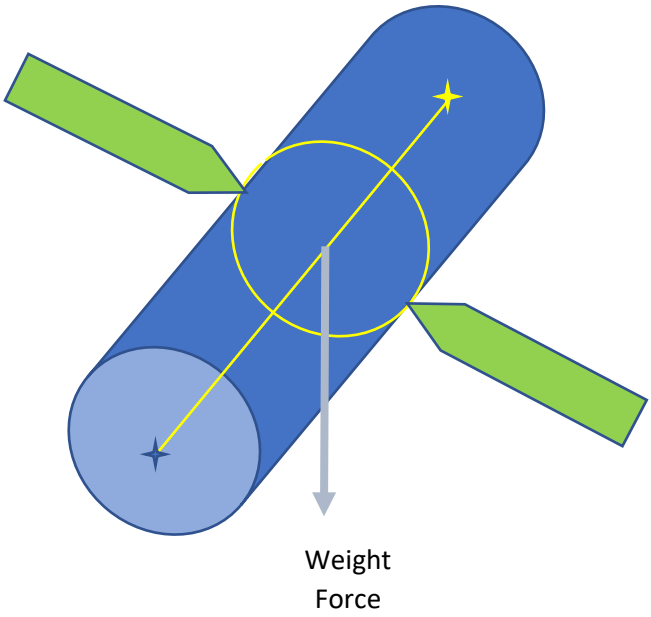

Figure 18: Two-fingered gasp positioned at the centre of mass

2.9 Limitations of current models

Since the applications of the robotic grippers has now been explored, it is clear now why the modelling has to be done well to ensure that all the money and effort put into the robot gripper is worth the design. There are currently a few limitations of the popular models used for gripping in the robotic industries to ensure that the grasp is force-closure and not slipping. It should be noted that most models do have assumptions that could be seen as limitations since it cannot be applied to every scenario. However, it is almost impossible for any complex model not to have any assumptions. So, while the limitations may be pointed out for some of the models, these are still valid models for the applicable situations and many times may have been altered for improvement in specific scenarios.

Let us focus on the major models used in the robotic grasping industry. Firstly, Newton's first law of motion is a basic theory useful for modelling the grasp of an object, as there needs to be balanced forces and moments along each axis. This theory is one of the primary ideas in grasp modelling and an object being in equilibrium is a criterion for a force closure grasp.

Next is Coulomb's friction law. As long as the Coulomb's coefficient of static friction is constant, then Coulomb's friction law will work to model robotic grasp. However, in reality, the surface of objects used in the agricultural or other major industries would have a varied coefficient of static friction. It is likely the surface of the objects is not perfectly uniform and any irregularities will result in fluctuations of the coefficient of friction (Naboulsi & Nicholas, 2003). This means the experiment results or tabular data of the coefficient of static friction for materials in perfect condition may not represent the entire surface of the object. But Coulomb's friction law is still widely used for many applications. Other than possible discrepancies with the coefficient of static friction, it is simple because it is only influenced by two variables: the coefficient of static friction and the normal force. This is why it is still heralded as the main model for modelling slippage. It can still be accurate for an object with an irregular surface as long as the variation in the coefficient of static friction is accounted for in the model. Another limitation of Coulomb's friction cone is that it assumes the contact can be modelled from a point. This can be inaccurate when used for modelling slipping of a soft-fingered grasp with non-planar surface contact. The coefficient of static friction that makes up the friction cone does not depend on the contact area. However, the friction cones' orientation will change over a non-planar surface. Even when the area happens to be curved and unsymmetrical, Coulomb's friction cone is still being modelled as occurring at the middle point of the curve and the friction cone is orientated around that point. This does not account for the fact that the force distribution over the contact area would change the orientation of the cones at the points making up the surface.

This leads us to the next theory that is used in conjunction with Coulomb's friction law, Nguyen's theorem. Nguyen's theorem was derived from the use of hard finger examples and is widely used for these types of grasps in the robotics industry. Nonetheless, it has not been used as extensively to model soft finger contacts since it is a positional theory revolving around the assumption of a point contact. Nguyen attempted to expand his theorem to fingers that had a planar area contact

on objects. But what about non-planar contact areas? And is this expansion actually useable in a practical situation? There are many questions to be asked as to whether the current use of Nguyen's theorem with a point contact model is an accurate representation of a soft finger contact is.

Obviously, the positioning of fingers is important when making a force closure grasp and that there would be a wider range of options for position placement of soft fingers than hard fingers because soft fingers can produce an additional moment. But the question is whether Coulomb's friction law and Nguyen's theorem can be expanded to better account for the superior qualities of soft fingers grasping an object.

3 Research Approach

The objective of this research is to determine whether two of the current major grasp stability theorems, Nguyen's theorem and Coulomb's friction cone law, can be applied for a soft finger grasp of non-planar objects to effectively show the difference between hard and soft finger grasps.

As outlined in the review in section 2.9, both major grasp theorems have a limitation in that they model the contact between the grasping fingers and an object as a point. In actuality, soft fingers have a contact area not a point when grasping an object. To compensate for not including the contact area in the modelling of soft fingers, they are currently modelled as having a moment about the normal as well as the friction cone about the centre point. Hard fingers are simply modelled as having a friction cone at the point contact without a moment. This difference alone is meant to showcase how soft fingers have superior capabilities to hard fingers.

The idea for this research originally came from thoughts about the grasping of a cylinder as was outlined previously and seen in Figures 17 and 18. When the hard and soft fingers are grasping the cylinder through the centre of mass, the moment exerted by the soft fingers is the same as that of the hard fingers, 0 Nm. Thus, both soft and hard fingers are modelled identically in this situation as a point contact with a friction cone. Using Nguyen's and Coulomb's theorems in this scenario would show both soft and hard fingers with identical coefficients of static friction to be force closure in the same positions and slipping to occur in the same positions. It is hypothesised that a soft finger grasp would have a greater number of positions of force closure than a hard finger grasp due to its ability to form a more stable grasp. This exposes the potential for an expansion of Nguyen's and Coulomb's theorems when the grasp has a contact area rather than a point contact.

While Nguyen's theorem has been derived effectively for hard finger point contacts, it has not been safely expanded for use of soft fingers grasping an object with non-planar surfaces. Likewise, Coulomb's theorem has possible limitations for soft fingers grasping an object with a non-planar contact area. One might have doubts when using these current theories with a point-

contact model for soft fingers because soft finger contact is an area. Thus, the position of the fingers grasping the object is not limited to a single point. This does beg the question of whether the continued use of the point contact with Nguyen's theorem and Coulomb's law is acceptable when modelling the stability of a grasp using soft fingers.

An approach to highlight the difference in grasping between soft and hard fingers in this scenario is to think of an area contact as being made up by a set of points instead of a single point contact in its centre. Each contact point has an associated friction cone, and this makes up the 'set-of-cones', a term that will be used frequently in the remainder of this thesis.

4 Model

To expand Nguyen's and Coulomb's theorems to incorporate the contact area of a soft-fingered grasp, the set-of-cones idea will be applied to a grasping scenario of a two soft-fingered grasp of a cylinder through its centre of mass. To make a model of this situation as simple as possible, it will be modelled in two dimensions (2D) because of the assumption of the fingers' position always being in the middle of the longitudinal axis of the cylinder. If the surface area of contact between the fingertip and the cylinder were to be considered in a 2D model, it would be seen as an arc. In actuality, if a finger with a hemispherical tip was to contact the round side of a cylinder, the contact area would be in the shape of a circle when flattened. Using the set-of-cones model, the points that make up the arc have a friction cone associated with each point, ultimately forming a set of friction cones along the arc. This makes the cones of the points at the end of each arc the most important to look at as is seen in Figure 19, a simplified visualisation of the set-of-cones model. Figure 19 shows a set of cones at three points of the contact arc; the bottom point, the centre-point, and the top point. The set-of-cones would include a cone at every point about the contact arc length but the most important cones for this scenario are shown in Figure 19.

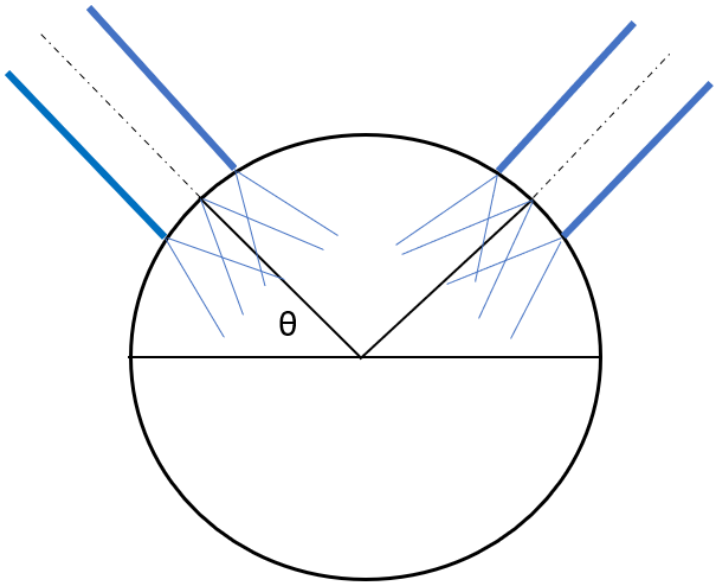

Figure 19: Schematic of the set-of-cones idea with a focus on the centre, top and bottom-most points in the arc

The set-of-cones idea can be modelled as a resultant friction cone for the grasping scenario presented in this research. The effects of using the resultant friction cone model with Coulomb's slipping law is outlined in section 4.1, while its impact on Nguyen's theorem is outlined in section 4.2.

4.1 Using the resultant cone model in Coulomb's friction law

The use of the set-of-cones in the contact area in a soft-fingered grasp expands Coulomb's friction cone at the centre point of the arc. On an arc segment of a 2D cylinder, there is a friction cone at each point along the arc. These friction cones can be encompassed by one larger resultant friction cone for simplicity. Since the arc is not straight, the friction cones' orientation with respect to the horizontal change along the arc. This can be seen in Figure 20 where the half-angle of the resultant extended friction cone, ϕ, is less than the half-angle of the individual friction cone, α, due to the change in the orientation of the cones with respect to the centre of curvature.

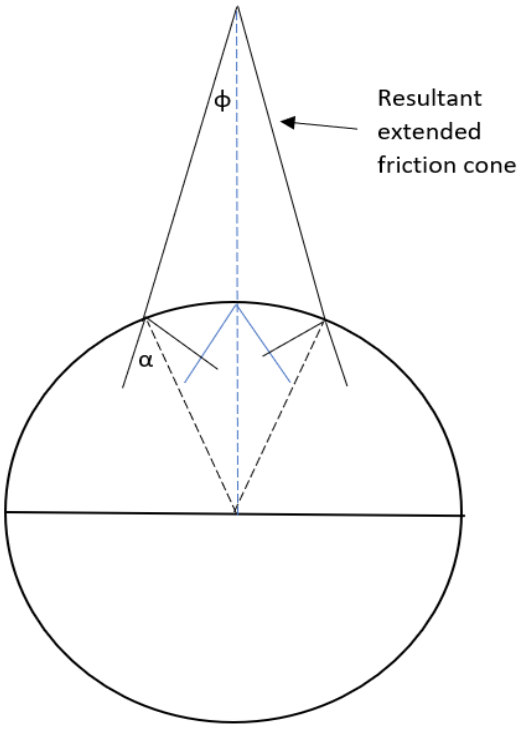

Figure 20: Diagram of Extended Friction cone

The outer limits of the cones at the extreme points make a truncated cone along the arc. This can be extended beyond the contact arc to create one large cone known as the resultant friction cone. Due to the curved surface, the half-angle of the extended cone is less than the angle of the friction cone at an individual point. Coulomb's friction cone equation, $\tan\alpha = \mu$, still only applies for the original friction cones at the points along the arc but the resultant friction cone is a way of geometrically showing how the connecting line between the cones at the contact point would have a significantly larger region to enter into when the resultant friction cone is used as opposed to the single Coulomb friction cone.

The validity of the resultant cone model's use would be done through the analysis of the resultant forces. In the resultant cone model, the resultant force would theoretically be shown as starting at the friction cone's original point. As long as the resultant force lies within the resultant friction cone, then Coulomb's law would not be broken.

It is important to note that Coulomb's original friction cone is valid for many situations and, unless proven wrong, is still valid for estimating slipping for curved objects. When a finger or any object is pressed flat against a flat planar surface, there is a distribution of pressure along the contact line that is normal to the surfaces in contact. Using the set-of-cones idea in this situation means there is a friction cone at each point in the contact line from a 2D perspective. Since the contact line is a straight line, the angle making up the friction cones with respect to the direction of the applied pressure is the same throughout. A depiction of this can be seen in Figure 21.

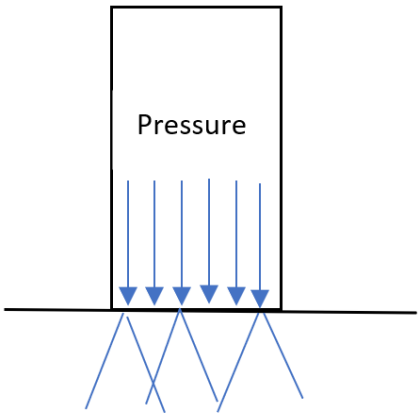

Figure 21: Pressure applied from an object to a flat surface

Usually, Coulomb's friction cone would be modelled as a single cone from the centre of the contact line. If the set-of-cones were to become a resultant cone, the resultant cone would also have the same angle as the single friction cone at the centre point. This is illustrated in Figure 22. The red cone depicts the standard Coulomb friction cone at a point, while the blue cone depicts the resultant friction cone. The cones are identical, so the limitations of the frictional forces have not changed because of the use of the resultant cone in this case. It would be the same to use the usual method of the Coulomb friction cone at the point using the net forces.

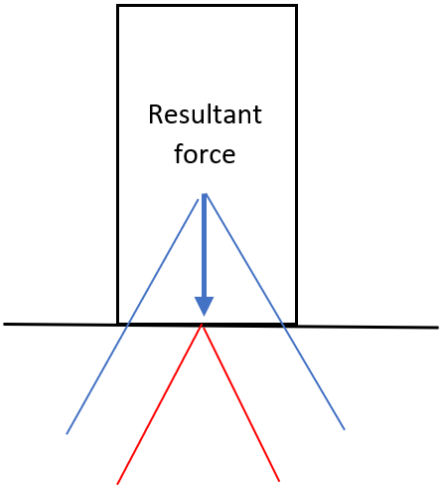

Figure 22: Schematics showing the similarities of the Resultant friction cone and Coulomb's friction cone for a planar contact

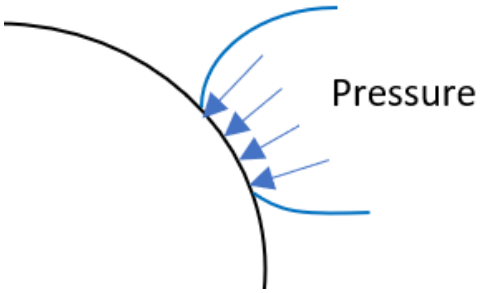

Figure 23: Pressure along the contact arc

The forces due to pressure applied when a contact line is curved results in the friction cones at the points of the contact arc having different orientations with respect to the normal force at the centre point of the arc, as can be seen from Figure 23. If the pressure distribution is symmetrical, as it is for two spheres in contact, the resultant force will act through the centre point. This

resultant force arises because of the distribution of the normal forces due to pressure along the contact arc length. The resultant normal force applied, $\vec{N}$, is the sum of the individual normal forces due to the pressure along the contact arc. Likewise, the resultant friction force, $\vec{f}$, from the contact is the sum of the individual frictional forces at each point.

$$\vec{N} = \sum \vec{N_i} \tag{17}$$

$$\vec{f} = \sum \vec{f_i} \tag{18}$$

Thus, it is hypothesised that every point in the arc must be considered and the limitations of the overall friction cone should consider the limitations of the friction cones at every point that contributes towards the resultant force. The resultant cone a way of modelling this for the grasping scenario used in this research. If the resultant cone model is shown to be valid, this extends to the use in Nguyen's theorem, where there is a larger amount of positions where the fingers can grasp the cylinder and be in force closure.

4.2 Using the resultant cone model with Nguyen's theorem

As has been previously mentioned in the literature review, an object is successfully restrained if Nguyen's theorem and Coulomb's theorem are both met. Nguyen's theorem focuses on the geometry of the fingers' positioning when grasping an object rather than the actual forces. In the scenario of the symmetrical two-fingered grasp of a cylinder (as previously shown in Figure 19), Nguyen's theorem can be used to predict the maximum angle of contact before the grasp is no longer in force closure, an important condition for a stable grasp.

Currently, Nguyen's theorem is assessed based on the use of a point contact at the centre of the contact arc. This is shown in Figure 24, where the maximum angle of the centre position before the grasp is no longer force closure can be identified. When it comes to curved surfaces, the direction of the normal force changes as the angle of contact, θ, increases. In fact, the normal

force direction would gradually point downwards as the angle increases past the mid-plane of the uniformly curved object.

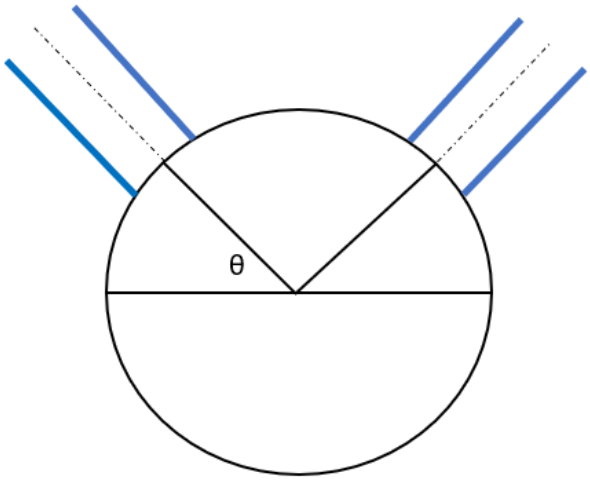

Figure 24: Centre Point contact schematic

As can be seen from Figure 25, the alternate angle rule shows that θ and α, the angle of the friction cone, are equal when the fingers are positioned for the maximum angle before slipping. Thus, the theoretical maximum angle of a force closure grasp based on the centre point contact idea is:

$$\theta_{max} = tan^{-1}\mu \tag{19}$$

$$Since \ \propto = tan^{-1}\mu \tag{20}$$

Where μ is the coefficient of static friction, θ_{max} is the maximum angle of contact and α is the half-angle making up the friction cone. This is a simple model that only depends on the coefficient of static friction of the objects in contact. An equilibrium analysis of the scenario completed through matrix operations can be found in Appendix 3.

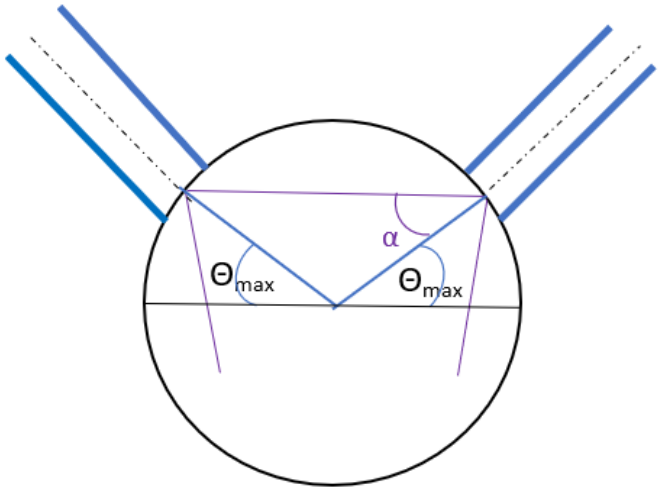

Figure 25: Maximum angle before the grasp is no longer in force closure calculations

When expanding the centre-point contact model to the resultant cone model for use in Nguyen's theorem, the most important points to look at are the top and bottom points in the arc. This is because these form the outer limits of the resultant cone. Depending on the orientation of the grasp, the friction cones corresponding to the top or bottom point of the arc will be the last friction cones to have a line connecting to the top/bottom point of the second contact arc. Thus, whether a certain grasp meets Nguyen's condition and is in force closure is dictated by the friction cones at the outer points.

In the particular two-fingered grasp scenario being analysed in this research, the friction cone corresponding to the top point in the contact arc is the first to break Nguyen's condition when increasing the angle of contact above the horizontal. This is because the two fingers are being placed above the horizontal mid-line of the cylinder. Hence, the friction cones begin to orientate downwards increasingly as the angle of contact increases. The friction cones of the top points in the grasp are the first not to have a line connecting their corresponding friction cones as the angle of contact above the horizontal increases. Figure 26 shows the maximum angle before Nguyen's theorem is no longer being met for the top point of the contact arc.

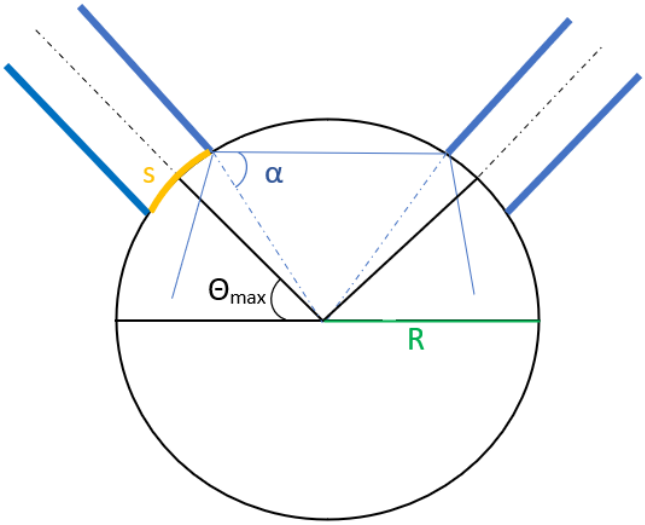

Figure 26: Schematic showing the maximum angle of force closure using the top-point theory

The equation for the maximum angle of contact before the grasp is no longer in force closure for the top-point theory was derived using Figure 26:

$$\theta_{max} = tan^{-1}\mu - \frac{s}{2R} \tag{21}$$

Where s is the arc length of the contact area from a 2D perspective and R is the radius of curvature of the object being held. The derivation of this and similar equations can be seen in Appendix 4.

The friction cone corresponding to the bottom points in the two-fingered grasping scenario outlined in this research is hypothesised to be the friction cone that dictates whether a soft-fingered grasp is in force closure. As the angle of contact, θ, increases, the friction cones begin to angle downwards with respect to the horizontal until there can no longer be a line between corresponding friction cones. The friction cones of the bottom points of contact are the last friction cones to reach the point where it can no longer have a connecting line between them as the angle of contact increases. Using the resultant cone theory in this grasping scenario, it can be said that Nguyen's theorem is met until there is no longer a connecting line within both resultant friction cones. As the contact angle increases, it is the friction cone at the lowest contact point that controls this condition. This reasoning arises from the fact that a hard contact fingertip in

the shape of a hemisphere only contacts the cylinder or disk at one point. This point has a contact area, but it is so minimal compared to a soft contact it is labelled as a point. Therefore, even with one point the hard finger can grasp an object in a force-closure grasp for a certain set of contact angles.

For the soft finger, the bottom point of the arc is the last point of the arc to start slipping based on the Nguyen's friction cone theorem. If only one point is needed for the hard finger to hold an object without slipping, then the grasped object is still in force closure as long as the bottom point obeys Nguyen's theorem. This idea is illustrated in Figure 27.

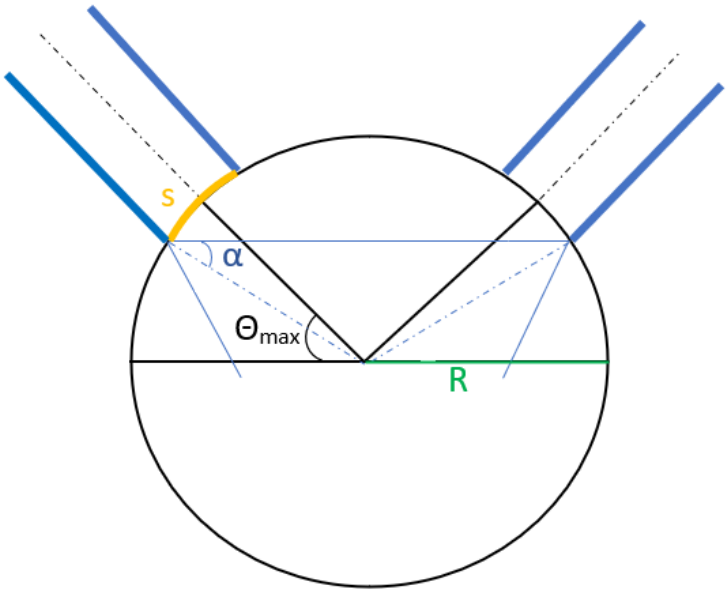

Figure 27: Schematic showing the maximum angle before slipping using the bottom point in the arc theory

Using this idea, the new equation for calculating the maximum contact angle of contact before the grasp is no longer in force closure for a symmetrical two-fingered grasp of a cylinder in 2D is:

$$\theta_{max} = tan^{-1}\mu + \frac{s}{2R} \tag{22}$$

As can be seen from the equation, using the bottom point as an indication of the state of the grasp instead of the centre point means that there is the addition of the value of s/2R before slipping occurs, overall increasing the maximum contact angle of the fingertips before slipping.

Using the resultant cone with Nguyen's theorem would indicate the superiority of the soft finger grasp over the hard finger grasp, even if they had the same coefficient of static friction. The larger contact area of the soft finger means more stability due to the additional torsion it can provide. Force-closure means that, as well as the grasp being in equilibrium, it has the ability to continue grasping in equilibrium while external changes happen. This can mean an addition of external forces or position changes, as seen in the example here, where the soft finger would theoretically be able to be positioned at a larger contact angle than the hard finger.

With the resultant cone model developed and applied for potential use in Coulomb's and Nguyen's theorems, an experimental method was designed to test its validity.

5 Methodology

Experiments had to be designed to test the validity of the resultant cone model. Since Coulomb's law and Nguyen's theorem are two conditions for a stable grasp of an object without slipping, the factor that was to be determined in the experiments was the positions of the fingers on the cylinder where these conditions were met. In particular, the position where the object was no longer grasped in a stable force closure grasp without slipping (i.e. becoming unrestrained) was to be quantified in terms of the angle of contact above the horizontal. The experimental results could then be compared to the predicted maximum angle from the theories, given that one of the conditions would have been broken.

The criteria of the initial design for the experiments included:

1) The object must be held in a two-fingered grasp

2) The contact angle made with the horizontal for each finger must be the same

3) The fingertips must be detachable and made from a few materials of various hardness levels

4) The grasping fingertips must have the ability to change their angle of contact

5) The fingers must be able to change the normal force exerted on the object in the grasp

5.1 Manufacturing Processes

The first step in the manufacturing process was making the cylinder that was to be grasped in the experiment. It was chosen to be a hard cylinder rather than made of a soft material because that meant the deformation of the soft fingers against the object could be observed easier than two objects deforming together.

The manufacturing process chosen for making the hard cylinder was 3D printing. At the University of Waikato, there is access to a large range of 3D printers. The material used in the 3D printers was Polylactic acid (PLA) which is a bioplastic. PLA is a hard material with a Shore A hardness of

67.0 – 85.0 (MatWeb, 2020). This indicates a relatively hard material when looking at the Shore A durometer hardness scales, somewhere between a tire tread and a shoe heel as can be seen from Figure 28.

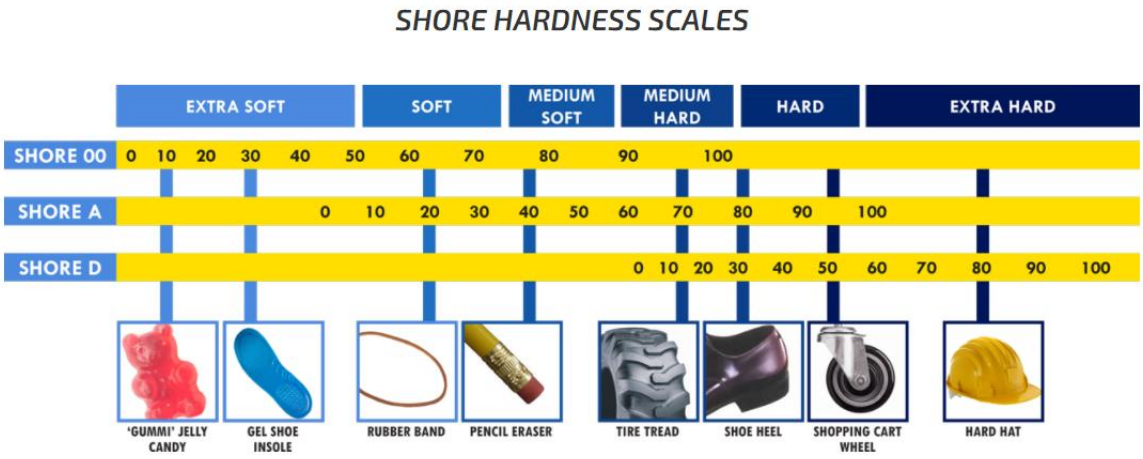

Figure 28: Durometer Shore Hardness Scale (Smooth-On, 2020)

The high Shore A hardness of PLA was an excellent material property to have in this experiment because it would ensure that there was little to no deformation of the object due to the set of forces that would be applied on it.

The dimensions of the cylinder were chosen roughly as an object weight/size that would be held well with the fingers. It was decided that the cross-section would have a diameter of 6cm and the width of the cylinder would be 2.5cm. The width was chosen to be 2.5cm because when looking ahead to the fingertip sizes, the width of the cylinder would have to be able to encompass the deformation of the fingertip. If the fingertip were to be modelled as approximately human-sized, 2.5cm would be enough to encompass the width.

The fingertips themselves had to be used and attached to whatever mechanism would be holding and adjusting the fingers. This was because fingertips of different hardness levels had to be used in the experiment. Since most fingertip models are modelled as hemispherical, this was to be replicated. The fingertip was modelled as being roughly the size of a human finger. According to the 2003 research by Kiran Dandekar Balasundar, I. Raju Mandayam, A. Srinivasan, the average

width of the human finger was found to be between 16-20mm (Dandekar, Raju, & Srinivasan, 2003). The larger diameter of 20mm was taken for a larger experimental setup that would make observations easier.

To analyse the changes in behaviour of the grasping fingertips holding the cylinder, at least two different hardness levels of the fingertip materials had to be chosen. A hard fingertip was 3D printed from PLA. Two softer fingertips were made from silicone rubber, one being of a Shore A hardness level of 30A and the other 15A.

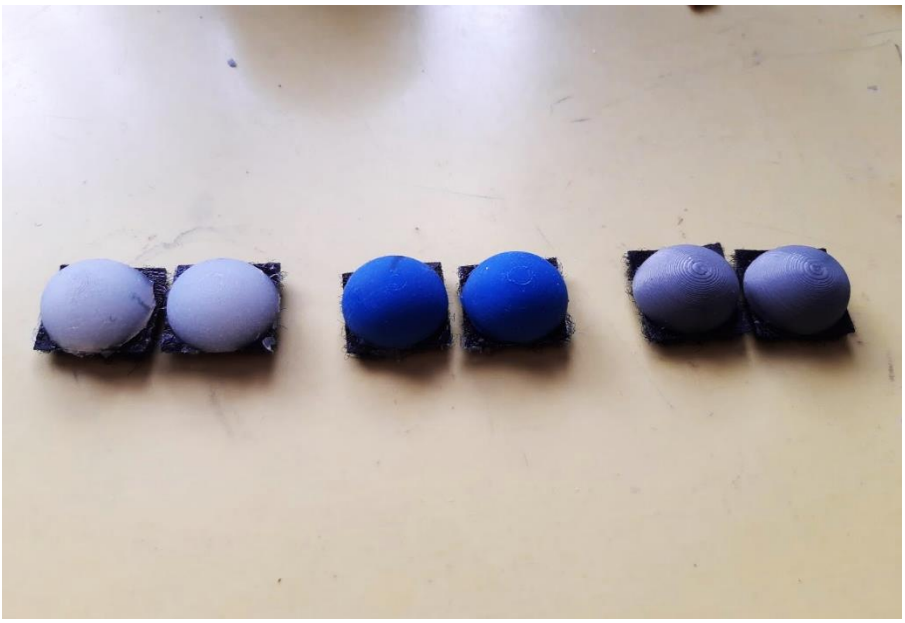

Figure 29: The three fingertips: (From left) 15A shore hardness silicone rubber, 30A shore hardness silicone rubber and PLA

The 3D printed PLA fingertip was the hardest fingertip, the 30A shore hardness silicone rubber fingertip was the second softest fingertip and the 15A shore hardness silicone rubber fingertip was the softest fingertip. These fingertips can be seen in Figure 29.

The fingertips were to be made detachable from the base of the fingertip holder so that they could easily be swapped during experimentation. A simple idea to execute this was to use Velcro and this can be seen in Figure 30. Velcro was attached to the fingertips and the fingertip holder and this allowed an easy way for the fingertips to be removed and connected again.

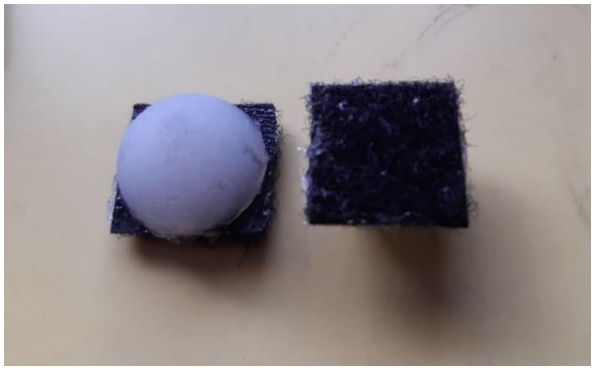

Figure 30: Velcro to make the fingertips detachable

5.2 The coefficient of static friction

The key aim of the experiment was to measure the maximum angle of contact before the object became unrestrained for each of the three hardness levels of the fingertips. This angle could then be compared to the maximum angles predicted by the models. If can be recalled, the variables involved included the radius of curvature of the cylinder, the arc length of contact and the coefficient of static friction. The first two of these variables could be practically found in the actual experiment, but the coefficient of static friction for each fingertip type had to be predetermined.

The method to measure the coefficient of static friction involves a piece of material on a longer rectangular piece of the other material. The rectangular piece should be raised on an incline until the smaller piece begins to slide, as demonstrated in Figure 31.

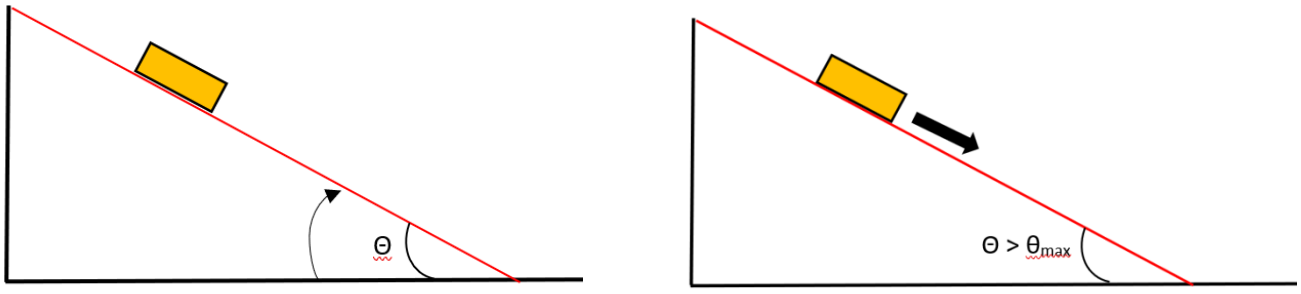

Figure 31: Schematic of Coefficient of static friction experiment

The angle just before sliding is the maximum angle before slipping:

$$tan\theta_{max} = \mu \tag{23}$$

Using the equation above, the coefficient of static friction can then be calculated. To make the rectangular part that would form the incline, 3D printing was once again utilised to make a PLA piece. The material was also PLA because the larger rectangular piece was representing the cylinder.

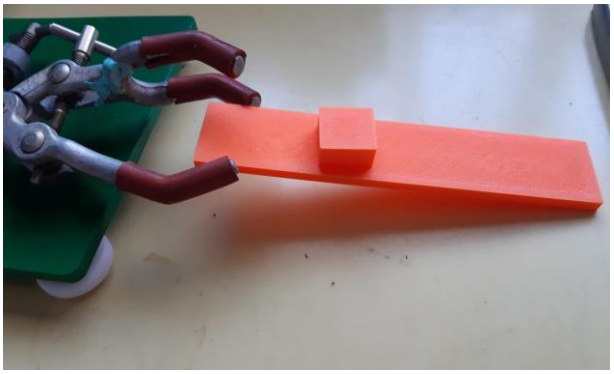

Figure 32: Actual coefficient of static friction experiment

Figure 32 shows the basic setup of the experiment. The smaller piece was 3D printed as a small rectangle to represent the hard PLA fingers and made in a mould for the softer fingers. For each material type, three trials were done to determine the average maximum angle before slipping and the coefficient of static friction was then found using equation 23.

The results for each fingertip were averaged and are now presented in the Table 3. Full results can be seen in Appendix 5.

Table 3: Average coefficient of static friction values

Fingertip type	Coefficient of static friction
PLA fingertip	0.11687
30A shore hardness silicone rubber	0.8310
15A shore hardness silicone rubber	1.1509

The higher coefficient of static friction of the softer materials means that there can be higher amounts of friction between the fingertip and the object before slipping, and thus, objects can be held more securely. Using Nguyen's theorem as well, the much higher coefficient of static friction would result in a higher maximum angle of contact before it was no longer in force closure in the two-finger grasp scenario for the model. This would be the case even if Nguyen's theorem was used with a point-contact model.

5.3 The actual experiment

The key aim of the experiment was to measure the maximum angle of contact of the fingers positioned above the horizontal on the cylinder, where any slight increase in the angle of contact of the fingers on the cylinder would result in the object becoming unrestrained. The normal force applied by the fingers onto the cylinder would have to be reasonably consistent throughout the trials. The maximum angle of contact was always to be considered as the angle from the horizontal to the centre-point of the contact arc.

5.3.1 Normal Force

The maximum angle that would be measured in this experiment would be affected if the normal force applied varied significantly between trials. To ensure that the normal force applied to the cylinder at the maximum angle of contact was approximately the same in each trial, visual inspection was used. This involved using photographs to inspect the arc length of contact between the fingertip and the cylinder. As Hertzian's theorem states, the arc length of contact is directly proportional to the force applied to the objects in contact. The photographs had to be taken level and parallel to the experimental setup so that they could then be analysed to determine the length. The reason that photographs were taken for visual analysis of the arc lengths rather than simply using a physical ruler on the experimental setup was due to the delicate nature of the setup. With the cylinder being supported only by the fingers, any external force could adjust the setup and cause slipping. This meant it would be challenging to bring any measuring equipment close to the cylinder and measure the arc length of the fingertip on the cylinder accurately. The arc of contact was taken as the arc of contact between the fingers and the cylinder that could be seen from the image taken parallel to the cylinder surface. This ensured that there was consistency in the method of measurement of the arc lengths.

A diameter line was drawn on the cylinder's cross-section to be a reference for when calculating the contact arc length and it would be confirmed to be horizontal using a ruler before the picture was captured. To accurately quantify the length of the arc, an app called 'ImageMeter' was installed. Using the reference line as the horizontal reference, grid lines were automatically created. Then, the heights to the top and bottom points of the arc were measured using the ImageMeter app as demonstrated in Figure 33.

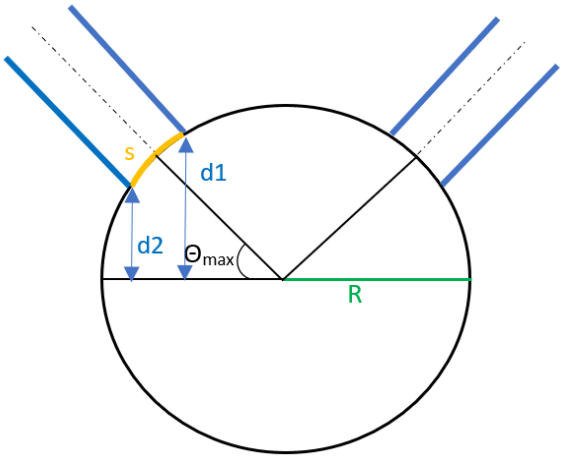

Figure 33: Schematic showing the vertical distances to the top and bottom points of the arc

These heights were to be used in the following formula to calculate the arc length.

$$arc\ length = R \times \ (sin^{-1}\left(\frac{d1}{R}\right) - sin^{-1}\left(\frac{d2}{R}\right)) \tag{24}$$

R is the radius of the cross-section, d1 is the height to the top point and d2 is the height to the bottom point. The equation must be calculated in radians. Explanation of full calculations can be seen in Appendix 6.

5.3.2 The mid-angle

In a similar fashion to how the arc length was measured, visual analysis of the experiment was to be used to measure the mid-angle and other angles of contact. The ImageMeter app was used to measure the vertical distance to the top and bottom points of the contact arc. The angles corresponding to these points were found, as shown below:

$$\theta_{top} = sin^{-1}\left(\frac{d1}{R}\right) \tag{25}$$

$$\theta_{bottom} = \ sin^{-1}\left(\frac{d2}{R}\right) \tag{26}$$

Since the angle of contact was always taken as the middle angle of the centre of the contact arc, the mid-angle was calculated as:

$$\theta_{mid} = \frac{\theta_{top} + \theta_{bottom}}{2} \tag{27}$$

5.3.3 Static setup before the experiment

Before completing each trial, the equipment had to be set up correctly to ensure minimal error and accurate results.

An important aspect of the setup that was considered was that the fingertip holders had to be the same height and horizontal so that the positions of the fingertips would be approximately the same. This would make the experiment symmetrical like the model and it would ensure that the normal force applied by both fingers would be similar. It was decided to make the fingers always positioned horizontally since the hemispherical fingertip is a continuous surface so the contact does not always have to be about the centre-point of the hemisphere.

With the fingertip holders correctly aligned, the fingertips themselves also had to be attached in such a way that would be uniform with the orientation of the fingertip holders. A diameter line was drawn on the fingertips for a reference and it was attached with the reference line of the fingertips meeting the reference mid-line of the fingertip holder. It was also visually checked that the fingertip outlines matched the outlines of the holder's cross-section. To confirm this alignment, a ruler was once again used to confirm both fingertips were the same height by measuring the vertical distance from the table to the centre point of the fingertip.

5.3.4 Methodology for completing the experiment

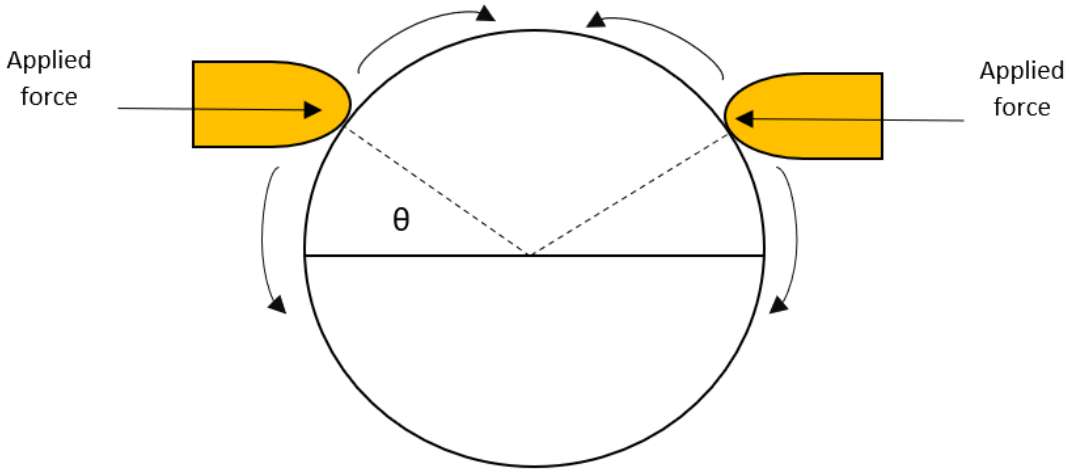

Figure 34: Schematic of the method of testing for the maximum angle before slipping

Once the setup of the experiment was complete, the initial trials began. The outline of the steps for a trial of each fingertip material is outlined below and a visual schematic can be seen in Figure 34.

Firstly, the fingers were aligned close together by moving the clamps closer. A ruler was used to ensure the fingers were pointing exactly at each other and the clamps were moved close together at a fixed position. The diameter line on the cross-section of the cylinder was aligned to be horizontal by using a ruler to check whether the line was concurring with the ruler's horizontal lines. The cylinder was placed between the fingers at the mid-line approximately and the contact arc length was noted by using the Imagemeter app.

The cylinder was gradually moved downwards to increase the contact angle that the fingers made with the cylinder. The administrator of the experiment had to hold the cylinder throughout the experiment until the stage where it could be tested where it would slip. The experiment administrator had to adjust the position of the fingertips so that approximately the same contact arc length was observed as the contact angle increased. This was confirmed by using the ImageMeter app at various trial stages. Eventually, the contact angle would increase such that

the cylinder would visibly begin to slip. This was done by the experimenter slowly loosening their grip on the cylinder to see whether any slipping occurred, keeping the fingers in the same position. Slipping was defined as any slight movement that caused the cylinder to move vertically downwards. Sometimes the slipping could be slow, so the key here was to wait a few moments to ensure there was no slipping.

If slipping did occur, the cylinder was moved upwards a little so that the contact angle was decreased. At this new position, the grip on the cylinder from the experimenter was once again loosened to check if any slipping would occur. If it did not slip, this position was taken as the maximum angle of contact before the object began to slip for that particular arc length.

Two pictures were taken of the maximum angle position in each trial, with the camera being parallel to the experimental setup. The first was a closeup of the contact of the right finger holding the cylinder. And the second was a closeup of the contact of the left finger holding the cylinder. The pictures were then analysed using the ImageMeter app, as seen in Figure 36.

The previous steps were repeated until there were twenty suitable trials for each hardness level of the fingertips. Trials with contact arc lengths that were not within approximately 1mm of the average at the maximum contact angle position were discarded and redone. A reason for an arc length not being within 1mm of the average would have been due to positioning of the fingers by the experimenter not exerting the same normal force as in the other trials. Note that the pictures had to be taken parallel to the experimental setup to take a realistic image of the reference line. The arc length measurement was defined as the arc line where the fingertip appeared to coincide with the cylinder circumference from a parallel perspective. This was also a rule for consistency so that a consistent method was done to measure the arc lengths to get the most consistent results.

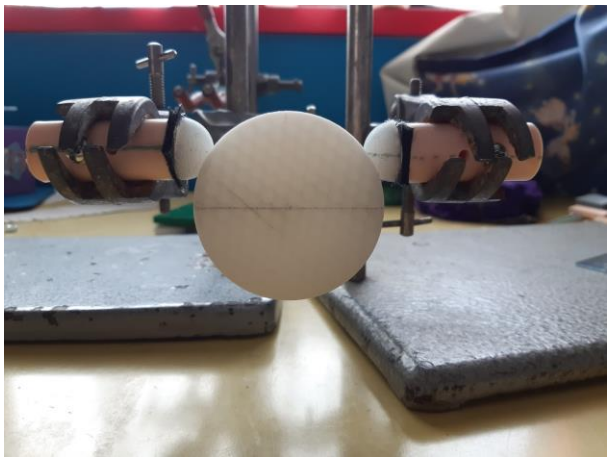

Figure 35: Two soft fingertips holding the cylinder without any support

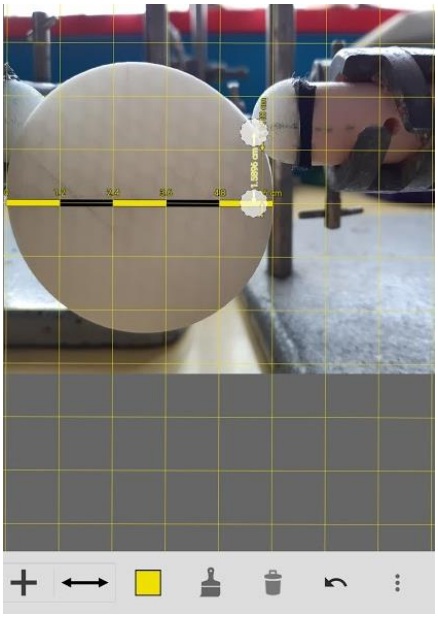

Figure 36: ImageMeter app being used to measured vertical distances of the right finger

6 Experimental Results

Twenty trials of the experiment for each fingertip type were recorded and the averages of the results are recorded in Table 4, where RF refers to the right finger and LF refers to the left finger. Calculations using the results from the trials were completed on Microsoft Excel for simplicity, but sample calculations can be found in Appendix 6. The maximum angle before slipping was calculated as the angle from the horizontal to the centre-point of the contact arc. For full results, refer to Appendix 7. The error for the population averages was calculated as the standard error (SE) of the population.

Table 4: Results of the experiment

Fingertip	Mean LF arc length (cm)	Mean RF arc length (cm)	Population mean arc length (cm)	Mean LF max angle (°)	Mean RF max angle (°)	Population mean max angle (°)
PLA	-	-	-	6.7	6.0	6.4±0.3
30A shore hardness silicone rubber	0.397	0.401	0.399±0.003	17.7	16.7	17.2±0.3
15A shore hardness silicone rubber	0.639	0.629	0.634±0.008	24.9	24.1	24.5±1.3

When looking at the data of the 20 trials for the 30A and 15A shore hardness fingers, it was a criterion that the arc lengths recorded should be within a specific frame of similarity of arc lengths. This was to ensure that approximately the same normal force was applied each trial. Due to this method of measuring the arc length using the ImageMeter app, there would be fluctuations in the measured arc lengths naturally. It was decided that when the entire population was counted, the average arc lengths for each trial should all be approximately within 1mm of each other. Therefore, after the initial 20 trials, a few had to be discarded as not

applicable to the experiment since their applied force was not similar to the other trials. The link between the applied normal force and the maximum angle of contact meant that the applied normal force had to be held reasonably constant. To make up for the discarded few, more trials were done until a full 20 trials could be used with arc length averages that were all within 1mm of each other for both 30A and 15A shore hardness fingers.

In looking at the results, it is clear that the hard PLA finger grasp had the lowest maximum contact angle before the object became unrestrained, with an average of just 6.4 degrees. This is a very low contact angle and was expected for such a hard material with a low coefficient of static friction. The two soft-fingered silicone rubber grasps had a much higher range of angle positions before the object became unrestrained. Within the two silicone rubber fingers, the softer 15A shore hardness finger with the higher coefficient of static friction had a higher maximum angle of contact of 24.5 degrees than the 30A shore hardness finger's maximum angle of contact of 17.2 degrees. This is a predictable trend since the larger the coefficient of static friction, the wider the angle of the friction cone, increasing the positions where both Coulomb's and Nguyen's conditions are met.

With the experiment results finalised, the reason that the object became unrestrained lay in either of the two conditions. Either the object began to slip due to Coulomb's law or the geometry of the grasp positioning meant that Nguyen's condition was not met, meaning the object was no longer in force closure and could become unrestrained. During the experiment, it was observed that at the positions near the maximum angle of contact, the fingers would visibly begin to slide over the edges of the cylinder. This confirmed that the object was not becoming unrestrained due to it not being in equilibrium or force closure but because of slipping. One possibility was that the object was becoming unrestrained due to the frictional forces becoming larger than the limits of a friction cone. The results of the experiment were then compared to the predicted maximum angles of slipping using the original and resultant friction cones with Coulomb's law. This is outlined in section 7.

7 Analysis of the results

7.1 Analysis of experimental results utilising Coulomb's theory

Using Coulomb's friction law required analysis and measurement of the force applied to the object at the maximum contact angle found from the experiment. The University of Waikato own accurate scales, so the idea was to use a scale to measure an applied force. According to the resultant friction cone theory, when the fingers are positioned at the maximum angle of contact before slipping, the resultant applied contact force due to the normal and frictional forces is along the line of the upper limit of the resultant friction cone, as seen in Figure 37. If the contact angle increased past the maximum angle, more friction would have to be applied to obtain the same frictional force in the opposite direction of the weight force, W. This means that the resultant force would ultimately direct outside of the extended friction cone and hence, slipping would occur.

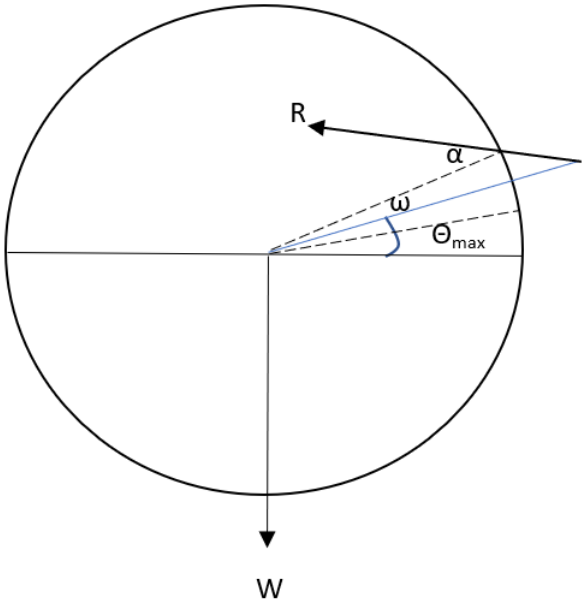

Figure 37: Resultant force using the extended cone model

Using the resultant friction cone model to calculate the resultant and normal forces acting on the object due to grasping differs from using Coulomb's law with a point contact friction cone to calculate the normal force. The similarity is that both methods use ideas of the friction cone to predict the relationship between the applied normal force and the allowable friction force. The difference is that the resultant friction cone incorporates all friction cones along the length of the arc and the variations in their orientations. Coulomb's friction cone assumes one friction cone in the centre of the arc. An equilibrium analysis can be done to estimate the resultant force, R, at the maximum angle of contact before slipping. Θ_{max} is the maximum angle of contact before slipping occurs, α is the half-angle of the friction cone of the top point in the arc, ω is the angle from the line from the centre-point of the arc to the top point in the contact arc and W is the weight force of the cylinder.

The equation for calculating the resultant force, R, using the extended friction cone model is:

$$R = \frac{W}{2\sin(\alpha - \omega - \theta_{max})} \tag{28}$$

$$where\ \alpha = tan^{-1}\mu\ and\ \omega = \frac{s}{2R}$$

The resultant force can then be resolved into the normal force, N, by using the formula:

$$N = Rcos(\alpha - \omega) \tag{29}$$

Using the maximum angles measured for each hardness level of the fingertip that was obtained in the experiments, the resultant and normal forces were calculated as shown in Table 5.

Table 5: Results of the calculated forces using the resultant cone model

Fingertip type	Resultant Force (N)	Normal Force (N)
30A shore hardness	0.390	0.316
15A shore hardness	0.395	0.289

The normal force applied at the maximum angle of contact before slipping using the original centre-point friction cone for Coulomb's law can also be estimated using a free body diagram. To

understand this relationship more, a simple Excel model was made using the relationships that could be found using the free body diagram before slipping:

$$W + Nsin\theta_{max} = \mu N cos\theta_{max} \quad (30)$$

This model was such that the weight force, coefficient of static friction and the maximum angle before slipping were all inputs. The normal force applied was the variable being calculated. The model implied that the maximum angle before slipping for a certain coefficient of static friction would not change even if the object's weight changed. This is because the normal force can be increased indefinitely in the model to balance the weight force while still being within the Coulomb friction cone. However, the normal force applied by the fingers cannot be increased indefinitely and instead was kept at a constant force in the experiments. The overall conclusion from the Excel model was that, for a given applied normal force and coefficient of static friction, there is a maximum angle before slipping that can be calculated for a certain weight of an object.

The cylinder had a weight of 0.0255kg, giving it a weight force of approximately 0.245N. With the inputs of this weight force, the coefficient of static friction of 1.1509 for the 15A shore hardness finger and the maximum angle before slipping of 24.5 degrees, the excel model was used to calculate the approximate normal force applied. The normal force calculated was 0.198 N. When the coefficient of static friction was changed to 0.8310 and the maximum angle to 17.2 degrees to correspond to the 30A shore hardness finger, the normal force calculated was 0.251N. If the normal force used for the 30A shore hardness finger (0.251 N) was applied for the 15A shore hardness finger, the excel model calculates the maximum angle as approximately 29.9 degrees. This shows that the maximum angle before slipping depends on the normal force applied and, hence, the object's weight.

The calculated normal force using the resultant cone theorem is slightly different from when using the original centre-point cone theorem. The normal forces using the centre-point friction cone were calculated as 0.251 N and 0.198 N for the 30A and 15A shore hardness fingers, respectively. These normal forces are smaller than the normal forces predicted by the resultant friction cone model. This is because the angle making up the resultant friction cone is slightly smaller than the angle of the centre-point friction cone. Thus, the original centre-point friction

cone predicts that less normal force has to be applied for the same allowable friction force to be generated. Both ideas showed the 15A shore hardness finger exerting a lower normal force than the 30A shore hardness force even though the resultant force was larger for the 15A shore hardness finger. This shows that the soft fingers or the materials with a higher coefficient of static friction do not have to exert as high a normal force to generate an allowable friction force that can balance external forces. The hard fingers have to exert much higher forces to get the small amount of friction force needed to keep the object in grasp due to their very low coefficient of static friction.

The method for finding the normal force was chosen to be through the use of one of the scales that the University of Waikato own. The University of Waikato owns some Kern PCB scales, which are precision scales that can measure up to 0.01 of a gram. It can be recalled that Hertzian's theory states that the contact area is proportional to the normal force applied. Thus, the arc lengths measured in the previous experiment for a certain finger material are proportional to the normal force being applied on the cylinder by the finger of that material. Experimentally, a finger pressed on the scale to deform such that the arc length is similar to the ones used in the experiment would measure the normal force applied in the experiment before slipping.

A test was devised to check if the normal forces predicted by the extended friction cone model were similar to the normal forces that would produce the same arc lengths recorded in the previous experiment. This process will be referred to as the test for the remainder of this thesis, while the main data came from the first experiment. The test would involve measuring the contact arc length of the fingertips on the cylinder when the normal force predicted from the resultant friction cone model was applied to the fingertips from the cylinder. The cylinder would be clamped and positioned directly above the centre of the fingertip. When it pressed down on the fingertips with a vertically downward force, a reaction force would act vertically upward on the fingertips to balance the downward normal force due to the cylinder. The finger-cylinder setup would be placed on a scale to measure any vertical reaction force and, due to the system being in a state of equilibrium, the reaction force would be equivalent to the applied normal force onto the fingertips from the cylinder. Due to the reaction forces, the applied normal force onto the fingertips from the cylinder would be the same as the applied normal force onto the cylinder

from the fingertips. Hence, the reaction force measured from the scale would be equivalent to the normal force the fingertips applied to the cylinder in the slipping experiment with the inclusion of the weight force from the fingertip resting on the scale. A visual description can be seen in Figure 38, where N is the normal force applied and w is the weight force.

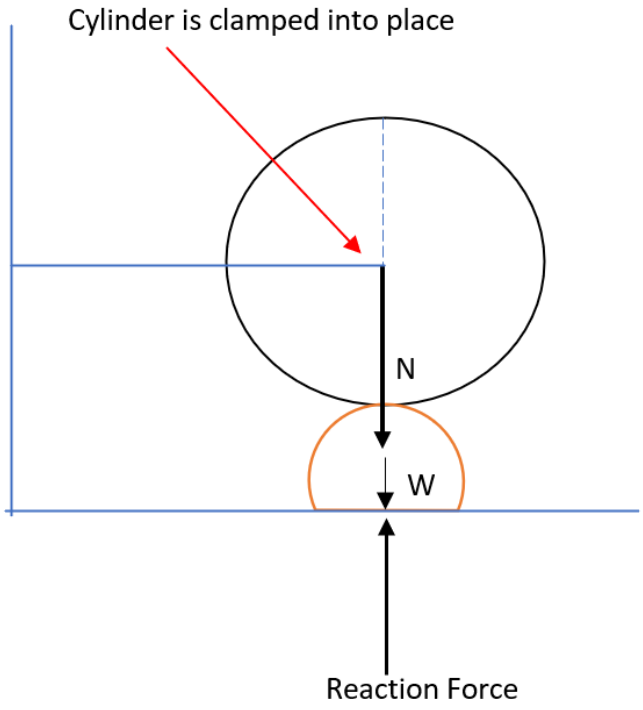

Figure 38: Forces acting in the setup for the scale experiment

With the consideration of the weight force of the fingertip in mind, the scale could be used to replicate the normal forces calculated using the resultant cone theorem at the maximum angle before slipping. Theoretically, the arc length measured when the scale reading is equivalent to the predicted normal force should be similar to the arc length measured in the slipping experiment for that certain fingertip material if the model is to be shown to be accurate for the grasping situation. In the original experiments, the average contact arc length of the 30A shore hardness fingertip before slipping was 0.399cm and the average contact arc length of the 15A shore hardness fingertip before slipping was 0.634cm. The arc length would need to be measured

as the fingertip against the cylinder since different shapes in contact have different deformation patterns. The methodology for this test for each fingertip type is outlined below and a picture of the setup can be seen in Figure 39.

Firstly, the cylinder was clamped to hover just above the plate of the scale, with its reference diameter line kept vertical. The scale was turned on and zeroed. A fingertip was placed on the scale and its mass was noted. The cylinder was then lowered onto the centre of the fingertip. When the predicted normal force from the resultant friction cone model with the additional fingertip mass was reached, the cylinder was clamped so that it could no longer move.

A picture of the setup was taken with care being taken to keep the photograph parallel to the setup and in a similar fashion to the previous experiment. The ImageMeter app was once again used to measure the distances of the outer points of contact of the fingertip in regard to the vertical reference line so that the arc length could be calculated from these distances. Calculated arc lengths are done similarly to the previous experiments that can be seen, for example, in Appendix 6. The distances d1 and d2, reported in the earlier experiment data, were horizontal instead of vertical in this test because the reference line was vertical instead of horizontal. The test was repeated 20 times for each fingertip type.

Figure 39: Setup of the test measuring the normal force using a scale

The results from the test can be seen in the Table 6 and full results of each trial can be seen in Appendix 8:

Table 6: Results of the normal force test using the Resultant cone model

Fingertip	Experimental arc length before slipping (cm)	Normal Force predicted from Resultant cone model (N)	Average normal force during Test (N)	Average Arc length measured during test (cm)
30A shore hardness	0.399±0.003	0.316	0.308±0.003	0.379±0.008
15A shore hardness	0.634±0.008	0.289	0.294±0.002	0.598±0.008

The results from the trials indicate that the resultant cone model's prediction of the normal force is similar to the normal force from the actual experiment. During the test, the normal force had to be averaged because of the difficulty in getting the normal force value to be exactly the same

as the force predicted from the extended model. The normal forces predicted from the extended models were within the range the average normal forces during the test using the standard error. The average arc length of the 30A shore hardness finger measured in the test was very similar to the experimental arc length measured before slipping, with an error of 5.01%. The average arc length of the 15A shore hardness finger measured in the test was also very similar to the experimental average arc length measured before slipping, with an error of 5.67%.

A possible reason for any error between the calibrated arc lengths and the original arc lengths was due to the difficulty in getting the normal force reading from the scale to exactly match the target normal force for that particular fingertip type. The scale tended to fluctuate even when it had settled down after a force was applied. Consequently, the average force in a set of fluctuated forces had to be taken. This may have resulted in an error of the calculated overall average normal force applied in the test and hence, the arc lengths recorded may have been actually corresponding to slightly different normal forces. Another possible reason for error is due to the method of measuring the arc lengths with the Imagemeter app. While it was an efficient app that allowed the user to zoom in to see the arc contact effectively, any small change to the points of the distance measured could change the reading significantly in relation to the arc size. Overall, the error is low and the arc lengths from the test are agreeable with the arc lengths measured during the slipping experiment.

The fact that the average arc lengths measured in the test for the predicted normal force from the resultant friction cone model were similar to the average arc lengths measured from the grasp at the maximum angle before slipping indicates that the resultant cone model predicted the normal force applied just before slipping in the two-fingered cylinder grasp well. As a preliminary analysis, this indicates that the resultant friction cone equation used to predict the forces in a grasp just before the slipping point could be a more accurate model for the two-fingered soft contact grasp of a cylinder than the centre-point model. This is the start of what could suggest that soft finger contact can be better modelled with a set of friction cones.

To confirm that the resultant cone model was the more suitable model for the given grasping situation, the test was repeated so that the normal force predicted from using the centre-point

friction cone model with Coulomb's law could be used instead for the sake of comparison. The averaged results can be seen in Table 7 with full results in Appendix 8.

Table 7: Results of the normal force test using Coulomb's theory with a centre-point cone

Fingertip	Experimental arc length before slipping (cm)	Normal Force predicted from the centre-point model (N)	Average normal force during Test (N)	Average Arc length measured during test (cm)
30A shore hardness	0.399±0.003	0.251	0.243±0.002	0.335±0.008
15A shore hardness	0.634±0.008	0.198	0.185±0.003	0.513±0.011

Since the centre-point friction cone model predicted lower applied normal forces just before slipping than the resultant cone model, the contact arc lengths corresponding to the lower normal forces were also smaller than those predicted by the resultant cone model. The difference in the average arc lengths measured during the test was 16.04% for the 30A shore hardness finger and 19.09% for the 15A shore hardness finger. These errors are significantly larger than the errors using the resultant cone theory. For the general grasping scenario, the original centre-point friction cone would have been used with Coulomb's theory to predict the normal force applied for a given maximum angle of contact. Naturally, error in this calculation would occur due to uncertainties about material properties and measurement tactics to confirm the normal force. Thus, the errors of 16.04% and 19.09% may have still been acceptable by itself. However, the fact that the slight alteration of the centre-point friction cone to the resultant cone model caused the error to decrease significantly for the two-fingered grasping scenario of the cylinder indicates that the resultant cone model is a more accurate representation of the grasp in this experiment.

This is an important finding because this points towards the original hypothesis being potentially correct, that a soft fingered contact should be modelled as a set of Coulomb's friction cones

instead of a single point Coulomb friction cone in the grasping of a non-planar object. The moment that is also used in a soft finger grasp model was not considered in the experiments conducted in this research due to the fact that the two-fingered grasp was applied in the centre of the cylinder so that no external moments were acting on the cylinder at the grasping position. The reason the resultant cone model worked as a predictor of the normal force applied at a maximum angle before slipping instead of the original centre-point friction cone in this experiment is that it considered the sum of the forces applied at the points along the arc rather than simply a representative cone in the centre of the arc. For a non-planar contact, this is particularly important because the differences in the angles of the applied forces with respect to the horizontal result in a set of friction cones for each point with different orientations. The resultant cone model used on planar soft contacts would become identical to the original centre-point friction cone due to no differences in the orientation of the friction cones along the contact area. This shows that Coulomb's centre-point friction cone is still relevant for many grasping scenarios, including hard contact grasping of any objects or soft contact grasping of planar surfaces. It is only limited in soft contact grasping of non-planar surfaces such as a cylinder, in which the resultant friction cone model can be used.

In the case of the two-fingered grasp of the cylinder executed in the first slipping experiment in this research, there is little difference in the prediction of the normal force applied at slipping between the centre-point friction model and the resultant cone model. This is due to the resultant cone model's resultant cone having a very slight difference in its half-angle. If this preliminary analysis is further proven to be true, the use of the resultant cone model instead of the centre point cone in heavier weight scenarios would mean a more significant difference in predicted forces just before slipping. This will be significant for the robotic grasping industry, where grasp models for a range of objects are further becoming more accurate to this day.

It should be noted that in this experiment, the range of arc length values did vary within each test. For example, the average arc length for the 15A shore hardness finger ranged from 0.559cm to 0.686cm for the resultant cone test and from 0.428cm to 0.596cm for the centre-point test. This fluctuation in the range of contact arc lengths did correspond with the fluctuations in the normal force read on the screen of the scale. An overlap can be seen in the range of arc lengths

measured for the resultant cone and Coulomb's original model since it was difficult to obtain the exact normal force that the scale was required to be set at. Therefore, it can be understood as to why there are some fluctuations of the arc lengths in the data sets and why further research at a larger scale may need to be done to further verify this preliminary analysis.

7.2 Effect of resultant friction cone model on Coulomb's theorem

The calibration tests indicated that the resultant cone model was a more accurate contact model than the centre-point cone model from the results in this particular research. With that in mind, it is important to examine how the resultant cone model modifies the predictions using Coulomb's law. Due to the resultant friction cone model, the allowable friction forces are limited by the cones at the outer points of the contact arc. For the scenario of the symmetrical two soft-fingered grasp of a cylinder, the resultant friction cone has a slightly smaller half-angle than the original centre-point friction cone. As a result, the resultant friction cone implies that a slightly higher net normal force has to be applied to ensure that forces are within the resultant friction cone than when using the centre-point friction cone for soft finger grasping.

An explanation for this is that the normal forces at each point of the contact arc are at a different angle with respect to the horizontal when there is a soft area contact. The hard point contact has its normal force applied at a point which is why the point friction cone is applicable. Since the distribution of applied normal forces for a soft finger contact are not all in the same direction, the maximum frictional forces allowable at each point to offset the weight force of the cylinder will also be varied. This is due to the difference in orientation of the friction cones at each point. Thus, to achieve the desired friction force without slipping to keep the cylinder held in equilibrium, a higher net normal force would have to be applied for a soft finger contact than would be estimated from the centre-point friction cone.

While the resultant cone is an effective way of visualising and implementing the set-of-cones theory for the grasping scenario presented in this research, the fundamental idea remains that the most limiting cone dictates the state of the grasp. In terms of Coulomb's theory, the object

is not slipping if all the friction forces at each point making up the contact area are within each friction cone.

7.3 Application to Nguyen's theorem

Using Coulomb's friction law with the resultant friction cone model had a more accurate prediction of the forces at the maximum angle before slipping from the experiment completed in this research. While further research can be done to further prove that the resultant friction cone model is applicable for various grasping scenarios, it needs to be confirmed that the grasp up to the maximum angle before slipping is also in force closure. If this is so, the conditions for a stable grasp is that both Nguyen's and Coulomb's theorems are met.

In using Nguyen's theorem to confirm that the soft two-fingered grasp is in force closure, the resultant friction cone theorem can be used since it was a more accurate contact model for soft-fingered grasp than the original centre point contact model. The grasp scenario in this experiment involved a two-fingered soft material grasp that was symmetrical.

The calculation of the maximum angle of contact for the object to be in force closure for the softer fingertips are shown below using the centre-point, lowest-point and highest-point friction cones.

Centre-point contact model:

$$\theta_{max} = tan^{-1}\mu$$

30A shore hardness

$$\theta_{max} = tan^{-1}0.8310$$

$$\theta_{max} = 39.72658°$$

15A shore hardness

$$\theta_{max} = tan^{-1}1.1509$$

$$\theta_{max} = 49.01311°$$

Lowest point in the arc model:

$$\theta_{max} = tan^{-1}\mu + \frac{s}{2R}$$

30A shore hardness

$$\theta_{max} = tan^{-1}0.8310 + \frac{0.39919}{2 * 3}$$

$$\theta_{max} = 43.53857°$$

15A shore hardness

$$\theta_{max} = tan^{-1}1.1509 + \frac{0.63380}{2 * 3}$$

$$\theta_{max} = 55.06641°$$

Highest point in the arc model:

$$\theta_{max} = tan^{-1}\mu - \frac{s}{2R}$$

30A shore hardness

$$\theta_{max} = tan^{-1}0.8310 - \frac{0.39919}{2 * 3}$$

$$\theta_{max} = 35.91460°$$

15A shore hardness

$$\theta_{max} = tan^{-1}1.1509 - \frac{0.63380}{2 * 3}$$

$$\theta_{max} = 42.96076°$$

The maximum angles before Nguyen's theorem is broken for each point contact is outlined in Table 8.

Table 8: Maximum angle before Nguyen's theorem is broken for different contact point models.

	Centre-point model (°)	Lowest arc-point model (°)	Highest arc-point model (°)
30A shore hardness finger	39.7	43.5	35.9
15A shore hardness finger	49.0	55.1	43.0

The outline of the resultant friction cone is made up of the outer friction cone lines of the lowest arc-point and the highest arc-point of the contact arc between the soft fingers and the object being held. Therefore, when using the resultant friction cone as the contact model when assessing Nguyen's condition in the cylinder grasp scenario, it is the lowest point in the contact arc that dictates whether or not the grasp is meeting Nguyen's theorem; a condition for a force closure grasp. This is because in the grasping scenario analysed in this research, the two fingers are above the centreline of the cylinder and therefore, the point friction cones begin to angle downwards as the angle of contact increases. The friction cone of the lowest point in the arc starts to angle downwards at the largest contact angle out of all the contact points in the arc and this results in Nguyen's theorem being broken, i.e. no line existing between the resultant friction cones, is dictated by the friction cone of the lowest point in the contact arc.

Table 8 shows that using the lowest arc-point model for Nguyen's theorem shows that there is a larger angle of positions where Nguyen's condition is met when using the resultant friction cone instead of just the centre-point friction cone for both fingertip types of different shore hardness levels. For example, the 30A shore hardness finger grasp the lowest arc-point model predicted a maximum contact angle of 43.5 degrees before Nguyen's condition was no longer met. This is higher than the centre-point model's prediction of 39.7 degrees. Since the lowest-point contact model is essentially estimating the same maximum angle that would meet Nguyen's condition for the resultant friction cone, it can be said that using the resultant friction cone model for a soft fingered grasp when evaluating Nguyen's condition results in a wider

range of positions for Nguyen's condition to be met, and hence where the object is grasped in force closure.

The use of the resultant friction cone model for soft-fingered grasps demonstrates a difference between soft-fingered grasps and hard-fingered grasps. The difference is that the soft-fingered grasp has a contact area rather than a point. The contact area results in a wider cone for use in demonstrating the range of force-closure positions of the soft-fingered grasp through Nguyen's condition.

It is also interesting to note that, while the experimental maximum angles of contact for the silicone rubber fingers corresponded to the resultant cone's use with Coulomb's law, it did not correspond to the maximum angles before Nguyen's condition is no longer met. This shows how the maximum angle before Nguyen's theorem is broken as predicted by the resultant cone theorem (shown in table as lowest arc-point model) is larger than the maximum experimental angle before slipping for both 30A and 15A shore hardness levels. This translates to the fact that the grasp was a force closure grasp without slipping up to the maximum experimental angle before slipping. After that maximum angle, Coulomb's law would be broken but Nguyen's condition would still be met up to a greater angle. This reiterates that while it is important to have a force closure grasp, it is also necessary to model when slipping occurs. When both Coulomb's and Nguyen's conditions are met, a grasp is considered ideal.

This research aimed to investigate whether the resultant cone model is a more accurate model than the centre-point cone model when modelling a grasp with soft finger contact. The idea for this research came from the idea of a grasping scenario where two fingers are holding a cylinder in the plane of its centre of mass. Using the original centre-point contact model in Nguyen's and Coulomb's theorems, the hard and soft finger grasp would be modelled identically in this scenario due to there being no external moments involved. This research has indicated the potential of the resultant cone model in this grasping scenario to differentiate between the soft and hard fingers. For the grasping scenario where the fingers are placed in the plane of the centre of mass, the use of the resultant cone model increases the range of positions where the grasp is in force closure for the soft finger grasp as compared to the hard

finger grasp. It also alters the angle of the resultant cone in use for Coulomb's slipping theory. The resultant cone model highlights the differences between the hard and soft finger grasp even in a position where no external moments are acting on the object, which was the aim of the research.

Further research should be done to confirm that the set-of-cones idea can be used for a wider range of grasping scenarios and geometries. The resultant cone model in the grasping scenario used in this research meant that the friction cone of the bottom point was of the most relevance when applying it to Nguyen's theorem. An example of a different scenario can be seen in Figure 40. The two grasping fingers are placed below the mid-diameter line. In this scenario, the use of the resultant cone in Nguyen's theorem showed that it was the top-point friction cone that was the last point to have a line connecting it to its equivalent point in the other finger within their friction cones. This stresses the importance of further research into a range of grasping scenarios to verify how the resultant cone model can be applied into different scenarios that include different object shapes, materials and positions of finger placement.

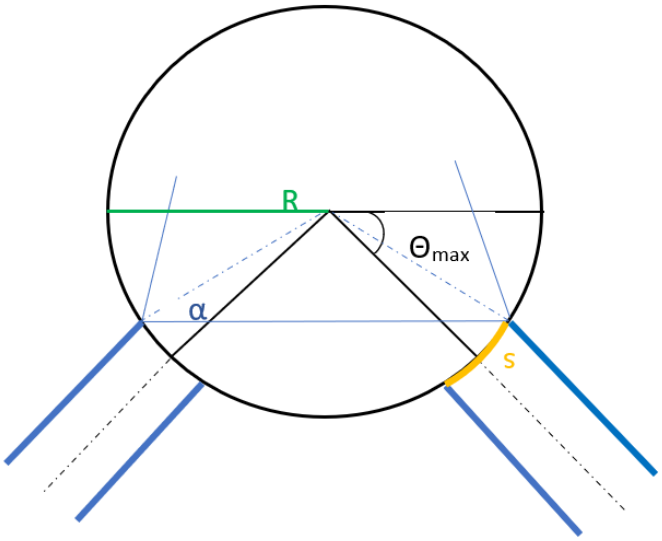

Figure 40: Schematic of grasping scenario where the grasping soft fingers are below the mid-line of the cylinder

8 Insight into Nguyen's theorem

In the process of planning and preparing for an experiment to test the maximum angle before an object is no longer restrained, another experiment was designed that would involve an asymmetric grasp as shown in Figure 41. The idea was to keep the right finger positioned at the horizontal line across the middle plane of the cylinder. That way, the only finger being moved would be the left finger. The symmetrical experiment was ultimately decided upon as the main experiment in this research, but the positions for force closure using Nguyen's theorem were determined, with an interesting result.

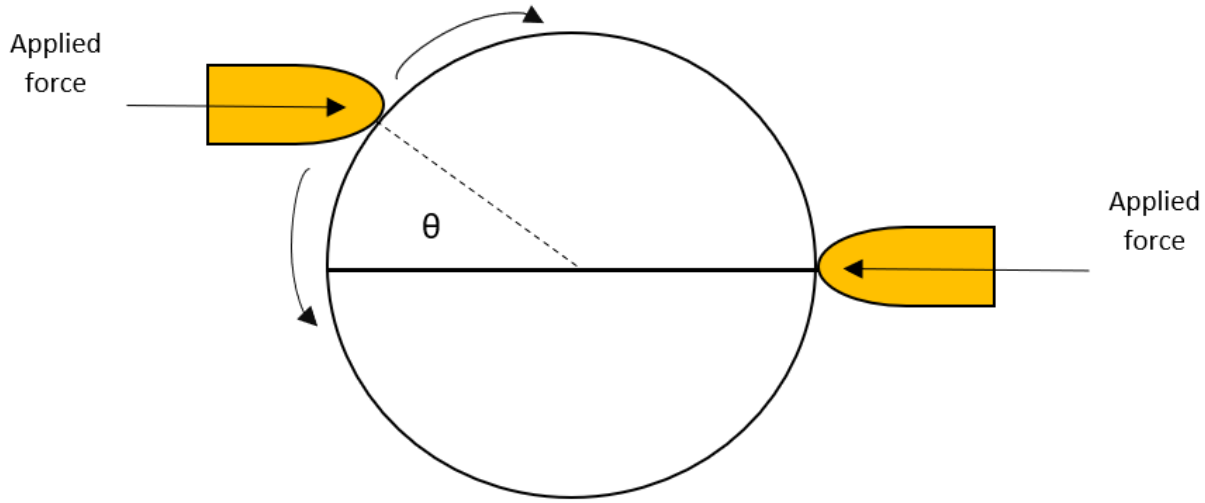

Figure 41: Schematic of the iterated experiment

The full derivations of the equations for Nguyen's theorem using the centre-point and bottom-point contact models can be seen in the Appendix 9 but a simplified diagram of the relationships can be seen in Figures 42 and 43.

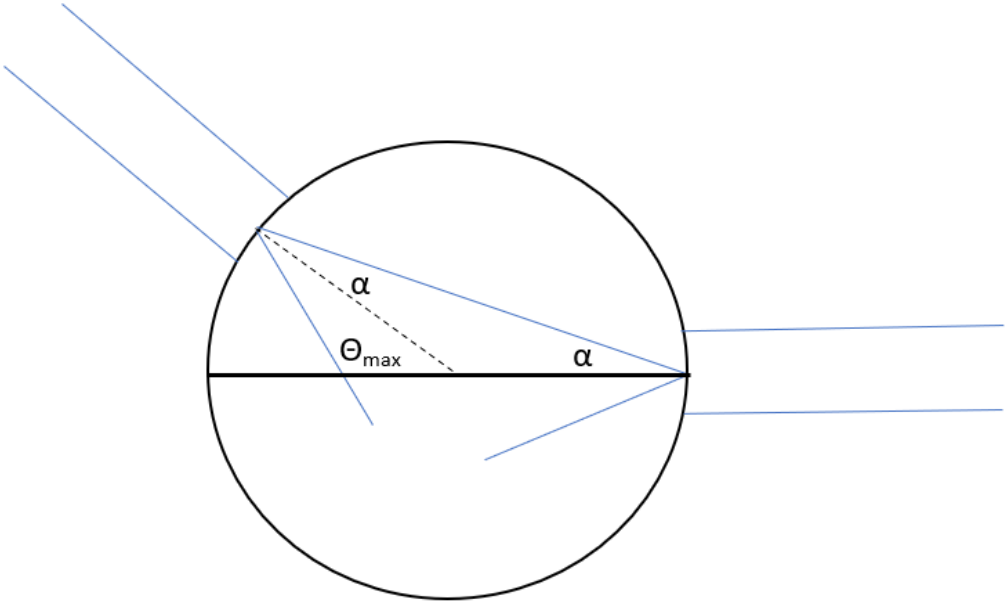

Figure 42: Schematic of the derivation of the maximum angle for the alternative experiment using the centre-point model in Nguyen's theorem

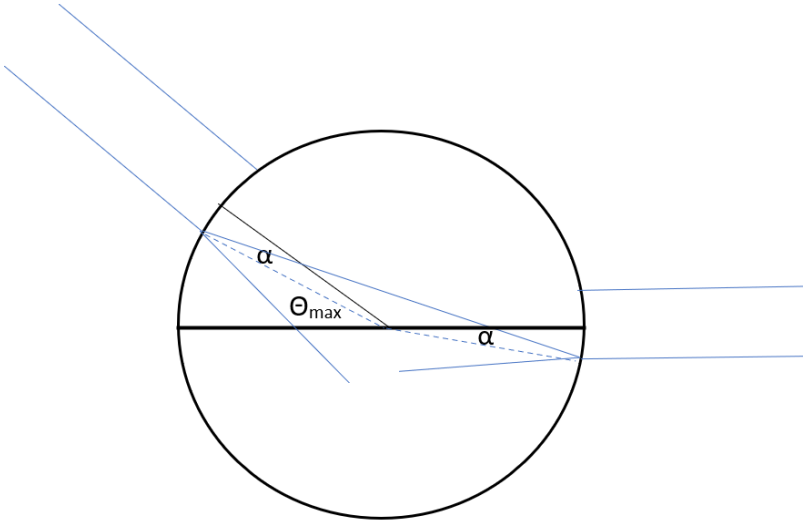

Figure 43: Schematic of the derivation of the maximum angle for the alternative experiment using the bottom-point model in Nguyen's theorem

The original centre-point contact model can be used in Nguyen's theorem to calculate the maximum angle of the left finger before the object is no longer held in force closure by using the following equation:

$$\theta_{max} = 2\alpha \tag{31}$$

$$Where\ \alpha = \ tan^{-1}\mu$$

The maximum angle before slipping for the bottom point in the arc model can be calculated by:

$$\theta_{max} = 2\alpha + \frac{s}{r} \tag{32}$$

Using these formulae for the different materials of the fingertips, noting that the hard PLA fingertip only uses the centre-point contact model, the maximum angle before the object was no longer grasped in force closure was calculated for all fingertip types and models. The results can be seen in Table 9. In a similar fashion to the main experiment, the maximum angle before slipping and the contact arc lengths were measured and calculated for this new scenario. Refer to Appendix 9 for the full results. These results were used to calculate the average arc length for each type of soft finger used in the trials so to be used in the theoretical models.

Table 9: The maximum angle estimations using the two models in Nguyen's theorem

Fingertip type	Contact arc length (cm)	Centre point model (°)	Bottom point set-of-cones model (°)
PLA	-	13.3	-
30A shore hardness	0.430	79.5	87.7
15A shore hardness	0.596	98.0	109.4

As can be seen from Table 9, the maximum angles for the position models are very large for the 30A shore hardness and 15A shore hardness materials. In fact, for the soft fingertips, both models

predict that the left finger will be over 90 degrees above the horizontal. This essentially means the left finger will have to be placed on the right side of the disk as it goes over 90 degrees. In this scenario, a free-body-force and moment analysis shows that the fingers cannot be applying a positive normal force while grasping the object in equilibrium. The two forces applied by the fingers are on the same side with regards to the centre of mass. If both are applied as positive toward the object, as the force applied from fingers always should be, the moments will not sum to zero and hence, the object cannot be in equilibrium.

It can be recalled, a force closure grasp is one where the fingers are placed on the object such that they can oppose any external disturbances to the object. Due to the fact that the fingers can only apply positive forces to an object, the predicted angles for force closure using Nguyen's theorem are impossible angles if they were to fit the definition of force closure as well as being in equilibrium. This suggests a potential limitation to the use of Nguyen's theorem, in that it may not fully consider the fact that the direction of the applied force from the fingers can only be positive.

Nguyen's theorem predicted a more realistic maximum angle of contact for the hard finger grasp with a very low coefficient of static friction. Thus, potential reasons for the limitation may be due to the high coefficient of static friction or the fact that it may not register the direction of the force and these potential reasons can be investigated in further research. If we bring up the case of the iron-on-iron hard point contact with the very high coefficient of static friction, similar to those of the 30A shore hardness and 15A shore hardness fingers, using Nguyen's theorem through the centre point model would also estimate a similar maximum angle before the grasp is no longer in force closure. Even with the point contact grasps, the contact angle being over 90 degrees is not practically achievable for equilibrium since this would require a negative pull force. This also emphasises the importance of an equilibrium analysis for grasping scenarios. Nguyen's and Coulomb's theorems are conditions for a stable grasp in force closure without slipping but equilibrium is the basic necessity required to ensure an object is restrained.

9 Conclusion and Recommendations

Soft materials are often used for fingertips in robotic grasping due to their ability to produce additional moments. In the design of robotic grasping, theoretical modelling is necessary to predict when and if an object will slip in a certain grasp. Coulomb friction laws and Nguyen's theorem must be met to ensure that an object is in a stable force closure grasp and that no slipping will occur.

This research aimed to look into how current grasp models could be expanded for use for soft fingers that have an area contact rather than a point contact. In certain grasping scenarios where the fingers are applied at the centre of mass, hard and soft fingers are both modelled identically as point contacts, even though soft fingers are thought of as superior to hard fingers in grasping. It was proposed that the contact should be modelled as a set-of-cones at each point making up the area of contact. An experiment was derived that tested the maximum angle the fingers could be raised around the edge of a cylinder without slipping. Three sets of fingertips were used, with one being hard PLA, one being 30A shore hardness silicone rubber, and the last being a 15A shore hardness silicone rubber.

In the analysis of the results, the set-of-cones approach was used as a resultant friction cone model that considered the set of friction cones at each point over the area of contact. The sum of the friction cones made up the overall resultant cone. This resultant cone had a different half-angle to the original Coulomb cone at a point due to it incorporating the change of orientation of the friction cones over the curved surface of the object. The normal forces at the maximum angle of contact before slipping were estimated with Coulomb's theory using the resultant cone model and the original centre-point model and compared to the experimental data. The results showed that the resultant cone model more accurately predicted the normal force applied before slipping than the original point cone model for both types of soft material focussed on in this research. This research has provided preliminary results suggesting that the resultant cone model may be more suitable for soft contact grasps than the centre-point model. Further research may confirm the resultant cone model for a variety of scenarios, then it can be said that the resultant cone

expands the range of positions of the finger for a force closure grasp according to Nguyen's theorem.

While the results of this research suggest that the resultant cone model is more accurate for the modelling of the two-fingered soft contact grasp, there were limitations in the research that mean more investigation into the model should be done. Further research could include the use of force sensors during the experiment itself to measure the forces being applied at the maximum angle of contact instead of using calibration practices with the arc lengths. It may also be beneficial to repeat the experiment on a larger scale with a heavier object being grasped. This would result in there being a larger difference in the predicted normal forces at the maximum angle before slipping for the centre-point friction cone and resultant friction cone models. Hence, this would make comparison of the experimental and theoretical results easier since it would be more obvious when the resultant cone model was more accurate. The set-of-cones idea that was used to model the resultant friction cone could also be explored with a variety of grasping scenarios in terms of object shape and finger placement to investigate its versatility. If the set-of-cones theory is found to be a useful theory for use in a variety of soft finger grasping scenarios, it can contribute to changes in how soft-fingered grasps are modelled in the robotic grasping industry and lead to more accurate predictions for a stable grasp.

References

Bicchi, A., & Kumar, V. (2000). *Robotic grasping and contact: A review.* Paper presented at the Proceedings 2000 ICRA. Millennium Conference. IEEE International Conference on Robotics and Automation. Symposia Proceedings (Cat. No. 00CH37065). Retrieved from https://www.researchgate.net/publication/2855409_Robotic_Grasping_and_Contact_A_Review

Caraza, J.-A. N., & Yun, X. (1991). Force-Closure Grasps With Two Palms. (Science Technical Report No. MS-CIS-91-83). https://repository.upenn.edu/cis_reports/438

Chandra, S. J. J. E. S. T. (2014). Modelling of Soil behaviour. (2-5), 68.

Chen, X.-Q., Niu, H., Li, D., & Li, Y. J. I. (2011). Modeling hardness of polycrystalline materials and bulk metallic glasses. *Intermetallics, 19*(9), 1275-1281. https://www.sciencedirect.com/science/article/pii/S0966979511000987?casa_token=918b5LGqgZkAAAAA:yJNppJ75h6Vdi7WMJAPwCZB6x-hLKRQZzOaFZTiQ7NUbu2sz2PuhfS6lgS14hLkbn4ctWIqTaw

Cutkosky, M. R. (1989). On grasp choice, grasp models, and the design of hands for manufacturing tasks. *Transactions on robotics automation, 5*(3), 269-279. https://www.researchgate.net/publication/3298011_On_grasp_choice_grasp_models_and_the_design_of_hands_for_manufacturing_tasks

Dandekar, K., Raju, B. I., & Srinivasan, M. A. (2003). 3-D finite-element models of human and monkey fingertips to investigate the mechanics of tactile sense. *J Biomech Eng., 125*(5), 682-691. https://pubmed.ncbi.nlm.nih.gov/14618927/

Davis, D. (2002). Friction. *Eastern Illinois University*. https://www.ux1.eiu.edu/~cfadd/1150/04Nwtn/frict.html

Dillard, D. A. (2018). A review of Winkler's foundation and its profound influence on adhesion and soft matter applications. *Soft Matter*(19). https://pubs.rsc.org/lv/content/articlehtml/2018/sm/c7sm02062g?casa_token=XaA--9cVSTMAAAAA:dQp69LZAuITvfqQZnJKlQus8hEnx727D6BSV1o3g5EoYD8kdbDUud7HSAvrSV5_H7oH_gxmnPqkAQDM

EngineeringToolBox. (2004). Friction and Friction coefficients. https://www.engineeringtoolbox.com/friction-coefficients-d_778.html

Fakhari, A., Kao, I., & Keshmiri, M. J. R. J. (2019). Modeling and control of planar slippage in object manipulation using robotic soft fingers. *ROBOMECH, 6*. https://robomechjournal.springeropen.com/articles/10.1186/s40648-019-0143-0

Fakhari, A., Keshmiri, M., Kao, I., & Hadian Jazi, S. J. A. R. (2016). Slippage control in soft finger grasping and manipulation. *Advanced Robotics, 30*(2), 97-108. https://www.tandfonline.com/doi/full/10.1080/01691864.2015.1105149?casa_token=X4Jju1yg4KoAAAAA%3ATYf7cjdf8jER5S5lusxIo5uSwx4FRZhdjuBbQHCrACiDQjcSTe0a3VkWZ4b1GbtdGz2wQfqVGc7-JQ

Harada, K., Tsuji, T., Uto, S., Yamanobe, N., Nagata, K., & Kitagaki, K. (2014). *Stability of soft-finger grasp under gravity.* Paper presented at the 2014 IEEE International Conference on Robotics and Automation (ICRA). Retrieved from https://www.researchgate.net/publication/286680290_Stability_of_soft-finger_grasp_under_gravity

Hongyan, C., Ran, A., & Ligang, C. (2016). Applicability of the hertz contact theory to rolling rubber cylinders model. *International Journal of Mechanical Engineering and Applications, 4*(6), 242-248.

http://www.sciencepublishinggroup.com/journal/paperinfo?journalid=220&doi=10.11648/j.ijmea.20160406.15

Khurshid, A., Ghafoor, A., & Malik, M. A. (2011). Robotic grasping and fine manipulation using soft fingertip. In *Advances in Mechatronics*: IntechOpen. Retrieved from https://www.intechopen.com/books/advances-in-mechatronics/robotic-grasping-and-fine-manipulation-using-soft-fingertip

Kim, H.-J., & Kim, D.-E. (2009). Nano-scale friction: A review. *International Journal of Precision Engineering and Manufacturing, 10*(2), 141-151. https://www.researchgate.net/publication/225135933_Nano-scale_friction_A_review

Kucher, D. (2020). Film-like Story of the First Real Robot Unimate in History. *somagnews*. https://www.somagnews.com/film-like-story-first-real-robot-unimate-history/

Li, Z., Li, P., Yang, H., & Wang, Y. J. B. e. (2013). Stability tests of two-finger tomato grasping for harvesting robots. *Biosystems Engineering, 116*(2), 163-170. https://www.sciencedirect.com/science/article/abs/pii/S1537511013001244

MatWeb. (2020). Overview of materials for Polylactic Acid (PLA) Biopolymer. http://www.matweb.com/search/DataSheet.aspx?MatGUID=ab96a4c0655c4018a8785ac4031b9278&ckck=1

Montana, D. J. (1991). *The condition for contact grasp stability.* Paper presented at the ICRA. Retrieved from https://ieeexplore.ieee.org/document/131612

Montana, D. J. (1992). Contact stability for two-fingered grasps. *IEEE Transactions on Robotics and Automation, 8*(4), 421-430. https://ieeexplore.ieee.org/document/149939

Moran, M. E. J. J. o. r. s. (2007). Evolution of robotic arms. *Journal of Robotic Surgery, 1*(2), 103-111. https://www.ncbi.nlm.nih.gov/pmc/articles/PMC4247431/#:~:text=Unimate%20introduced%20the%20first%20industrial,a%20robotic%20arm%20in%201993.

Murray, R. M., Li, Z., Sastry, S. S., & Sastry, S. S. (1994). *A mathematical introduction to robotic manipulation*: CRC press. Retrieved from https://books.google.co.nz/books?hl=en&lr=&id=D_PqGKRo7oIC&oi=fnd&pg=PR13&dq=A+mathematical+introduction+to+robotic+manipulation&ots=dmMkBj29ou&sig=eAt0wiNHzPIoRB6XgpTUCV2iwYc#v=onepage&q=A%20mathematical%20introduction%20to%20robotic%20manipulation&f=false

Naboulsi, S., & Nicholas, T. (2003). Limitations of the Coulomb friction assumption in fretting fatigue analysis. *International journal of solids structures, 40*(23), 6497-6512. https://www.sciencedirect.com/science/article/pii/S0020768303004013?casa_token=c78GdGXgACgAAAAA:WVCRD_90unesOxdhACKW8rMv8L0C7zlP8_6gDlfRtumksHGXtmu0tLtv89qrhZO5KBu7KwsJlw

Naeini, S., Ziaie moayed, R., & Allahyari, F. (2014). Subgrade Reaction Modulus (K s) of Clayey Soils Based on Field Tests. *Journal of Engineering Geology*. https://www.researchgate.net/publication/286926667_Subgrade_Reaction_Modulus_K_s_of_Clayey_Soils_Based_on_Field_Tests

Napier, J. R. (1956). The prehensile movements of the human hand. *The Journal of bone joint surgery. British volume, 38*(4), 902-913. https://online.boneandjoint.org.uk/doi/abs/10.1302/0301-620X.38B4.902

Nguyen, V.-D. (1986). *The Synthesis of Stable Force-Closure Grasps*. Retrieved from Massachusetts institute of Technology: https://apps.dtic.mil/sti/pdfs/ADA186419.pdf

Nguyen, V.-D. (1987). *Constructing force-closure grasps in 3D.* Paper presented at the Proceedings. 1987 IEEE International Conference on Robotics and Automation. Retrieved from https://ieeexplore.ieee.org/document/1088014

Popov, V. L. (2010). *Contact mechanics and friction*: Springer. Retrieved from https://link.springer.com/book/10.1007%2F978-3-662-53081-8

Reuleaux, F. (2013). *The kinematics of machinery: outlines of a theory of machines* (Reissued ed.): Dover Publications

Rimon, E., & Burdick, J. (1996). *On force and form closure for multiple finger grasps.* Paper presented at the Proceedings of IEEE International Conference on Robotics and Automation, Minneapolis, MN, USA. Retrieved from https://ieeexplore.ieee.org/document/506972

SeoulNationalUniversity. (n.d.). Grasp Statics. *Seoul National University Lecture Notes*. http://robotics.snu.ac.kr/edX/2014-1/lecturenotes/SNUx_Chapter_3.pdf

Shake, M. (2020). Ten Popular Industrial Robot Applications. *Jabil*. https://www.jabil.com/blog/ten-popular-industrial-robot-applications.html

Slater, A. (2020). AGRO ROBOTS | WHICH ROBOTS ACTUALLY WORK ON FARMS? https://www.foodunfolded.com/things-you-did-not-know/agro-robots-which-robots-actually-work-on-farms

Smooth-On. (2020). Durometer Shore Hardness Scale. https://www.smooth-on.com/page/durometer-shore-hardness-scale/

Sonka, M., Hlavac, V., & Boyle, R. (2014). *Image processing, analysis, and machine vision* (4 ed.): Cengage Learning. Retrieved from https://kgut.ac.ir/useruploads/1550563201478ety.pdf

Team, R. O. M. (2017). Robotics in Agriculture: Types and Applications. https://www.robotics.org/blog-article.cfm/Robotics-in-Agriculture-Types-and-Applications/74

Xydas, N., & Kao, I. J. T. I. J. o. R. R. (1999). Modeling of contact mechanics and friction limit surfaces for soft fingers in robotics, with experimental results. *The International Journal of Robotics Research, 18*(9), 941-950. https://journals.sagepub.com/doi/abs/10.1177/02783649922066673

Younis, W. (2010). *Up and running with Autodesk Inventor Simulation 2011: a step-by-step guide to engineering design solutions*: Elsevier. Retrieved from https://www.sciencedirect.com/book/9780123821027/up-and-running-with-autodesk-inventor-simulation-2011

Zhang, B., Xie, Y., Zhou, J., Wang, K., Zhang, Z. J. C., & Agriculture, E. i. (2020). State-of-the-art robotic grippers, grasping and control strategies, as well as their applications in agricultural robots: A review. *Computers and Electronics in Agriculture, 177*, 105694. https://www.sciencedirect.com/science/article/abs/pii/S0168169920311030

Zhang, L. E., Ciocarlie, M., & Hsiao, K. (2011). *Grasp evaluation with graspable feature matching.* Paper presented at the RSS Workshop on Mobile Manipulation: Learning to Manipulate. Retrieved from https://foswiki.cs.rpi.edu/foswiki/pub/RoboticsWeb/LabPublications/ZCHRSS11.pdf

Zhu, X. (2012). *Tutorial on hertz contact stress.* Paper presented at the Opti. Retrieved from https://wp.optics.arizona.edu/optomech/wp-content/uploads/sites/53/2016/10/OPTI-521-Tutorial-on-Hertz-contact-stress-Xiaoyin-Zhu.pdf

Zuo, K. J., & Olson, J. L. J. P. S. (2014). The evolution of functional hand replacement: From iron prostheses to hand transplantation. *The Canadian Journal of Plastic Surgery, 22*(1), 44-51. https://www.researchgate.net/publication/265055193_The_evolution_of_functional_hand_replacement_From_iron_prostheses_to_hand_transplantation

Appendices

Appendix 1 Force analysis for fingers positioned away from the centre of mass

A 1.1 Soft Finger grasp

Equations being used:

Overall equation:

$$F_0 = G.f_c \tag{33}$$

Which is the equation for equilibrium if it is in balance. F_0 is the matrix of applied forces and torques in the x, y and z directions as is mapped to the origin of choice. G is the grasp matrix and f_c is the matrix of contact forces as is applied at their contact points.

Grasp map equation for each **Soft** contact:

$$G_i = \begin{bmatrix} R_{ci} & 0 \\ \widehat{p_{ci}}.R_{ci} & R_{ci} \end{bmatrix} \begin{bmatrix} 1&0&0&0 \\ 0&1&0&0 \\ 0&0&1&0 \\ 0&0&0&0 \\ 0&0&0&0 \\ 0&0&0&1 \end{bmatrix} \tag{34}$$

The R matrix represents how the coordinate frame of the contacts relates to the coordinate frame at the origin. The p matrix represents the position of the contact force in relation the origin.

To find $\widehat{p_{ci}}$ from p, the following rule needs to be used:

$$\text{If } v = \begin{bmatrix} x \\ y \\ z \end{bmatrix}, \text{ then}$$

$$\hat{v} = \begin{bmatrix} 0 & -z & y \\ z & 0 & -x \\ -y & x & 0 \end{bmatrix} \tag{35}$$

Please note the meaning of the subscripts and the superscripts. The subscripts c1, c2 refer to contact force 1 and 2 respectively, as can be seen from the diagram. The superscripts, 1, 2 and 3

after the subscripts correspond to the force component from that contact force in the x, y and z direction respectively.

The labelling of the coordinate systems for each contact force was taken by the typical notations used by Murray et al. 1994 in their published textbook.

$$R_{c1} = \begin{bmatrix} 0 & 1 & 0 \\ 0 & 0 & 1 \\ 1 & 0 & 0 \end{bmatrix} P_{c1} = \begin{bmatrix} 0 \\ -r \\ 0 \end{bmatrix} \quad R_{c2} = \begin{bmatrix} 1 & 0 & 0 \\ 0 & 0 & -1 \\ 0 & 1 & 0 \end{bmatrix} P_{c2} = \begin{bmatrix} 0 \\ r \\ 0 \end{bmatrix}$$

$$\therefore \widehat{p_{c1}} = \begin{bmatrix} 0 & 0 & -r \\ 0 & 0 & 0 \\ r_1 & 0 & 0 \end{bmatrix} \widehat{p_{c2}} = \begin{bmatrix} 0 & 0 & r \\ 0 & 0 & 0 \\ -r & 0 & 0 \end{bmatrix}$$

$$\widehat{p_{c1}}.R_{c1} = \begin{bmatrix} 0 & 0 & -r \\ 0 & 0 & 0 \\ r_1 & 0 & 0 \end{bmatrix} \begin{bmatrix} 0 & 1 & 0 \\ 0 & 0 & 1 \\ 1 & 0 & 0 \end{bmatrix} = \begin{bmatrix} -r & 0 & 0 \\ 0 & 0 & 0 \\ 0 & r & 0 \end{bmatrix}$$

$$\widehat{p_{c2}}.R_{c2} = \begin{bmatrix} 0 & 0 & r \\ 0 & 0 & 0 \\ -r & 0 & 0 \end{bmatrix} \begin{bmatrix} 1 & 0 & 0 \\ 0 & 0 & -1 \\ 0 & 1 & 0 \end{bmatrix} = \begin{bmatrix} 0 & r & 0 \\ 0 & 0 & 0 \\ -r & 0 & 0 \end{bmatrix}$$

$$G_1 = \begin{bmatrix} 0 & 1 & 0 & 0 & 0 & 0 \\ 0 & 0 & 1 & 0 & 0 & 0 \\ 1 & 0 & 0 & 0 & 0 & 0 \\ -r & 0 & 0 & 0 & 1 & 0 \\ 0 & 0 & 0 & 0 & 0 & 1 \\ 0 & r & 0 & 1 & 0 & 0 \end{bmatrix} \begin{bmatrix} 1 & 0 & 0 & 0 \\ 0 & 1 & 0 & 0 \\ 0 & 0 & 1 & 0 \\ 0 & 0 & 0 & 0 \\ 0 & 0 & 0 & 0 \\ 0 & 0 & 0 & 1 \end{bmatrix} = \begin{bmatrix} 0 & 1 & 0 & 0 \\ 0 & 0 & 1 & 0 \\ 1 & 0 & 0 & 0 \\ -r & 0 & 0 & 0 \\ 0 & 0 & 0 & 1 \\ 0 & r & 0 & 0 \end{bmatrix}$$

$$G_2 = \begin{bmatrix} 1 & 0 & 0 & 0 & 0 & 0 \\ 0 & 0 & -1 & 0 & 0 & 0 \\ 0 & 1 & 0 & 0 & 0 & 0 \\ 0 & r & 0 & 1 & 0 & 0 \\ 0 & 0 & 0 & 0 & 0 & -1 \\ -r & 0 & 0 & 0 & 1 & 0 \end{bmatrix} \begin{bmatrix} 1 & 0 & 0 & 0 \\ 0 & 1 & 0 & 0 \\ 0 & 0 & 1 & 0 \\ 0 & 0 & 0 & 0 \\ 0 & 0 & 0 & 0 \\ 0 & 0 & 0 & 1 \end{bmatrix} = \begin{bmatrix} 1 & 0 & 0 & 0 \\ 0 & 0 & -1 & 0 \\ 0 & 1 & 0 & 0 \\ 0 & r & 0 & 0 \\ 0 & 0 & 0 & -1 \\ -r & 0 & 0 & 0 \end{bmatrix}$$

$$G = [G_1 \, G_2]$$

$$G = \begin{bmatrix} 0 & 1 & 0 & 0 & 1 & 0 & 0 & 0 \\ 0 & 0 & 1 & 0 & 0 & 0 & -1 & 0 \\ 1 & 0 & 0 & 0 & 0 & 1 & 0 & 0 \\ -r & 0 & 0 & 0 & 0 & r & 0 & 0 \\ 0 & 0 & 0 & 1 & 0 & 0 & 0 & -1 \\ 0 & r & 0 & 0 & -r & 0 & 0 & 0 \end{bmatrix}$$

$$\text{Contact forces: } f_c = \begin{bmatrix} {f_{c1}}^1 \\ {f_{c1}}^2 \\ {f_{c1}}^3 \\ {f_{c1}}^4 \\ {f_{c2}}^1 \\ {f_{c2}}^2 \\ {f_{c2}}^3 \\ {f_{c2}}^4 \end{bmatrix} \in R^8$$

$$F_0 = G.f_c$$

$$F_0 = \begin{bmatrix} {f_{c1}}^2 + {f_{c2}}^1 \\ {f_{c1}}^3 - {f_{c2}}^3 \\ {f_{c1}}^1 + {f_{c2}}^2 \\ -r{f_{c1}}^1 + r{f_{c2}}^2 \\ {f_{c1}}^4 - {f_{c2}}^4 \\ r{f_{c1}}^2 - r{f_{c2}}^1 \end{bmatrix}$$

If block is in force closure and balanced:

$$\begin{bmatrix} {f_{c1}}^2 + {f_{c2}}^1 \\ {f_{c1}}^3 - {f_{c2}}^3 \\ {f_{c1}}^1 + {f_{c2}}^2 \\ -r{f_{c1}}^1 + r{f_{c2}}^2 \\ {f_{c1}}^4 - {f_{c2}}^4 \\ r{f_{c1}}^2 - r{f_{c2}}^1 \end{bmatrix} + \begin{bmatrix} 0 \\ 0 \\ -mg \\ 0 \\ mgr_1 \\ 0 \end{bmatrix} = \begin{bmatrix} 0 \\ 0 \\ 0 \\ 0 \\ 0 \\ 0 \end{bmatrix}$$

Mgr_1 is seen as positive in the anticlockwise direction about the origin when looking at it from the right side as shown in the diagram. As can be seen from the final equation on the fifth line, the soft finger can produce torque to balance the external moment due to the weight force when the fingers are placed away from the centre of mass. From the equation it can look like they will cancel each other out. It is just because if positive is around the anticlockwise direction of the applied normal force, then since they are applied in opposite directions, one will appear to be in the opposite clockwise direction if looking from the right side as seen from the diagram. However, the torques will be working to balance the external torques so from one side will be both looking as going in the same direction. F_{c1} will actually be going in a negative applied direction from their

applied normal position (i.e. anticlockwise). Overall, the sum of the torque will not cancel each other but instead add together to reach a magnitude of mg_{r1} and in the opposite direction to the mgr_1.

A 1.2 Hard Finger grasp

The grasp map for a hard finger grasp is seen below:

$$G_i = \begin{bmatrix} R_{ci} & 0 \\ \widehat{p_{ci}}.R_{ci} & R_{ci} \end{bmatrix} \begin{bmatrix} 1 & 0 & 0 & 0 \\ 0 & 1 & 0 & 0 \\ 0 & 0 & 1 & 0 \\ 0 & 0 & 0 & 0 \\ 0 & 0 & 0 & 0 \\ 0 & 0 & 0 & 0 \end{bmatrix} \tag{36}$$

The positioning and coordinate matrices, p and R, are the same as in the soft finger scenario. The major difference here is the wrench matrix basis not containing a torque. Calculations will proceed from calculation the grasp matrices for each contact point.

$$G_1 = \begin{bmatrix} 0 & 1 & 0 & 0 & 0 & 0 \\ 0 & 0 & 1 & 0 & 0 & 0 \\ 1 & 0 & 0 & 0 & 0 & 0 \\ -r & 0 & 0 & 0 & 1 & 0 \\ 0 & 0 & 0 & 0 & 0 & 1 \\ 0 & r & 0 & 1 & 0 & 0 \end{bmatrix} \begin{bmatrix} 1 & 0 & 0 & 0 \\ 0 & 1 & 0 & 0 \\ 0 & 0 & 1 & 0 \\ 0 & 0 & 0 & 0 \\ 0 & 0 & 0 & 0 \\ 0 & 0 & 0 & 0 \end{bmatrix} = \begin{bmatrix} 0 & 1 & 0 & 0 \\ 0 & 0 & 1 & 0 \\ 1 & 0 & 0 & 0 \\ -r & 0 & 0 & 0 \\ 0 & 0 & 0 & 0 \\ 0 & r & 0 & 0 \end{bmatrix}$$

$$G_2 = \begin{bmatrix} 1 & 0 & 0 & 0 & 0 & 0 \\ 0 & 0 & -1 & 0 & 0 & 0 \\ 0 & 1 & 0 & 0 & 0 & 0 \\ 0 & r & 0 & 1 & 0 & 0 \\ 0 & 0 & 0 & 0 & 0 & -1 \\ -r & 0 & 0 & 0 & 1 & 0 \end{bmatrix} \begin{bmatrix} 1 & 0 & 0 & 0 \\ 0 & 1 & 0 & 0 \\ 0 & 0 & 1 & 0 \\ 0 & 0 & 0 & 0 \\ 0 & 0 & 0 & 0 \\ 0 & 0 & 0 & 0 \end{bmatrix} = \begin{bmatrix} 1 & 0 & 0 & 0 \\ 0 & 0 & -1 & 0 \\ 0 & 1 & 0 & 0 \\ 0 & r & 0 & 0 \\ 0 & 0 & 0 & 0 \\ -r & 0 & 0 & 0 \end{bmatrix}$$

Cancel out the column of 0's in both G1 and G2.

$$G = \begin{bmatrix} 0 & 1 & 0 & 1 & 0 & 0 \\ 0 & 0 & 1 & 0 & 0 & -1 \\ 1 & 0 & 0 & 0 & 1 & 0 \\ -r & 0 & 0 & 0 & r & 0 \\ 0 & 0 & 0 & 0 & 0 & 0 \\ 0 & r & 0 & -r & 0 & 0 \end{bmatrix}$$

$$f_c = \begin{bmatrix} {f_{c1}}^1 \\ {f_{c1}}^2 \\ {f_{c1}}^3 \\ {f_{c2}}^1 \\ {f_{c2}}^2 \\ {f_{c2}}^3 \end{bmatrix}$$

$$F_0 = G.f_c$$

$$F_0 = \begin{bmatrix} {f_{c1}}^2 + {f_{c2}}^1 \\ {f_{c1}}^3 - {f_{c2}}^3 \\ {f_{c1}}^1 + {f_{c2}}^2 \\ -r{f_{c1}}^1 + r{f_{c2}}^2 \\ 0 \\ r{f_{c1}}^2 - r{f_{c2}}^1 \end{bmatrix}$$

For force closure and equilibrium:

$$\begin{bmatrix} {f_{c1}}^2 + {f_{c2}}^1 \\ {f_{c1}}^3 - {f_{c2}}^3 \\ {f_{c1}}^1 + {f_{c2}}^2 \\ -r{f_{c1}}^1 + r{f_{c2}}^2 \\ 0 \\ r{f_{c1}}^2 - r{f_{c2}}^1 \end{bmatrix} + \begin{bmatrix} 0 \\ 0 \\ -mg \\ 0 \\ mgr_1 \\ 0 \end{bmatrix} = \begin{bmatrix} 0 \\ 0 \\ 0 \\ 0 \\ 0 \\ 0 \end{bmatrix}$$

Note that for the hard finger grasp case, the fifth line shows that there is no torque from the applied contact forces that can oppose the external torque due to the weight force. Thus, it is impossible for the hard finger grasp to hold a cylinder or rectangle in such a way.

Appendix 2 Force analysis of grasp through the centre of mass

A 2.1 Soft Finger grasp

$$R_{c1} = \begin{bmatrix} 0 & 1 & 0 \\ 0 & 0 & 1 \\ 1 & 0 & 0 \end{bmatrix} \quad P_{c1} = \begin{bmatrix} 0 \\ -r \\ 0 \end{bmatrix} \quad R_{c2} = \begin{bmatrix} 1 & 0 & 0 \\ 0 & 0 & -1 \\ 0 & 1 & 0 \end{bmatrix} \quad P_{c2} = \begin{bmatrix} 0 \\ r \\ 0 \end{bmatrix}$$

$$\therefore \widehat{p_{c1}} = \begin{bmatrix} 0 & 0 & -r \\ 0 & 0 & 0 \\ r_1 & 0 & 0 \end{bmatrix}$$

$$\widehat{p_{c1}}.R_{c1} = \begin{bmatrix} 0 & 0 & -r \\ 0 & 0 & 0 \\ r_1 & 0 & 0 \end{bmatrix}\begin{bmatrix} 0 & 1 & 0 \\ 0 & 0 & 1 \\ 1 & 0 & 0 \end{bmatrix} = \begin{bmatrix} -r & 0 & 0 \\ 0 & 0 & 0 \\ 0 & r & 0 \end{bmatrix}$$

$$\widehat{p_{c2}}.R_{c2} = \begin{bmatrix} 0 & 0 & r \\ 0 & 0 & 0 \\ -r & 0 & 0 \end{bmatrix}\begin{bmatrix} 1 & 0 & 0 \\ 0 & 0 & -1 \\ 0 & 1 & 0 \end{bmatrix} = \begin{bmatrix} 0 & r & 0 \\ 0 & 0 & 0 \\ -r & 0 & 0 \end{bmatrix}$$

$$G_1 = \begin{bmatrix} 0 & 1 & 0 & 0 & 0 & 0 \\ 0 & 0 & 1 & 0 & 0 & 0 \\ 1 & 0 & 0 & 0 & 0 & 0 \\ -r & 0 & 0 & 0 & 1 & 0 \\ 0 & 0 & 0 & 0 & 0 & 1 \\ 0 & r & 0 & 1 & 0 & 0 \end{bmatrix}\begin{bmatrix} 1 & 0 & 0 & 0 \\ 0 & 1 & 0 & 0 \\ 0 & 0 & 1 & 0 \\ 0 & 0 & 0 & 0 \\ 0 & 0 & 0 & 0 \\ 0 & 0 & 0 & 1 \end{bmatrix} = \begin{bmatrix} 0 & 1 & 0 & 0 \\ 0 & 0 & 1 & 0 \\ 1 & 0 & 0 & 0 \\ -r & 0 & 0 & 0 \\ 0 & 0 & 0 & 1 \\ 0 & r & 0 & 0 \end{bmatrix}$$

$$G_2 = \begin{bmatrix} 1 & 0 & 0 & 0 & 0 & 0 \\ 0 & 0 & -1 & 0 & 0 & 0 \\ 0 & 1 & 0 & 0 & 0 & 0 \\ 0 & r & 0 & 1 & 0 & 0 \\ 0 & 0 & 0 & 0 & 0 & -1 \\ -r & 0 & 0 & 0 & 1 & 0 \end{bmatrix}\begin{bmatrix} 1 & 0 & 0 & 0 \\ 0 & 1 & 0 & 0 \\ 0 & 0 & 1 & 0 \\ 0 & 0 & 0 & 0 \\ 0 & 0 & 0 & 0 \\ 0 & 0 & 0 & 1 \end{bmatrix} = \begin{bmatrix} 1 & 0 & 0 & 0 \\ 0 & 0 & -1 & 0 \\ 0 & 1 & 0 & 0 \\ 0 & r & 0 & 0 \\ 0 & 0 & 0 & -1 \\ -r & 0 & 0 & 0 \end{bmatrix}$$

$$G = [G_1\, G_2]$$

$$G = \begin{bmatrix} 0 & 1 & 0 & 0 & 1 & 0 & 0 & 0 \\ 0 & 0 & 1 & 0 & 0 & 0 & -1 & 0 \\ 1 & 0 & 0 & 0 & 0 & 1 & 0 & 0 \\ -r & 0 & 0 & 0 & 0 & r & 0 & 0 \\ 0 & 0 & 0 & 1 & 0 & 0 & 0 & -1 \\ 0 & r & 0 & 0 & -r & 0 & 0 & 0 \end{bmatrix}$$

Contact forces: $f_c = \begin{bmatrix} {f_{c1}}^1 \\ {f_{c1}}^2 \\ {f_{c1}}^3 \\ {f_{c1}}^4 \\ {f_{c2}}^1 \\ {f_{c2}}^2 \\ {f_{c2}}^3 \\ {f_{c2}}^4 \end{bmatrix} \in R^8$

$$F_0 = G.f_c$$

$$F_0 = \begin{bmatrix} {f_{c1}}^2 + {f_{c2}}^1 \\ {f_{c1}}^3 - {f_{c2}}^3 \\ {f_{c1}}^1 + {f_{c2}}^2 \\ -r{f_{c1}}^1 + r{f_{c2}}^2 \\ {f_{c1}}^4 - {f_{c2}}^4 \\ r{f_{c1}}^2 - r{f_{c2}}^1 \end{bmatrix}$$

If block is in force closure and balanced:

$$\begin{bmatrix} {f_{c1}}^2 + {f_{c2}}^1 \\ {f_{c1}}^3 - {f_{c2}}^3 \\ {f_{c1}}^1 + {f_{c2}}^2 \\ -r{f_{c1}}^1 + r{f_{c2}}^2 \\ {f_{c1}}^4 - {f_{c2}}^4 \\ r{f_{c1}}^2 - r{f_{c2}}^1 \end{bmatrix} + \begin{bmatrix} 0 \\ 0 \\ -mg \\ 0 \\ 0 \\ 0 \end{bmatrix} = \begin{bmatrix} 0 \\ 0 \\ 0 \\ 0 \\ 0 \\ 0 \end{bmatrix}$$

In this example, there is no external moment acting on the cylinder about the origin of choice since it is placed at the centre of mass. Thus, the fifth line of the matrices equation is as follows:

$$r{f_{c1}}^2 - r{f_{c2}}^1 + 0 = 0$$

This means that it is possible for each moment produced by the soft fingertips to be equal to zero or equal and opposite to each other. The ability of the soft fingertips to produce torque is not utilised by this scenario as opposed to scenario before.

A 2.2 Hard Finger grasp

$$G_1 = \begin{bmatrix} 0 & 1 & 0 & 0 & 0 & 0 \\ 0 & 0 & 1 & 0 & 0 & 0 \\ 1 & 0 & 0 & 0 & 0 & 0 \\ -r & 0 & 0 & 0 & 1 & 0 \\ 0 & 0 & 0 & 0 & 0 & 1 \\ 0 & r & 0 & 1 & 0 & 0 \end{bmatrix} \begin{bmatrix} 1 & 0 & 0 & 0 \\ 0 & 1 & 0 & 0 \\ 0 & 0 & 1 & 0 \\ 0 & 0 & 0 & 0 \\ 0 & 0 & 0 & 0 \\ 0 & 0 & 0 & 0 \end{bmatrix} = \begin{bmatrix} 0 & 1 & 0 & 0 \\ 0 & 0 & 1 & 0 \\ 1 & 0 & 0 & 0 \\ -r & 0 & 0 & 0 \\ 0 & 0 & 0 & 0 \\ 0 & r & 0 & 0 \end{bmatrix}$$

$$G_2 = \begin{bmatrix} 1 & 0 & 0 & 0 & 0 & 0 \\ 0 & 0 & -1 & 0 & 0 & 0 \\ 0 & 1 & 0 & 0 & 0 & 0 \\ 0 & r & 0 & 1 & 0 & 0 \\ 0 & 0 & 0 & 0 & 0 & -1 \\ -r & 0 & 0 & 0 & 1 & 0 \end{bmatrix} \begin{bmatrix} 1 & 0 & 0 & 0 \\ 0 & 1 & 0 & 0 \\ 0 & 0 & 1 & 0 \\ 0 & 0 & 0 & 0 \\ 0 & 0 & 0 & 0 \\ 0 & 0 & 0 & 0 \end{bmatrix} = \begin{bmatrix} 1 & 0 & 0 & 0 \\ 0 & 0 & -1 & 0 \\ 0 & 1 & 0 & 0 \\ 0 & r & 0 & 0 \\ 0 & 0 & 0 & 0 \\ -r & 0 & 0 & 0 \end{bmatrix}$$

Cancel out the column of 0's in both G1 and G2.

$$G = \begin{bmatrix} 0 & 1 & 0 & 1 & 0 & 0 \\ 0 & 0 & 1 & 0 & 0 & -1 \\ 1 & 0 & 0 & 0 & 1 & 0 \\ -r & 0 & 0 & 0 & r & 0 \\ 0 & 0 & 0 & 0 & 0 & 0 \\ 0 & r & 0 & -r & 0 & 0 \end{bmatrix}$$

$$f_c = \begin{bmatrix} {f_{c1}}^1 \\ {f_{c1}}^2 \\ {f_{c1}}^3 \\ {f_{c2}}^1 \\ {f_{c2}}^2 \\ {f_{c2}}^3 \end{bmatrix}$$

$$F_0 = G.f_c$$

$$F_0 = \begin{bmatrix} {f_{c1}}^2 + {f_{c2}}^1 \\ {f_{c1}}^3 - {f_{c2}}^3 \\ {f_{c1}}^1 + {f_{c2}}^2 \\ -r{f_{c1}}^1 + r{f_{c2}}^2 \\ 0 \\ r{f_{c1}}^2 - r{f_{c2}}^1 \end{bmatrix}$$

For force closure and equilibrium:

$$\begin{bmatrix} {f_{c1}}^2 + {f_{c2}}^1 \\ {f_{c1}}^3 - {f_{c2}}^3 \\ {f_{c1}}^1 + {f_{c2}}^2 \\ -r{f_{c1}}^1 + r{f_{c2}}^2 \\ 0 \\ r{f_{c1}}^2 - r{f_{c2}}^1 \end{bmatrix} + \begin{bmatrix} 0 \\ 0 \\ -mg \\ 0 \\ 0 \\ 0 \end{bmatrix} = \begin{bmatrix} 0 \\ 0 \\ 0 \\ 0 \\ 0 \\ 0 \end{bmatrix}$$

As can be seen from the fifth line equation in the matrices, there is no external moment due to the weight force, mg. There is also no possible moment about the y-axis that can produced from the hard fingertips in the case that it was needed to balance an external moment. This is why it is possible for a hard finger to hold a cylinder when it is holding it through the centre of mass as opposed to away from the centre of mass.

A 2.3 Comparison of soft finger and hard finger

For the scenario where the fingers are positioned at the centre of mass of the object, the final force analysis equations are similar for the soft and hard fingers.

Soft Finger

$$\begin{bmatrix} {f_{c1}}^2 + {f_{c2}}^1 \\ {f_{c1}}^3 - {f_{c2}}^3 \\ {f_{c1}}^1 + {f_{c2}}^2 \\ -r{f_{c1}}^1 + r{f_{c2}}^2 \\ {f_{c1}}^4 - {f_{c2}}^4 \\ r{f_{c1}}^2 - r{f_{c2}}^1 \end{bmatrix} + \begin{bmatrix} 0 \\ 0 \\ -mg \\ 0 \\ 0 \\ 0 \end{bmatrix} = \begin{bmatrix} 0 \\ 0 \\ 0 \\ 0 \\ 0 \\ 0 \end{bmatrix}$$

Hard Finger

$$\begin{bmatrix} {f_{c1}}^2 + {f_{c2}}^1 \\ {f_{c1}}^3 - {f_{c2}}^3 \\ {f_{c1}}^1 + {f_{c2}}^2 \\ -r{f_{c1}}^1 + r{f_{c2}}^2 \\ 0 \\ r{f_{c1}}^2 - r{f_{c2}}^1 \end{bmatrix} + \begin{bmatrix} 0 \\ 0 \\ -mg \\ 0 \\ 0 \\ 0 \end{bmatrix} = \begin{bmatrix} 0 \\ 0 \\ 0 \\ 0 \\ 0 \\ 0 \end{bmatrix}$$

The component of the fifth line of the soft finger, $f_{c1}{}^4 - f_{c2}{}^4$, is equal to 0 since there is no external moment to balance. The equations are hence identical. When the need for a produced moment from the finger is eliminated, the theory shows that the soft finger and the hard finger behave the same and have similar grasp mechanics as each other.

Of course, this is one particular model. It is not to say that soft finger and hard finger are identical in their ability. Soft fingers are known to be generally superior in grasping than hard fingers. So, while the equations are identical, the issue of stability and force-closure needs to be addressed. Stability refers to the ability of the object to return to its original position after a disturbance. In the case of the soft finger, any movement away from the centre of mass can be balanced by the moments the fingers can produce. The hard finger cannot produced such a moment and thus, slipping would occur if the grasp moves away from the centre of mass due to a disturbance.

Appendix 3 2D Force Analysis

2D Force analysis of two-fingered grasp around a cylinder with relation to the contact angle.

$$\begin{bmatrix} F_{c1x} \\ F_{c1y} \\ F_{c2x} \\ F_{c2y} \end{bmatrix} = \begin{bmatrix} {F_{c1}}^1 cos\theta + {F_{c1}}^2 sin\theta \\ -{F_{c1}}^1 sin\theta + {F_{c1}}^2 cos\theta \\ -{F_{c2}}^1 cos\theta - {F_{c2}}^2 sin\theta \\ -{F_{c2}}^1 sin\theta + {F_{c2}}^2 cos\theta \end{bmatrix}$$

$$\begin{bmatrix} f_0 \\ \tau_0 \end{bmatrix} = \begin{bmatrix} R_{ci} & 0 \\ [-p_y \quad p_x]R_{ci} & 1 \end{bmatrix} \begin{bmatrix} f_{ci} \\ \tau_{ci} \end{bmatrix}$$

$$R_{c1} = \begin{bmatrix} 1 & 0 \\ 0 & 1 \end{bmatrix} \qquad R_{c2} = \begin{bmatrix} 1 & 0 \\ 0 & 1 \end{bmatrix} \qquad p_{c1} = \begin{bmatrix} -Rcos\theta \\ 0 \end{bmatrix} \qquad p_{c2} = \begin{bmatrix} Rcos\theta \\ 0 \end{bmatrix}$$

For contact 1:

$$[-p_y \quad p_x]R_{c1} = \begin{bmatrix} 0 \\ -Rcos\theta \end{bmatrix} \begin{bmatrix} 1 & 0 \\ 0 & 1 \end{bmatrix} = [0 \quad -Rcos\theta]$$

For contact 2:

$$[-p_y \quad p_x]R_{c2} = [0 \quad Rcos\theta]$$

$$G_1 = \begin{bmatrix} 1 & 0 & 0 \\ 0 & 1 & 0 \\ 0 & -Rcos\theta & 1 \end{bmatrix} \begin{bmatrix} 1 & 0 \\ 0 & 1 \\ 0 & 0 \end{bmatrix} = \begin{bmatrix} 1 & 0 \\ 0 & 1 \\ 0 & -Rcos\theta \end{bmatrix}$$

$$G_2 = \begin{bmatrix} 1 & 0 & 0 \\ 0 & 1 & 0 \\ 0 & Rcos\theta & 1 \end{bmatrix} \begin{bmatrix} 1 & 0 \\ 0 & 1 \\ 0 & 0 \end{bmatrix} = \begin{bmatrix} 1 & 0 \\ 0 & 1 \\ 0 & Rcos\theta \end{bmatrix}$$

$$G = [G_1 \quad G_2]$$

$$G = \begin{bmatrix} 1 & 0 & 1 & 0 \\ 0 & 1 & 0 & 1 \\ 0 & -Rcos\theta & 0 & Rcos\theta \end{bmatrix}$$

$$\begin{bmatrix} f_0 \\ \tau_0 \end{bmatrix} = \begin{bmatrix} 1 & 0 & 1 & 0 \\ 0 & 1 & 0 & 1 \\ 0 & -Rcos\theta & 0 & Rcos\theta \end{bmatrix} \begin{bmatrix} F_{c1x} \\ F_{c1y} \\ F_{c2x} \\ F_{c2y} \end{bmatrix} = \begin{bmatrix} F_{c1x} + F_{c2x} \\ F_{c1y} + F_{c2y} \\ -F_{c1y}Rcos\theta + F_{c2y}Rcos\theta \end{bmatrix}$$

Expanding the F terms

$$\begin{bmatrix} f_x \\ f_y \\ \tau_z \end{bmatrix} = \begin{bmatrix} {F_{c1}}^1 cos\theta + {F_{c1}}^2 sin\theta - {F_{c2}}^1 cos\theta - {F_{c2}}^2 sin\theta \\ -{F_{c1}}^1 sin\theta + {F_{c1}}^2 cos\theta - {F_{c2}}^1 sin\theta + {F_{c2}}^2 cos\theta \\ {F_{c1}}^1 sin\theta R cos\theta - {F_{c1}}^2 cos\theta R cos\theta - {F_{c2}}^1 sin\theta R cos\theta + {F_{c2}}^2 cos\theta R cos\theta \end{bmatrix} + \begin{bmatrix} 0 \\ -mg \\ 0 \end{bmatrix}$$

$$= \begin{bmatrix} 0 \\ 0 \\ 0 \end{bmatrix}$$

This is the overall equilibrium analysis in 2D. With the fingers placed directly in the plane of the centre of mass along the length of the cylinder, there are no external torques. Assuming the forces applied by the two fingers are equal, the third line of the matrix shows that they cancel each other out so there are no torques acting on the cylinder. Thus, the only aspect being investigated is whether the forces applied can balance the weight force, mg, and keep the cylinder grasped well.

Appendix 4 Derivation of maximum angle of force closure using Nguyen's theorem

The derivations of the maximum angle before the grasp is no longer in force closure applies to the two-fingered scenario used in this research.

A 4.1 Centre-point model

The friction cone from the point of contact (centre point of an arc contact) begins to point downwards as the angle of contact, θ, increases. Nguyen's rule is that there must be a line in the friction cone that connects the contact points to each other.

The θ_{max} in this scenario is the angle made with the horizontal and the line of contact. Since the top part of the friction cone is horizontal, the alternate angle rule can be used. This is between two parallel lines and the angles on alternate sides of the line connecting these parallel lines are equal.

$$Thus,\ \theta_{max} = \alpha \tag{37}$$

A 4.2 Bottom point in the arc model

The bottom point in the arc model is similar to Nguyen's except the cone being focused on is the one around the bottom point of the arc rather than the centre. The angle of contact, θ, is still associated with the centre point of the contact, whether that is a point or an area contact. That is why the formula is slightly less simple than the original Nguyen's theorem.

Using the alternate angle rule, the angle to the bottom point, θ_{bottom}, is equal to α. The angle required for θ_{max} is greater than this. The difference in angle between θ_{max} and θ_{bottom} can be found by using the arc length, s, and the radius, r.

It can be seen that the distance along the circumference of the shape to the middle point from the bottom point is half an arc length. This can be used as a fraction of the actual circumference of the circle cross-section to find the difference in the angles, θ_{diff}.

$$\theta_{diff} = \frac{\frac{1}{2}s}{2\pi r} \times 2\pi$$

$$\theta_{diff} = \frac{s}{2r}$$

Adding this angle to the bottom point, θ_{max} can be found.

$$\theta_{max} = \theta_{bottom} + \frac{s}{2r} \tag{38}$$

A 4.3 Top point of the arc model

This is very similar to the previous model, except this time the difference in angle between the middle point and the angle to the top point friction cone being looked at needs to be subtracted from the top point. This is because the top point is larger than the middle point.

Using the same approach as in the previous model, the θ_{max} can be worked out as:

$$\theta_{max} = \theta_{top} - \frac{s}{2r} \tag{39}$$

Appendix 5 Results from the coefficient of static friction experiment

Table 10: Results of the coefficient of static friction experiment

Fingertip type	Trial 1 (°)	Trial 2 (°)	Trial 3 (°)	Average angle (°)	Average static frictional coefficient
PLA	7	6.5	6.5	6.67	0.11687
30A shore hardness	37	40	42	39.67	0.8310
15A shore hardness	48	49	50	49	1.1509

Appendix 6 Sample Calculations of the arc length and experimental maximum angle

PLA Finger:

No arc length is needed to be calculated since the PLA finger is a point contact.

An example vertical distance from the horizontal mid-line to the contact point is from trial 7 right finger, 0.3528cm.

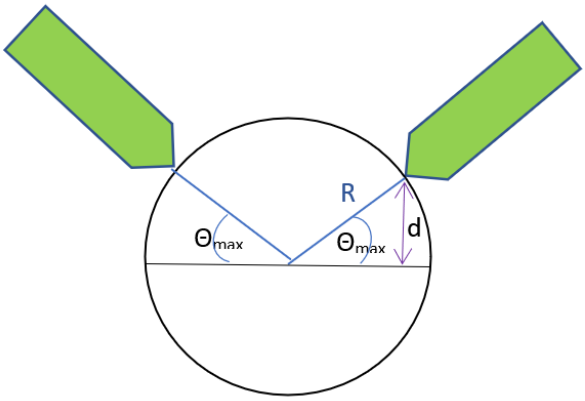

Figure 44: Schematic showing distance for hard finger calculations

To work out the θ_{max}, a right-angle triangle can be imagined with its borders being the radius R as the hypotenuse, d as the opposite side, and the horizontal mid line as the adjacent line.

$$\theta_{max} = sin^{-1}\left(\frac{d}{R}\right) \tag{40}$$

So for the example d of 0.3528cm:

$$\theta_{max} = sin^{-1}(\frac{0.3528}{3})$$

$$\theta_{max} = 0.1179\ rad$$

$$\theta_{max} = 6.754°$$

30A shore hardness/15A shore hardness Finger calculations

In an expansion from the PLA finger, the Imagemeter app was used to find two vertical distances, d1 and d2. These distances correspond to the height to the top point of the arc and the bottom respectively.

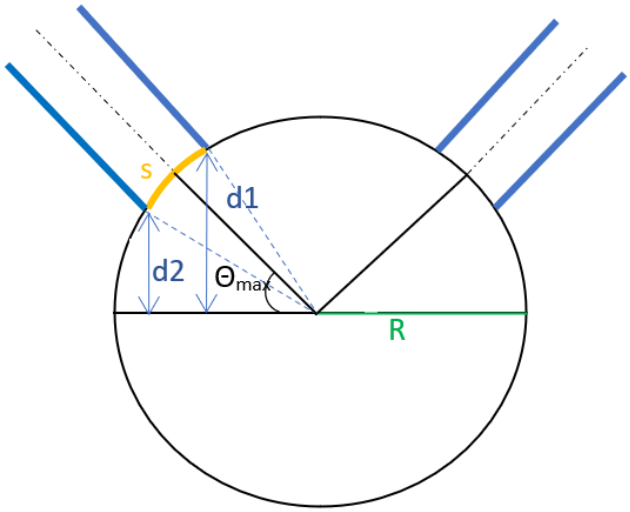

Figure 45: Schematic showing distances for 30A/15A shore hardness finger calculations

The maximum angle before slipping is directly in the centre of the arc of the top point and the bottom point. This means it is the average angle of the top angle and the bottom angle. Thus, the right-angle triangle approach that was done for the PLA finger will be utilised again in the triangles made from both d1 and d2 as the opposite side in the triangle. The angles found will be the contact angles for the top and bottom points, respectively.

$$\theta_{d1} = sin^{-1}\left(\frac{d1}{R}\right) \tag{41}$$

$$\theta_{d2} = sin^{-1}\left(\frac{d2}{R}\right) \tag{42}$$

$$\theta_{max} = \frac{\theta_{d1} + \theta_{d2}}{2} \tag{43}$$

To find the arc length of contact for the 30A/15A shore hardness fingers the total angle span from the arc length was used. It was used as a fraction of 2 pi and then multiplied by the circumference of the cross-section.

$$s = \frac{\theta_{d1} - \theta_{d2}}{2\pi} \times 2\pi R$$

$$s = (\theta_{d1} - \theta_{d2)} \times R \tag{44}$$

Appendix 7 Experimental Results

PLA Finger

Table 11: Experimental results from each trial for PLA finger

Trial	d LH (cm)	d RH (cm)	angle LH (°)	angle RH (°)	Average Angle (°)
1	0.2404	0.2659	4.596229778	5.084988637	4.840609207
2	0.214	0.188	4.090573062	3.592889751	3.841731407
3	0.3834	0.364	7.342481162	6.969059274	7.155770218
4	0.3488	0.4138	6.676689829	7.928274752	7.30248229
5	0.2894	0.2887	5.535741377	5.522309872	5.529025624
6	0.2791	0.2181	5.338136764	4.169081152	4.753608958
7	0.324	0.3528	6.200037133	6.753611911	6.476824522
8	0.3191	0.3031	6.105911785	5.7986775	5.952294642
9	0.4548	0.3887	8.719660292	7.444552367	8.08210633
10	0.3498	0.3151	6.695919211	6.029087039	6.362503125
11	0.3167	0.2947	6.059815624	5.637447015	5.848631319
12	0.3457	0.2721	6.617083536	5.203878846	5.910481191
13	0.3238	0.2925	6.196194954	5.595227436	5.895711195
14	0.3508	0.2853	6.71514935	5.457075449	6.0861124
15	0.3971	0.2566	7.606374416	4.906694312	6.256534364
16	0.5134	0.3972	9.85371998	7.608301234	8.731010607
17	0.4308	0.3327	8.256216689	6.367199213	7.311707951
18	0.4209	0.3809	8.06520632	7.294342519	7.67977442
19	0.3317	0.3063	6.34798244	5.860110688	6.104046564
20	0.4375	0.3774	8.385538647	7.226957107	7.806247877

30A shore hardness Finger

Vertical Distances

Table 12: Experimental results of the vertical distances to the top/bottom points for 30A shore hardness fingers

Trial	d1 LF (cm)	d2 LF (cm)	d1 RF (cm)	d2 RF (cm)
1	1.1564	0.7656	1.1431	0.7563
2	1.1477	0.7863	1.0644	0.6943
3	1.125	0.7578	1.111	0.7043
4	1.1205	0.7277	1.0526	0.6784
5	1.1092	0.7769	1.1342	0.7423
6	1.0988	0.7066	1.1088	0.7447
7	1.167	0.7736	1.1891	0.8117
8	1.179	0.804	1.1419	0.7498
9	1.1493	0.79	1.0855	0.7009
10	1.103	0.745	1.0167	0.6137
11	0.9839	0.5843	1.134	0.7823
12	1.0652	0.6588	0.9182	0.5576
13	1.0867	0.7107	1.0482	0.6679
14	1.0662	0.6616	0.9948	0.5899
15	1.0858	0.7129	0.9609	0.601
16	1.0668	0.6745	0.9834	0.5653
17	0.939	0.5732	0.8365	0.454
18	1.145	0.7766	1.1256	0.7745
19	1.0945	0.719	0.9937	0.585
20	1.0791	0.6996	1.0287	0.6245

Calculated values

Table 13: Calculated values using the experimental results for 30A shore hardness finger

Trial	LF mid angle (deg)	RF mid angle (deg)	LF arc length (cm)	RF arc length (cm)	Average angle (deg)	Average arc length (cm)
1	18.72907548	18.49975932	0.412976918	0.408191854	18.6144174	0.410584386
2	18.84373203	17.08133005	0.382125188	0.387448149	17.96253104	0.384786669
3	18.32786657	17.65702263	0.387090948	0.427167971	17.992446	0.40712946
4	17.98485537	16.80493233	0.413305689	0.391170293	17.39489385	0.402237991
5	18.35396442	18.26983037	0.35030934	0.413030263	18.3118974	0.381669801
6	17.55430968	18.03197246	0.411679187	0.383167271	17.79314107	0.397423229
7	18.91790302	19.52461322	0.416196913	0.40072309	19.22125812	0.408460001
8	19.34329361	18.42324276	0.39772603	0.413609054	18.88326819	0.405667542
9	18.89688958	17.3619531	0.380022431	0.403262892	18.12942134	0.391642661
10	17.97534785	15.8070018	0.37661816	0.419179409	16.89117482	0.397898784
11	15.18825002	18.66270562	0.41439249	0.3714564	16.92547782	0.392924445
12	16.74153522	14.26700689	0.424742809	0.372314517	15.50427105	0.398528663
13	17.47053197	16.6571847	0.39446719	0.397247703	17.06385834	0.395857447
14	16.7791608	15.35303599	0.422942215	0.420227998	16.06609839	0.421585107
15	17.48293799	15.11876035	0.391237008	0.373044045	16.30084917	0.382140526
16	16.91164961	14.99833408	0.410351885	0.433221925	15.95499184	0.421786905
17	14.62757897	12.44739491	0.378304177	0.391986132	13.53748694	0.385145155

18	18.71989144	18.49899049	0.38925031	0.37046541	18.60944097	0.37985761
19	17.63209686	15.29418725	0.39429386	0.42405842	16.46314205	0.40917664
20	17.28365779	16.03429619	0.39773769	0.42090643	16.65897705	0.40932066

15A shore hardness Finger

Vertical Distances

Table 14: Experimental Results of the vertical distances to the top/bottom points of the 15A shore hardness finger

Trial	d1 LF (cm)	d2 LF (cm)	d1 RF (cm)	d2 RF (cm)
1	1.6422	1.0967	1.5896	1.0342
2	1.6768	1.151	1.5995	1.0394
3	1.5603	1.0051	1.5154	0.9976
4	1.5055	0.9566	1.5362	0.9959
5	1.5436	0.9873	1.5716	0.9699
6	1.5717	0.9936	1.6023	1.0231
7	1.4787	0.9264	1.4994	0.98
8	1.5466	0.9555	1.5339	0.9219
9	1.528	0.894	1.5334	0.8909
10	1.4622	0.8469	1.5193	0.9138
11	1.4793	0.9346	1.4194	0.8173
12	1.5697	0.9348	1.5261	0.9671
13	1.5713	0.8982	1.5279	0.8888
14	1.4319	0.8468	1.4186	0.81
15	1.5638	1.001	1.3719	0.8307
16	1.4907	0.9491	1.4135	0.8667
17	1.5277	0.9573	1.3587	0.8774
18	1.5013	0.8895	1.4408	0.8896
19	1.6066	1.0163	1.564	0.9854
20	1.6421	1.0903	1.5177	0.9089

Calculated Values

Table 15: Calculated values for the 15A shore hardness finger

Trial	LF mid angle (deg)	RF mid angle (deg)	LF arc length (cm)	RF arc length (cm)	Average angle (deg)	Average arc length (cm)
1	27.3156424	26.08098239	0.615038171	0.619465951	26.69831239	0.617252061
2	28.27152645	26.24550839	0.598005957	0.625612164	27.25851742	0.611809006
3	25.45676224	24.88140728	0.615982261	0.571643827	25.16908476	0.593813044
4	24.3578831	25.09488769	0.603550587	0.597604226	24.72638539	0.600577407
5	25.09021285	25.22729594	0.615338997	0.666508062	25.15875439	0.640923533
6	25.46792403	26.11136951	0.641544347	0.646280764	25.78964677	0.643912555
7	23.75914842	24.52667454	0.60446553	0.571779753	24.14291148	0.588122642
8	24.80267293	24.323526	0.652449885	0.673027053	24.56309947	0.662738469
9	23.97847581	24.00742744	0.695439474	0.704965285	23.99295163	0.70020238
10	22.78367894	24.08032355	0.668756584	0.664574916	23.43200124	0.66666575
11	23.84810032	22.02349839	0.596529773	0.650768622	22.93579936	0.623649198
12	24.85253425	24.69169376	0.701292895	0.616336745	24.772114	0.65881482
13	24.50341111	23.92536107	0.741608739	0.700769236	24.21438609	0.721188988
14	22.45237094	21.9424032	0.63427057	0.657444901	22.19738707	0.645857736
15	25.45436721	21.64414601	0.624432191	0.583170933	23.54925661	0.603801562
16	24.11922732	22.45108308	0.594377746	0.592606057	23.2851552	0.593491902
17	24.61064069	21.96779367	0.628542134	0.519630322	23.28921718	0.574086228
18	23.6380895	22.97616271	0.669220365	0.599694136	23.30712611	0.634457251

19	26.09091927	25.29873311	0.658600209	0.641198884	25.69482619	0.649899546
20	27.24887066	24.01349503	0.621791509	0.667862761	25.63118284	0.644827135

Appendix 8 Results from the scale test

A 8.1 Using the resultant cone model

Note: Normal Forces in the table also contain the mass of the fingertips which was 2.38g.

<u>30A shore hardness finger</u>

Normal force predicted for the two-fingered 30A shore hardness finger grasp was 0.3159 N or 32.20g.

Target normal force included the mass of the fingertips was thus 34.58g

Table 16: Results of the arc lengths measured for the normal force predicted by the extended cone model for 30A shore hardness finger

Trial	**d1 (cm)**	**d2 (cm)**	**Arc length (cm)**	**Normal Force (g)**
1	1.1763	0.7892	0.388182306	33.21
2	1.2671	0.8752	0.393023281	34.02
3	1.387	0.9793	0.408965502	33.32
4	1.1716	0.7904	0.382233331	36.53
5	1.2933	0.9137	0.380620311	34.39
6	1.2784	0.9224	0.356840858	32.34
7	1.2329	0.9576	0.275687861	33.72
8	1.1722	0.8136	0.359459497	32.47
9	1.1959	0.798	0.399075949	34.51
10	1.128	0.7021	0.427343769	35.7
11	1.3111	0.9581	0.353819691	34.31
12	1.3374	0.976	0.362279877	35.11
13	1.3356	0.9416	0.395141531	35.2
14	1.2787	0.9223	0.357243708	34.48
15	1.4387	1.022	0.418051682	32.83
16	1.2564	0.8668	0.390703519	34.53
17	1.3049	0.9725	0.333083911	33.55
18	1.3373	0.9627	0.375580335	33.89
19	1.3621	0.9737	0.389493302	36.13
20	1.2872	0.8617	0.42693968	33.61

Average normal force measured: 34.1925 g ±0.2553g

Average arc length measured: 0.3787cm ±0.0078cm

15A shore hardness Finger

Normal force predicted by the extended cone model for the two-fingered 15A shore hardness finger grasp of the cylinder was 0.2889N or 29.45g. Including the mass of the fingertip, the target normal force was 31.83g.

Table 17: Results of the arc lengths for the normal force predicted by the extended cone theorem for the 15A shore hardness finger

Trial	**d1 (cm)**	**d2 (cm)**	**Arc length (cm)**	**Normal Force (g)**
1	0.6356	0.0512	0.588160619	31.61
2	0.3667	-0.1946	0.564627539	30.79
3	0.4818	-0.1128	0.59856344	33.78
4	0.9805	0.4243	0.559436711	31.16
5	0.8623	0.2585	0.607952634	33.84
6	0.9238	0.3618	0.565340139	31.68
7	0.9091	0.3111	0.602032662	32.49
8	0.8403	0.2258	0.618880281	32.28
9	0.8605	0.2529	0.611832537	31.88
10	0.9901	0.3101	0.685961705	32.47
11	1.1705	0.5708	0.603767579	33.8
12	1.1657	0.6024	0.566663624	31.9
13	1.1627	0.5925	0.573690152	30.84
14	1.1285	0.4717	0.662163446	32.13
15	1.2228	0.6326	0.594075062	32.01
16	1.1689	0.6057	0.566561814	32.7
17	1.2196	0.5758	0.64884681	33.52
18	1.2272	0.6658	0.564729337	32.87
19	1.2055	0.5956	0.614181402	32.55
20	1.1851	0.6258	0.562591717	33.1

Average normal force measured: 32.37g ± 0.2082g

Average arc length measured: 0.5980cm ± 0.0080cm

A 8.2 Using Coulomb's theory

30A shore hardness

The normal force predicted by Coulomb's theorem for the two-fingered grasp scenario of the cylinder using the 30A shore hardness finger was 0.2512 N or 25.61g. Including the mass of the fingertip the target reading force on the scale was 27.99g.

Table 18: Results of the arc lengths for the normal force predicted by Coulomb's law for the 30A shore hardness finger

Trial	**d1 (cm)**	**d2 (cm)**	**Arc length (cm)**	**Normal Force (g)**
1	1.0531	0.7521	0.301507318	25.87
2	1.045	0.7131	0.332580818	28.82
3	0.9721	0.6677	0.304924759	28.68
4	1.136	0.8096	0.327047411	27.88
5	1.038	0.684	0.354826707	27.78
6	1.0678	0.7345	0.333989502	27.9
7	1.0194	0.7612	0.258519835	26.67
8	1.106	0.7238	0.383241525	28.06
9	1.146	0.8098	0.336907726	27.68
10	1.1354	0.7131	0.423707248	28.81
11	1.3755	1.0726	0.303417016	27.55
12	1.2153	0.8512	0.364999835	27.51
13	1.4017	1.0812	0.321112816	27.98
14	1.3236	0.979	0.345362331	28.01
15	1.3441	1.0208	0.323929076	26.96
16	1.2987	0.9794	0.319905935	27.44
17	1.397	1.0309	0.367014812	28.49
18	1.3281	1.0065	0.32221917	27.89
19	1.4627	1.1105	0.353014107	27.56
20	1.4184	1.1054	0.313570657	24.71

Average Normal force measured: 27.6125g ± 0.2199g

Average arc length measured: 0.33459±0.00779

15A shore hardness finger

The normal force predicted by Coulomb's theory for the 15A shore hardness finger was 0.1977N was 20.15g. Including the mass of the fingertip the target normal force was 22.53g for the scale.

Table 19: Results of the arc lengths based on the predicted Normal force from Coulomb's law for the 15A shore hardness finger grasp

Trial	**d1 (cm)**	**d2 (cm)**	**Arc length (cm)**	**Normal Force (g)**
1	1.1861	0.6912	0.497172645	19.32
2	0.6966	0.1707	0.528631435	20.96
3	0.7833	0.2879	0.497679597	22.11
4	0.7439	0.2662	0.479742088	24.07
5	0.6582	0.156	0.504575585	22.68
6	0.7796	0.234	0.548653332	24.6
7	0.7417	0.1878	0.557096305	21.52
8	0.8878	0.296	0.595707043	21.48
9	0.5859	0.1169	0.470931724	19.34
10	0.6807	0.1493	0.534218872	19.99
11	1.3681	0.87	0.50041739	22.34
12	1.296	0.7766	0.522030488	22.17
13	1.3377	0.8668	0.472855474	22.04
14	1.3148	0.861	0.455548678	20.17
15	1.3411	0.7658	0.578885718	21.83
16	1.3773	0.7881	0.593055164	20.74
17	1.3544	0.7902	0.567579948	22.36
18	1.2207	0.7723	0.450086575	21.38
19	1.1565	0.6779	0.480653742	21.25
20	1.1122	0.6854	0.428252998	23.19

Average normal force measured: 21.677g±0.3117g

Average arc length measured: 0.5132cm ± 0.0109cm

Appendix 9 Maximum angle of force closure calculations for second experiment

A 9.1 Centre-point model

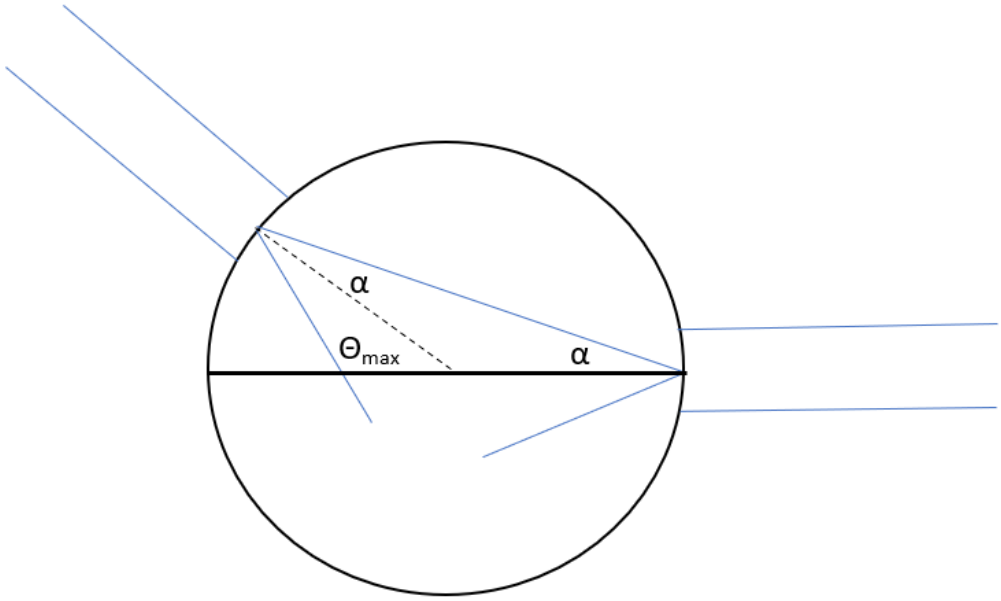

Figure 46: Schematic for calculating maximum angle before slipping for iterated experiment using the Centre-point model

The maximum angle of contact corresponding to the centre of the contact arc was calculated using basic geometry rules. The highest angle the left finger can go without the object slipping is when its top friction cone boundary aligns with the top friction cone boundary of the right finger. After this, if the angle continues to increase, there would no longer be a line connecting the two points of contact together within their friction cones, thus slipping would occur.

As can be seen Figure 46 above, there is an isosceles triangle with the two identical angles being α. The sum of the angles in a triangle adds up to π radians. It can also be seen that θ_{max} lies on a line with this angle. The rule here is that angles on a line add up to π radians.

Combining these rules together, θ_{max} can be calculated in radians as:

$$\theta_{max} = \pi - (\pi - 2\alpha)$$

$$\theta_{max} = 2\alpha \tag{45}$$

A 9.2 Bottom point in the arc model

The contact angle that is associated with the bottom point in the arc, θ_{bottom}, can be calculated using the same triangle and line rules that were seen in the previous Nguyen's model.

$$\theta_{bottom} = 2\alpha$$

However, for comparison purposes, the angle of importance is the angle going to the centre point of the contact arc i.e. θ_{max}. This is found using the theory that was outlined in Appendix 4 A 4.2.

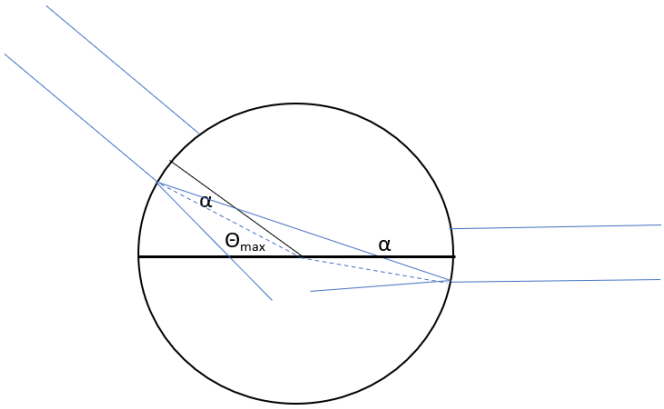

Figure 47: Schematic showing calculations of maximum angle using the bottom point model for the iterated experiment

$$\theta_{max} = 2\alpha + \frac{s}{R} \tag{46}$$

Appendix 10 Second Experiment Results

30A shore hardness Finger

Vertical Distances

Table 20: Results of the vertical distances to the top/bottom points of the 30A shore hardness finger

Trial	d1 LF (cm)	d2 LF (cm)	d1 RF (cm)	d2 RF (cm)
1	1.8577	1.5084	0.2276	-0.2382
2	1.6735	1.3037	0.1529	-0.2599
3	1.8077	1.4586	0.1886	-0.1615
4	1.8779	1.479	0.3091	-0.1461
5	1.7311	1.3155	0.1247	-0.2927
6	1.7562	1.3383	0.2079	-0.2582
7	1.8145	1.4135	0.1734	-0.2475
8	1.6448	1.3344	0.2009	-0.209
9	1.6535	1.3139	0.1244	-0.2291
10	1.7681	1.373	0.1954	-0.2307

Calculated Values

Table 21: Calculated values for the 30A shore hardness finger grasp

Trial	LF mid angle (deg)	RF mid angle (deg)	LF arc length (cm)	RF arc (cm)	Average arc length (cm)
1	34.22279503	-0.10152901	0.422792919	0.4662699	0.444531408
2	29.83190688	-1.02425694	0.426647495	0.4131925	0.419919989
3	33.07253336	0.259228506	0.416932308	0.3503026	0.383617434
4	34.14556388	1.561230837	0.482507744	0.4558073	0.46915754
5	30.62518341	-1.60839227	0.48348787	0.4179023	0.450695095
6	31.16249558	-0.48179131	0.488911156	0.4665866	0.477748879
7	32.66345185	-0.70936879	0.4768307	0.4212783	0.449054508
8	29.82936184	-0.07753046	0.358017815	0.4102199	0.384118854
9	29.71065316	-1.00160269	0.391278546	0.3537589	0.372518746
10	31.67436089	-0.33794542	0.46471663	0.4264664	0.44559152

15A shore hardness Finger

Vertical Distances

Table 22: Vertical distances to the top/bottom of the arc for 15A shore hardness finger

Trial	d1 LF (cm)	d2 LF (cm)	d1 RF (cm)	d2 RF (cm)
1	2.5042	2.1253	0.3303	-0.3399
2	2.575	2.183	0.3658	-0.2416
3	2.4231	2.1209	0.3896	-0.2558
4	2.4618	2.10037	0.3261	-0.324
5	2.3219	1.9696	0.0842	-0.4497
6	2.3724	1.9734	0.3091	-0.317
7	2.5528	2.2017	0.2733	-0.2829
8	2.4378	2.0289	0.3175	-0.324
9	2.506	2.1003	0.1537	-0.3154
10	2.4714	2.0314	0.3104	-0.3243

Calculated Values

Table 23: Calculated values for the 15A shore hardness finger grasp

Trial	LF mid angle (deg)	RF mid angle (deg)	LF arc length (cm)	RF arc length (cm)	Average arc length (cm)
1	50.8478354	-0.09225059	0.601117138	0.6716024	0.636359782
2	52.91054952	1.19223575	0.651295304	0.6085745	0.629934889
3	49.43023395	1.285264074	0.465121808	0.6468145	0.555968154
4	49.79090056	0.020172281	0.560669639	0.6513788	0.606024223
5	45.87372932	-3.50640936	0.506603953	0.5356124	0.5211082
6	46.69631952	-0.07585358	0.582662412	0.6272424	0.604952414
7	52.76383926	-0.09206973	0.581141251	0.5570004	0.569070833
8	48.45296305	-0.06242828	0.617613955	0.6427289	0.630171426
9	50.54279534	-1.54905452	0.639603945	0.4697512	0.554677597
10	49.04352668	-0.1334843	0.672666402	0.6358915	0.654278931